

Computer Aided Design of components for energy transfer

LOCAL LNG STATION



Edward Lisowski, Wojciech Czyżycki,
Grzegorz Filo, Katarzyna Łazarczyk

Bergen University College, 2013

Skriftserien, nr. 3/2014

~~Boken kan bestilles hos:~~
~~Høgskolen i Østfold~~
~~www.hio.no/nettbutikk/~~

ISBN 978-82-77-09779-8

Denne fagrapporten er vurdert av Shokri Amzin

Opplag:

45 eksemplarer

Grafisk produksjon:

BODONI

Computer Aided Design of components for
energy transfer

LOCAL LNG STATION

Scientific Committee:

Prof. Mons Erik Monstad

Prof. Edward Lisowski

Ragnar Gjengedal, PhD

Mariusz Domagała, PhD

Wojciech Czyżycki, PhD

Grzegorz Filo, PhD

Bergen University College, 2013

Table of contents

1. Introduction	5
1.1. Preface	5
1.2. Heat transfer in cryogenic conditions	7
1.2.1. Heat transfer by conduction	7
1.2.2. Heat transfer by convection	11
1.2.3. Heat transfer by radiation	14
1.2.4. Heat transfer by residual gas	16
1.3. References	19
2. SolidWorks simulation of the heat transfer of the vertical criogenic tank with Liqueified Natural Gas	21
2.1. Analysis of insulation materials of cryogenic tank walls	25
2.2. Simplifying assumptions and plan of the research	25
2.3. Thermal loads, boundary conditions and material parameters	35
2.4. Results of simulations	37
2.5. Summary	48
2.6. References	48
3. Simulation research of the thermal insulation supports of cryogenic tank	50
3.1. Arrangement of internal supports regard to external supports	50
3.2. Construction and materials of insulation inserts for the supports	54
3.3. Assumptions for the calculations	57
3.4. Simulation research of insulating inserts of supports in SolidWorks	59
3.5. Conclusions	69
3.6. References	70
4. Experimental research	72
4.1. Research of thermal properties of plastics at cryogenic temperatures	72
4.2. Strength tests of plastics at low temperatures	81
4.3. Conclusions	84
4.4. References	85
5. Online monitoring and diagnosis system of the LNG supply station	87
5.1. Mathematical description of the evaporation process	87
5.1.1. Evaporation of overheated liquid	88
5.1.2. Mass and heat exchange during the evaporation from open container	91
5.1.3. Vaporizing of cryogenic liquids	97
5.1.4. Vaporization of liquefied LNG	98
5.2. Idea of monitoring and diagnostics system of LNG supply station	104
5.2.1. Identification of measuring points	104

5.2.2. Requirements for the monitoring and diagnostics system	106
5.2.3. Main components of the system	107
5.3. Elements of the monitoring subsystem	109
5.3.1. Temperature sensors and transducers	109
5.3.2. Mass flow measurement	114
5.3.3. Measurement of the pressure	121
5.3.4. Structure of the measurement system	122
5.4. Design of the software	125
5.4.1. The data acquisition program	125
5.4.2. Database design	127
5.4.3. Initial assumptions on the module for results visualization	129
5.5. References	130

1. INTRODUCTION

1.1. PREFACE

Nowadays, due to the increase in energy prices, the interest in natural gas as a fuel of great ecological and economical properties is growing. The use of the natural gas is relatively easy if there are pipelines which allow to access it. However, there are systems, which cannot be connected to a stationary pipeline system, for example vehicles, or distant separate places [7]. An alternative solution for these systems is to use the natural gas in the liquefied form as a Liquefied Natural Gas (LNG) [7, 10]. LNG is produced from the natural gas by removing impurities, and then condensing in the process of cooling to about minus 160 degrees Celsius [2, 3, 5]. Condensation process of the liquefied natural gas is carried out in specialized cryogenic installations. Transition from the gas to the liquid causes a reduction in unit volume of gas about 650 times. This unique property is very important for the economics of transport and storage. Transport and storage of the LNG requires temperatures of minus 160 degrees Celsius or lower. LNG is odorless, colorless and non-toxic. After a vaporization we obtain a fuel with minimal impurity, almost completely devoid of the moisture. Liquefied natural gas is a clean fuel gas with a high octane number approximately equal to 130.

LNG supply stations can be used for realizing various tasks. The most important of them are:

- connection a gas pipeline to existing national network of gas pipelines as a temporary solution,
- an alternative solution for distant locations, which will not be able to connect to the system due to the technical and financial reasons. In

this case the LNG is an economically attractive energy source for manufacturing facilities and individual clients,

- as a temporary source for covering short-term peak demands and emergency power supplies,
- as fuel stations for combustion engines of vehicles, rail vehicles and vessels [4].

A typical LNG supply station is composed of the following components: cryogenic storage tank for LNG, installation of vaporizers, installation of gas odor transmission, system of safety valves and installation of pressure reduction. Usually, the most expensive element of the installation is a cryogenic tank in which the LNG is stored. However, considering current high energy prices, investments in this technology are cost-effective. This is confirmed by numerous examples of applications, especially at medium or large gas consumption. In Poland, the use of the liquefied natural gas continues to increase, both to heat buildings and power supply in industrial lines. This led manufacturers of industrial fittings to a wider interest in the production of components for this type of installation. Taking into consideration demands of the market, Cracow University of Technology together with the Chemet S.A. company developed a family of cryogenic tanks with various volumes and for various usages.

Nowadays, modern design tasks including the strength analyzes and simulations of heat flow are strongly supported with the use of computer systems. In the development process of the LNG local supply station various computer aided design systems were used, for example SolidWorks with CosmosWorks and FLOWorks applications, Pro/Engineer with Pro/Mechanica, etc [8]. While performing tasks related to the design of cryogenic installations, the constructor must realize, that the extremely low temperatures causes significant changes in properties of materials [2, 6, 9].

Some of the phenomena, particularly connected with the heat flow, are more intense than in the normal ambient temperatures. Therefore, the next section is devoted to the most important issues related to the heat exchange in cryogenic conditions.

1.2. HEAT TRANSFER IN CRYOGENIC CONDITIONS

In all cryogenic devices, there are complex heat transfer processes. The cryogenic conditions are quite different from those for devices which operate in normal temperature ranges [1, 2]. The designer of cryogenic tank must consider in the calculations many various phenomena related to the heat transfer between the environment and the fluid inside of the tank. For example, the following ways of heat transfer must be taken into account: conduction, convection and radiation [3, 5]. Obtaining and maintaining a cryogenic temperature requires a very efficient thermal insulation with special parameters [7, 10]. For the purpose of the cryogenic insulations, a completely new types of insulations and their manufacturing techniques have been developed [6, 8, 9].

1.2.1. HEAT TRANSFER BY CONDUCTION

The phenomenon of heat conduction in cryogenic tanks occurs mainly through the support elements, tubes, pipes, valves and other components, which are in contact with the container or a cryogenic liquid passes through them when refueling or operating. Conduction occurs between heat sources with different temperatures. In the case of the LNG tank, difference in temperature between the fluid and the environment can be above 200 degrees Celsius (for example: temperature of the LNG is minus 165 degrees Celsius and the ambient temperature is plus 35 degrees

Celsius). Under these conditions, thermal conductivity of solid bodies is strongly dependent on the temperature [3, 5]. Therefore, this dependency should be included in the calculations. In the construction of cryogenic equipment, decreasing of the heat flux can be achieved by:

- increasing the length of the components which have thermal contact with sources of heat at different temperatures,
- decreasing the contact area,
- selecting of materials with low thermal conductivity.

In the most practical applications, problem of the heat conduction in cryogenic devices can be reduced to one-dimensional problem in the steady state conditions [1, 2].

The heat conduction is described in the Fourier law [5]:

$$q = -\lambda \cdot \text{grad}(T), \quad (1.1)$$

where: q – elementary heat flux $\left[\frac{W}{m^2}\right]$, λ – thermal conductivity $\left[\frac{W}{m \cdot K}\right]$, $\text{grad}(T) = \frac{\partial T}{\partial n}$ – derivative of temperature in direction n (perpendicular to the isothermal surface).

The case of one-dimensional heat conduction through the body section F along the x axis perpendicular to the surface F is described by the equation:

$$Q = -\lambda \cdot F \cdot \frac{dT}{dx}. \quad (1.2)$$

Assuming that the cross section F is constant and the thermal conductivity λ does not depend on the temperature: $F = \text{const}$ and $\lambda = \text{const}$, which occurs for example for a rod with a length of δ and the temperatures

T_1 and T_2 at both ends ($T_1 > T_2$), after integration of the equation (1.2) the following solution is obtained:

$$Q = \frac{\lambda}{\delta} \cdot F \cdot (T_1 - T_2). \quad (1.3)$$

Equation (1.3) may only be used in case when $F = const$ and $\lambda = const$. In general, the coefficients of thermal conductivity strongly depend on the temperature. Hence, this dependence must be considered for cryogenic tanks. The temperature dependence of the thermal conductivity coefficient for typical construction materials is presented in fig. 1.1.

If we assume that both the thermal conductivity and the area of cross-section are variable: $\lambda = \lambda(T)$ and $F = F(x)$, after integration of the equation (1.2), the following dependence is obtained:

$$Q = - \left[\int_{T_1}^{T_2} \lambda(T) dT \right] / \left[\int_{x_1}^{x_2} \frac{dx}{F(x)} \right]. \quad (1.4)$$

Equation (1.4) can be transformed to the form:

$$Q = - \left[\int_0^{T_1} \lambda(T) dT - \int_0^{T_2} \lambda(T) dT \right] / \left[\int_{x_1}^{x_2} \frac{dx}{F(x)} \right]. \quad (1.5)$$

In the case of constant cross section area along the entire length of the bar δ the following dependency occurs:

$$\int_{x_1}^{x_2} \frac{dx}{F(x)} = \frac{x_2 - x_1}{F} = \frac{\delta}{F}. \quad (1.6)$$

Expressions $\int_0^{T_1} \lambda(T) dT$ and $\int_0^{T_2} \lambda(T) dT$ are the integrals of the heat conduction. Using these integrals allows to determine the amount of transferred heat, including dependence of the material thermal conductivity coefficient on the temperature.

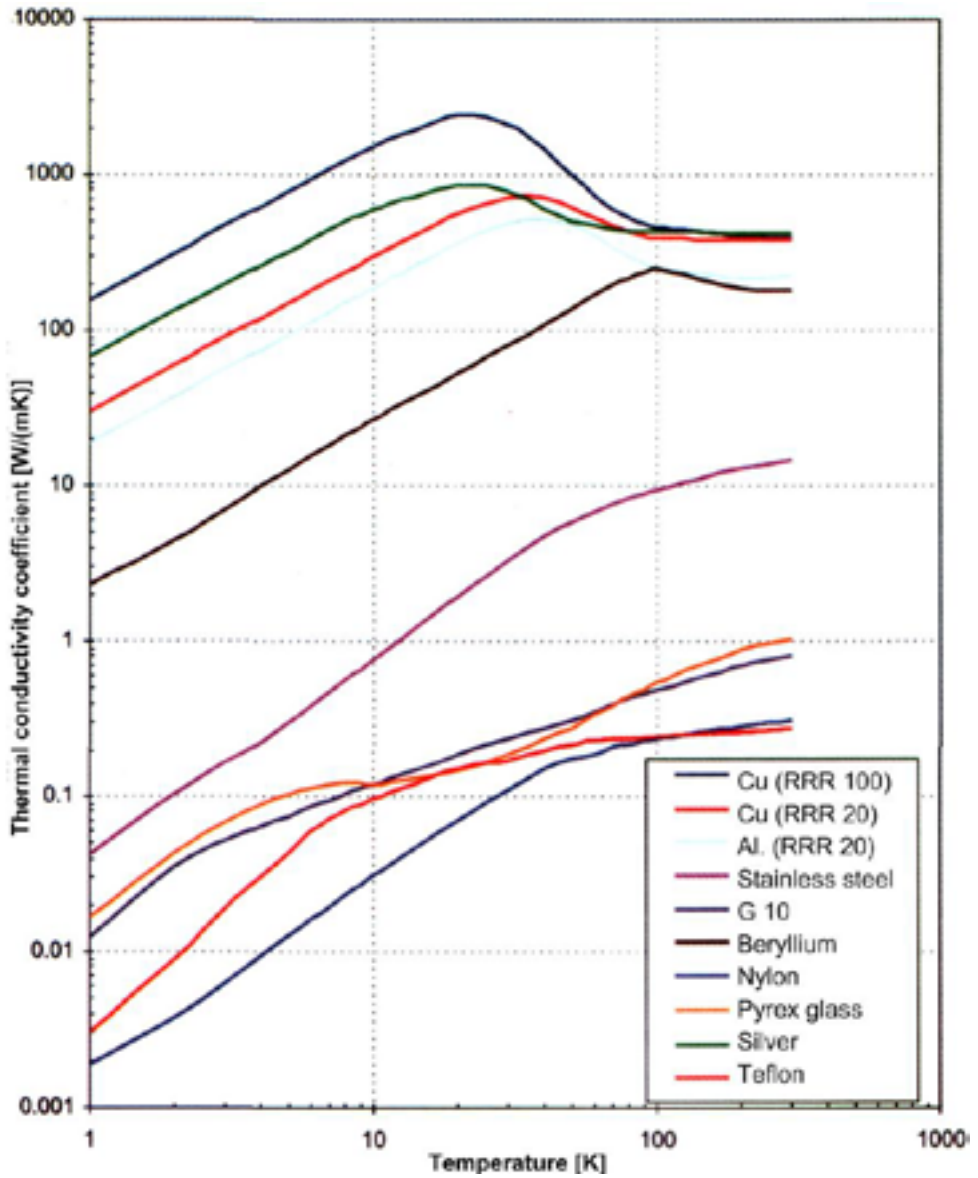


Fig. 1.1. Temperature dependence of thermal conductivity coefficient for typical construction materials [3]

Heat conduction in solid materials is a result of transfer of vibrational energy of atoms in the crystal lattice of quanta energy called phonons and by the movement of free electrons:

$$\lambda = \lambda_f + \lambda_e, \quad (1.7)$$

where: λ_f – phonon thermal conductivity coefficient, λ_e – electron thermal conductivity coefficient.

In metals, heat is conducted mainly by free electrons, whereas in insulation materials characterized by a small amount of these electrons, mainly by phonons. The following factors have the major impact on the phonon and electron thermal conductivity: amount of impurities and pollutants contained in the metals, technology of manufacturing, both: heat and mechanical treatments and the crystal structure.

1.2.2. HEAT TRANSFER BY CONVECTION

Convection is the process of heat transfer from fluid to solid body. If the liquid is in monophasic condition, the convection depends on both: the nature of the flow (laminar, turbulent or transitional) and the mechanism forcing the fluid movement (natural or forced convection). In the case of LNG tank, the convection at cryogenic temperatures do not differ in terms of physical from the convection observed at higher temperatures. The process of heat transfer from the solid body to the flowing cryogenic fluid describes the Newton's law [5]:

$$Q = \alpha \cdot F \cdot (T_s - T_f), \quad (1.8)$$

where: α – the heat transfer coefficient, F – solid body surface area, T_s – solid body temperature, T_f – fluid temperature.

Using the equation (1.8) requires calculation of the heat transfer coefficient α . Despite the dynamic development of analytical and numerical methods for describing the heat transfer processes, empirical and half-empirical dependences are still used in the design process. Expression for determining the heat transfer coefficient α is usually given as a function of dimensionless numbers, in particular: Nusselt number $Nu = \frac{\alpha d}{\lambda}$, Reynolds number $Re = \frac{\rho d w}{\mu}$, Prandtl number $Pr = \frac{\mu c_p}{\lambda}$, Grashof number $Gr = \frac{g \beta \rho^2 d^3 \Delta T}{\mu^2}$, Stanton number $St = \frac{Nu}{Re \cdot Pr} = \frac{\alpha}{w \rho c_p}$ and geometrical relations, like $\frac{l}{d}$.

General relation which describe convective heat transfer in a turbulent fluid flow has the following form:

$$Nu = f(Re, Pr), \quad (1.9)$$

and usually is presented in the form of products of polynomials with real number exponents: $Nu = Re^n Pr^m$.

Characteristic numbers Nu , Re , Pr and others describe a heat transfer by convection. The heat transfer depends on thermal properties of the fluid. In particular, thermal conductivity λ , viscosity μ , heat capacity c and density ρ are used. In the cryogenic conditions these properties strongly depend on the temperature. Hence, the heat transfer coefficient α is also a function of temperature.

In case of heat transfer to the gas at low temperature in a state of turbulent flow, the following equation can be used:

$$Nu = 0.023 \cdot Re^{0.8} Pr^{0.4} \left(\frac{T_s}{T_g} \right)^{-0.5}, \quad (1.10)$$

where gas parameters are determined at some distance from the wall (beyond the boundary layer), T_s – wall temperature, T_g – gas temperature in the core of the flow stream.

In the case of turbulent flow through the pipeline, when physical properties of the liquid do not change significantly, the following function can be used:

$$Nu = 0.023 \cdot Re^{0.8} Pr^{0.4}. \quad (1.11)$$

At a constant flow rate the following relation is valid:

$$\alpha = (const) \cdot \lambda^{0.6} \left(\frac{c_p}{\mu} \right)^{0.4} = f(T). \quad (1.12)$$

Heat transfer coefficient α should be determined for the average temperature of the fluid. The average temperature of the fluid and wall can also be used:

$$T_f = \frac{T_b + T_s}{2}, \quad (1.13)$$

where: T_f – the average temperature, T_b – temperature of the fluid at some distance from the wall, T_s – temperature of the wall.

Relations presented in (1.10) – (1.13) are commonly used in the design process of cryogenic equipment, when thermal properties of the fluid do not change significantly in the analyzed temperature range. The heat transfer coefficient α is calculated assuming the average temperature of the fluid and determining values of the following coefficients: λ , c_p and μ for this temperature. In some cases the assumption that the fluid properties remain constant along the pipeline cannot be made. In this situation the entire pipeline can be divided into small sections, and calculations of the heat transfer coefficient can be made separately for each section.

1.2.3. HEAT TRANSFER BY RADIATION

Heat transfer by radiation is a characteristic process of each body with a temperature above the absolute zero. This process is the result of transformation internal energy of this body into the radiation energy, which is emitted outside of the body in the form of the electromagnetic waves. If emitted energy reaches the surface of another body, it can be partially or completely absorbed and converted into the internal energy of the body. Heat transfer by radiation does not require contact of the bodies and can occur in a vacuum. In terms of statistics, the heat radiation is the emission of photons leaving the excited atoms. The photons then reach other atoms causing their excitation [2].

Thermal radiation includes electromagnetic waves with lengths from 0.4 to 1000 μm . Thus, it covers the range of visible radiation (from 0.38 to 0.77 μm), near infrared (from 0.77 to 25 μm) and far infrared (from 25 to 1000 μm).

The heat flux transmitted through the radiation of heat between two bodies with temperatures T_1 and T_2 ($T_1 > T_2$) can be determined from the Stefan-Boltzmann's law:

$$q_r = \sigma \cdot \varepsilon' \cdot (T_1^4 - T_2^4) \quad (1.14)$$

where: σ – constant of the black body radiation ($\sigma = 5.67 \cdot 10^{-8} \left[\frac{\text{W}}{\text{m}^2 \cdot \text{K}^4} \right]$),
 ε' – equivalent emissivity of the analyzed system.

If the heat transfer by radiation occurs in the lower temperature, the more spectrum of radiation is shifted towards the near and far infrared.

The radiation reaching the opaque body can be absorbed or reflected. It follows from the theoretical considerations, that if the body is in thermal equilibrium, it emits the same amount of radiation as it absorbs. It means

that the ability to reflect radiation is inversely proportional to the emissivity of the body. The important fact is that optical smoothness of the surface is not a good criterion for finding its low emissivity. Optically smooth surfaces reflect well only radiation of wave lengths from the range of visible light. This does not imply high reflectivity of wave lengths from the near and far infrared.

Comparison of the results of materials emissivity at cryogenic conditions leads to the following general conclusions:

- the best reflecting radiation materials (low emissivity) are good electrical conductors (copper, silver, gold, aluminum),
- emissivity of the surface diminishes when the temperature decreases,
- alloy containing a metal with high coefficient of radiation reflection has increased emissivity,
- emissivity of the surface area increases as a result of operations such as mechanical polishing,
- visual properties of surfaces (e.g. gloss) are not the reliable criteria for evaluating the reflection coefficient.

It follows from the equation (1.14) that if temperatures of the hot surface T_1 and the cold surface T_2 are defined, then reduction of the radiation heat transfer is only possible by decreasing the equivalent emissivity of the system. This involves selecting the appropriate materials for both surfaces and obtaining optimal state of the surfaces.

An effective way to reduce the heat transfer by radiation between two surfaces is placing the radiation shields between them. Hence, the shields have intermediate temperatures between T_1 and T_2 . It follows from the theoretical considerations that if the radiation shield and the heat exchanging surfaces are characterized by the same emissivity, the amount of heat exchanged by radiation between the surfaces decreases twice when one

shield is present. The use of N shields would reduce the heat radiation approximately $N+1$ times.

1.2.4. HEAT TRANSFER BY RESIDUAL GAS

Both, the kinetic theory of gases and laboratory tests confirm, that thermal conductivity of the gas, when the length of the particles free paths are small compared to the distance between the surfaces of the heat source, does not depend on the pressure of the gas [1, 2, 3]. Investigations of heat flux in the air, for the temperature of 300 degrees Celsius at a distance of 1 cm walls were carried out. The results showed, that reducing the pressure from 0.1 MPa to about 10 Pa did not cause significant changes in the heat flux. A significant decrease of the heat flux occurred when the pressure was reduced from 10.0 to 1.0 Pa. In case, when the pressure was less than approximately 0.1 Pa, the heat flux was almost proportional to the pressure value. Taking into consideration a constant heat flux caused by radiation, the following conclusion can be made: the heat flux generated by the residual gas is proportional to the pressure of the gas. In order to quantitatively estimate the heat flux generated by the residual gas, the accommodation coefficient α was defined:

$$\alpha = \frac{T_i - T_e}{T_i - T_w}, \quad (1.15)$$

where: T_i – the actual temperature of the gas particles before the collision, T_e – the actual temperature of the reflected particles (after impact), T_w – wall temperature. In case of complete thermal equilibrium between the wall and colliding particles, the α coefficient takes the value of one. If gas molecules are reflected from the wall perfectly elastically (no energy losses), α takes the value of zero. In practice, the α coefficient takes the value between zero

and one. In case when surfaces are rough and the temperature of the gas is close to the condensation temperature, the value of α is close to one.

In the simplest case there are of two parallel walls: the hot one and the cold one, the accommodation coefficient is equal to one on each wall and gas molecules can be divided into two groups. Molecules reflected from the warm surface have a velocity profile characteristic for this surface and the component of velocity vector towards the cold wall. The second group of molecules has a velocity profile given by the collision with the cold wall and moves toward the hot one. Martin Knudsen on the basis of these cases, developed a formula describing the heat flux between two cylindrical surfaces:

$$\dot{Q} = \frac{A_1}{2} \left(\frac{\alpha_1 \cdot \alpha_2}{\alpha_2 + \left(\frac{r_1}{r_2}\right) \cdot (1 - \alpha_2) \cdot \alpha_1} \right) \left(\frac{\gamma + 1}{\gamma - 1} \right) \left(\frac{R}{2\pi} \right)^{\frac{1}{2}} \left(\frac{P}{\sqrt{TM}} \right) (T_2 - T_1) \quad (1.16)$$

where: \dot{Q} – heat flux, A_1 – surface of the internal cylinder, α – adjustment coefficient, r – radius of the cylinder, γ – ratio of the specific heat $\frac{c_p}{c_v}$, R – universal gas constant, P – pressure, T – temperature [K], M – molar mass of residual gas molecules, the index of 1 refers to the inner cylinder, the index of 2 – to the outer cylinder. T without the index is the temperature measured at the point of pressure measurement.

If the free paths of the molecules have lengths comparable to the distance between the walls, the quotient $\frac{P}{\sqrt{T}}$ has a constant value. This phenomenon is known as the thermal effusion, the thermo-molecular pressure or the Knudsen effect.

For practical calculations of heat flow in systems different than two long, coaxial cylinders, it is convenient to express the radii ratio $\frac{r_1}{r_2}$ by using the ratio of the areas of inner and outer surface $\frac{A_1}{A_2}$. This substitution allows to perform calculations of heat flow between the surfaces in the shape of short cylinders, concentric spheres, etc. The general equation can be used for any coherent system of units. For the units commonly used in the cryogenics and systems associated with the vacuum [1, 2, 5], equation (1.16) can be written in the following form:

$$\dot{Q} = 2.43 \cdot 10^{-4} A_1 \left(\frac{\alpha_1 \cdot \alpha_2}{\alpha_2 + (A_1/A_2) \cdot (1 - \alpha_2) \cdot \alpha_1} \right) \left(\frac{\gamma + 1}{\gamma - 1} \right) \left(\frac{P}{\sqrt{TM}} \right) (T_2 - T_1) \quad (1.17)$$

where: \dot{Q} – heat flux [W], A_1, A_2 – surfaces [cm²], P – pressure [μ mHg], T, T_1, T_2 – temperatures [K].

Equation (1.17) was simplified by Corruccini. Assuming a suitably low pressure and a large length of a gas molecule free path in comparison to the size of the tank, the heat flux of the residual gas \dot{Q}_{gc} in tanks made of concentric spheres, coaxial cylinders and parallel surfaces can be written as:

$$\dot{Q} = \left(\frac{\gamma + 1}{\gamma - 1} \right) \cdot \alpha \cdot \left(\frac{R}{8\pi MT} \right)^{1/2} \cdot P \cdot (T_2 - T_1), \quad (1.18)$$

where \dot{Q}_{gc} – heat flux per time unit and the inner area unit, γ – ratio of the specific heat $\frac{C_p}{C_v}$, R – universal gas constant, P – pressure, M – molar mass of residual gas molecules, T – temperature at the point of pressure measurement [K], indexes 1 and 2 refer to the inner and the outer surface, respectively. The resulting accommodation coefficient α :

$$\alpha = \frac{\alpha_1 \cdot \alpha_2}{\alpha_2 + (A_1/A_2) \cdot (1 - \alpha_2) \cdot \alpha_1}. \quad (1.19)$$

Equation (1.18) can be written in the shorten form:

$$\dot{Q} = C \cdot \alpha \cdot P \cdot (T_2 - T_1), \quad (1.20)$$

where C is a constant factor:

$$C = \left(\frac{\gamma+1}{\gamma-1}\right) \cdot \left(\frac{R}{8\pi MT}\right)^{1/2}. \quad (1.21)$$

1.3. REFERENCES

- [1] Arkharov A., Marfenina I, Mikulin Ye.: *Cryogenic Systems*, Vol.1: *Basics of Theory and Design*, Moscow, 2000.
- [2] Bryson W. E.: *Cryogenics*, Hanser Gardner Publications, 1999;
- [3] Chorowski M.: *Kriogenika. Podstawy i zastosowania*, IPPU Masta, Gdańsk, 2007.
- [4] Dudek, S., Rudkowski, M. The comparative analysis of bus 6C(T)107 engine parameters fuelled pressed with compressed CNG and liquid natural gas LNG, *Journal of KONES*, Vol. 11, No. 1-2, s. 128--136, Institute of Aviation, Warsaw 2004.
- [5] Flynn T. M.: *Cryogenic Engineering*, 2nd edition, Dekker 2004.
- [6] Lisowski, E.; Czyżycki, W.; Łazarczyk, K.; *Simulation and experimental research of internal supports in mobile cryogenic tanks*, *Technical Transactions*, 8, 175-183, Wydawnictwo PK, 2010.
- [7] Lisowski E., Czyżycki W.: *Transport and storage of LNG in container tanks*, *Journal of KONES Powertrain and Transport*, Vol. 18, No. 3, p.p. 193-201, Warsaw 2011.

- [8] Lisowski, E.; Czyżycki, W.; *Modelowanie elementów maszyn i urządzeń w systemie CAD 3D SolidWorks z aplikacjami CosmosWorks i FloWorks*, Wydawnictwo PK, 2008.
- [9] Lisowski, E.; Czyżycki, W.; Łazarczyk, K.; *Using of polyamide in construction of supporting blocks of cryogenic tanks on example of LNG container*, Archives of Foundry Engineering, 10, 3/2010, 81 - 86, 2010.
- [10] Lisowski, E.; Czyżycki, W.; *Transport ciekłego LNG w zbiornikach kontenerowych*, Zeszyty Naukowe Politechniki Świętokrzyskiej. Nauki Techniczne, no. 12, 2009.

2. SOLIDWORKS SIMULATION OF THE HEAT TRANSFER OF THE VERTICAL CRYOGENIC TANK WITH LIQUIFIED NATURAL GAS

Simulations presented in this section were carried out with the use of CAD programs SolidWorks and SolidWorks Simulation (formerly Cosmosworks). The simulations are related to the new family of cryogenic tanks deployed to production in CHEMET SA company [6, 7, 8, 9, 10]. By utilizing results of previously conducted research on the cryogenic tank container for transport of the LNG [7, 10, 11], it was assumed that in the design of these tanks will be used a solution in the form of a double-wall tank. Internal cryogenic tank will be made of stainless steel 1.4301 according to the EN 10028-7 standard. The outer tank will be made of steel P355NL1 according to the EN 10028-3 standard. It has also been assumed, that due to the demand of the industry, there will be considered a number of sizes from 3.4 m^3 to 60.1 m^3 .

Proposed series of tank types consists of tanks with four main diameters (fig. 2.3) and three or four heights for each diameter will result in fifteen variants of capacity. In fig. 2.1 is shown LNG tank with a capacity of 8.8 m^3 , and in fig. 2.2 is presented variant of a 60.1 m^3 capacity tank. In the considered system, thermal insulation of the tank is placed between the outer and the inner wall [7]. The load of cryogenic tank is carried out by system of axial and radial thermal insulating inserts. The whole structure is supported on four external supports combined with the lower bottoms. External supports are attached to the foundation by bolts. There is also a reserved space under the tank assigned for pipe fittings and valves.



Fig. 2.1. LNG tank, capacity 8.8 m^3 with fragment with a cut piece of the wall



Fig. 2.2. LNG tank, capacity 60.1 m^3 with fragment with a cut piece of the wall

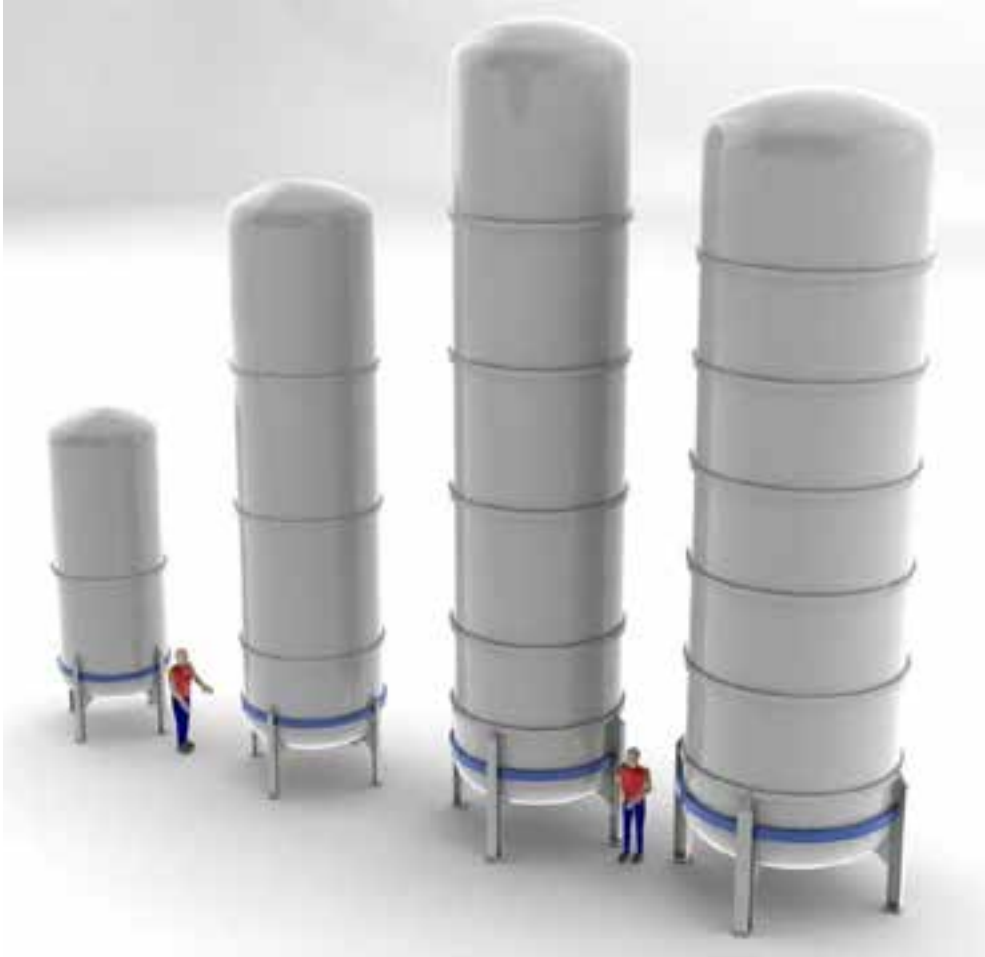


Fig. 2.3. Series of tank types, capacities (from left to right):
8.8, 27.5, 43.8 and 60.1m³

2.1. ANALYSIS OF INSULATION MATERIALS OF CRYOGENIC TANK WALLS

On the base of the own research results [6, 7, 9, 10] as well as the availability of thermal insulating materials and the bibliography [1, 2, 3, 5] it has been assumed, that an effective system of cryogenic tank wall insulation will be a combination of an insulation vacuum system and an insulation material. The outer surface of the cryogenic tank will be covered with the insulation material. The following insulation materials were considered: Cryo-lite, Cryotherm as well as the combination of Cryo-lite and Cryotherm.

Cryo-lite can be used in the temperature range from minus 268 degrees Celsius to plus 232 degrees Celsius. It has a form of a 25.4 mm thick mat. The specific weight is $Q_s = 157 \text{ N/m}^3$.

Cryotherm is formed from an inorganic fiberglass. It provides a very good thermal insulation. Furthermore, Cryotherm 233 type also has high strength properties. It can be used in the temperature down to minus 268 degrees Celsius. The specific weight is $Q_s = 1900 \text{ N/m}^3$ and thermal conductivity coefficient $\lambda = 0.037 \text{ W/(m K)}$.

2.2. SIMPLYFING ASSUMPTIONS AND PLAN OF THE RESEARCH

The following simplifying assumptions were made before carrying out the research [3, 4, 5, 8,]:

- The model is in thermal equilibrium state.
- For the purpose of comparison it was assumed that the inner surface of the inner tank has a constant temperature equal to the temperature of liquid gas.

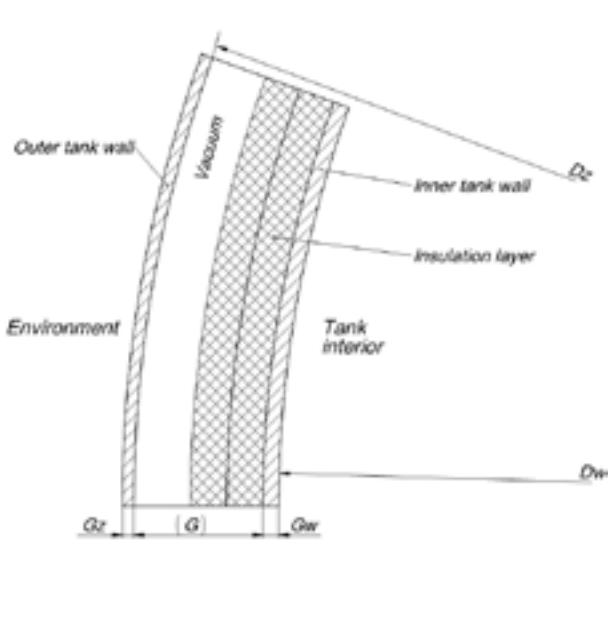
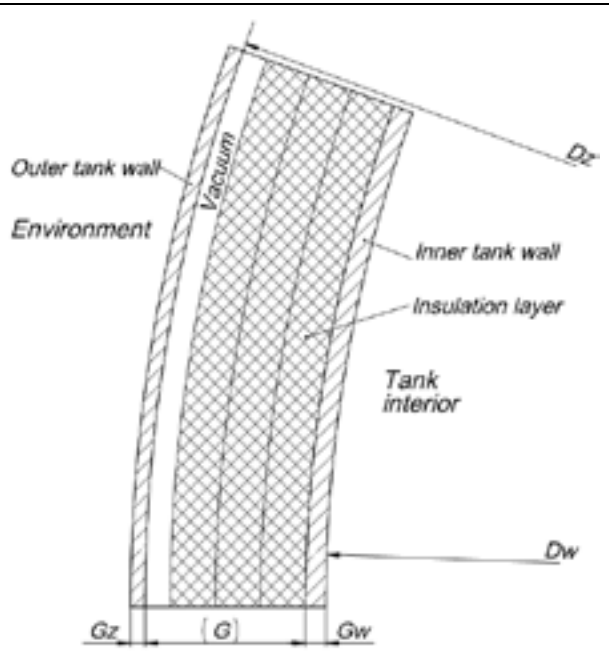
- Layers of Cryo-lite and Cryotherm allow the thermal radiation to go through. The radiation is lowered by the sheets of foil covering the insulation mats.
- For the MLI insulation type, the radiation between layers of insulating material, which is included in the apparent conductivity coefficient of the Cryotherm material, have been omitted.
- Heat transfer through foils which cover the mats have been omitted due to very small thickness of the foil.
- In the vacuum layer, the heat exchange takes place through radiation and conduction by the residual gas.
- At the low level vacuum or without the vacuum, heat exchange takes place by radiation and conduction of the gas layer.
- Heat transfer by the radiation inside the fibrous insulation is omitted due to the significant weakening of this process by insulation material.
- The outer surface of the tank exchange heat with the environment by convection at a specified ratio of penetration.
- For the FEM calculations it was assumed a multi-layer solid model.

Simulations were carried out using a rectangular section of the tank with a height of 250 mm and an aperture angle 20° (arc length is about. 316 mm). The use of wall with dimensions far beyond the distance between the walls allowed to reduce the impact of phenomena taking place at the edges of the considered model. Other dimensions of geometric model without considering the insulating material are as follows:

- distance between the walls: 89 mm,
- thickness of the outer wall: 8 mm,
- thickness of the inner wall: 11 mm.

Table 2.1. Considered versions of insulation

Ver.	Characteristics	Schematic drawing
1	Without insulation material <ul style="list-style-type: none"> • Medium level vacuum between walls 	
2	Insulation CL25 <ul style="list-style-type: none"> • One layer of Cryo-lite • Insulation material placed on the outer wall of inner tank • Thickness of the layer: 25 mm • Medium level vacuum 	

<p>3</p> <p>Insulation CL50</p> <ul style="list-style-type: none"> • Two layers of Cryo-lite • Insulation material placed on the outer wall of inner tank • Thickness of the layer: 2 x 25 mm = 50 mm • Medium level vacuum 	 <p>The diagram shows a cross-section of a tank wall assembly. From left to right, it consists of: an outer tank wall, a vacuum space, an inner tank wall, and an insulation layer. The insulation layer is shown as two parallel lines, representing two layers of material. Labels include: 'Environment' on the far left, 'Outer tank wall' pointing to the leftmost wall, 'Vacuum' in the space between the walls, 'Inner tank wall' pointing to the rightmost wall, 'Insulation layer' pointing to the two parallel lines, and 'Tank interior' on the far right. At the bottom, there are labels 'Gz' on the left, 'G' in a box in the center, and 'Gw' on the right. On the right side, there are labels 'Dz' at the top and 'Dw' at the bottom.</p>
<p>4</p> <p>Insulation CL75</p> <ul style="list-style-type: none"> • Three layers of Cryo-lite • Insulation material placed on the outer wall of inner tank • Thickness of the layer: 3 x 25 mm = 75 mm • Medium level vacuum 	 <p>The diagram shows a cross-section of a tank wall assembly, similar to the one above but with three layers of insulation. From left to right, it consists of: an outer tank wall, a vacuum space, an inner tank wall, and an insulation layer. The insulation layer is shown as three parallel lines, representing three layers of material. Labels include: 'Environment' on the far left, 'Outer tank wall' pointing to the leftmost wall, 'Vacuum' in the space between the walls, 'Inner tank wall' pointing to the rightmost wall, 'Insulation layer' pointing to the three parallel lines, and 'Tank interior' on the far right. At the bottom, there are labels 'Gz' on the left, 'G' in a box in the center, and 'Gw' on the right. On the right side, there are labels 'Dz' at the top and 'Dw' at the bottom.</p>

<p>5</p>	<p>Insulation MLI24</p> <ul style="list-style-type: none"> • Insulation material: Multilayer (MLI) • Insulation material placed on the outer wall of inner tank • 24 layers of MLI • Medium level vacuum 	
<p>6</p>	<p>Insulation MLI36</p> <ul style="list-style-type: none"> • Insulation material: Multilayer (MLI) • Insulation material placed on the outer wall of inner tank • 36 layers of MLI • Medium level vacuum 	

<p>7</p>	<p>Insulation MLI24+CL25</p> <ul style="list-style-type: none"> • Insulation material: MLI + Cryo-lite • Insulation material placed on the outer wall of inner tank • 24 layers of MLI • One layer of Cryo-lite 25 mm • Medium level vacuum 	<p>The diagram shows a cross-section of a tank wall. From left to right, it consists of: an outer tank wall, an environment, a vacuum space, an inner tank wall, an insulation layer, and the tank interior. The insulation layer is composed of 24 layers of MLI and one layer of Cryo-lite (CL) 25mm thick. The total thickness of the insulation is labeled as (G). The inner tank wall thickness is labeled as Dw. The outer tank wall thickness is labeled as Gz. The vacuum space is labeled as Vacuum.</p>
<p>8</p>	<p>Insulation MLI36+CL25</p> <ul style="list-style-type: none"> • Insulation material: MLI + Cryo-lite • Insulation material placed on the outer wall of inner tank • 36 layers of MLI • One layer of Cryo-lite 25 mm • Medium level vacuum 	<p>The diagram shows a cross-section of a tank wall, similar to the one above but with 36 layers of MLI. The insulation layer is labeled as 36 x MLI. The total thickness of the insulation is labeled as (G). The inner tank wall thickness is labeled as Dw. The outer tank wall thickness is labeled as Gz. The vacuum space is labeled as Vacuum.</p>

9	<p>Insulation MLI36+CL50</p> <ul style="list-style-type: none"> • Insulation material: MLI + Cryo-lite • Insulation material placed on the outer wall of inner tank • 36 layers of MLI • Cryo-lite 2 x 25 mm = 50 mm • Medium level vacuum 	<p>Outer tank wall Environment Vacuum Inner tank wall Insulation layer Tank interior</p> <p>G_z (G) G_w</p> <p>$2 \times 25\text{mm}$ $36 \times \text{MLI}$</p> <p>D_z D_w</p>
10	<p>Insulation CL25+MLI24</p> <ul style="list-style-type: none"> • Insulation material: Cryo-lite + MLI • Insulation material placed on the outer wall of inner tank • Cryo-lite 25 mm • 24 layers of MLI • Medium level vacuum 	<p>Outer tank wall Environment Vacuum Inner tank wall Insulation layer Tank interior</p> <p>G_z (G) G_w</p> <p>$24 \times \text{MLI}$ $\text{CL } 25\text{mm}$</p> <p>D_z D_w</p>

<p>11</p>	<p>Insulation CL25+MLI36</p> <ul style="list-style-type: none"> • Insulation material: Cryo-lite + MLI • Insulation material placed on the outer wall of inner tank • Cryo-lite 25 mm • 36 layers of MLI • Medium level vacuum 	<p>Outer tank wall Environment Vacuum Inner tank wall Insulation layer Tank interior Dz Dw 36 x MLI CL 25mm Gz (G) Gw</p>
<p>12</p>	<p>Insulation CL50+MLI24</p> <ul style="list-style-type: none"> • Insulation material: Cryo-lite + MLI • Insulation material placed on the outer wall of inner tank • Cryo-lite 2 x 25 mm =50 mm • 24 layers of MLI • Medium level vacuum 	<p>Outer tank wall Environment Vacuum Inner tank wall Insulation layer Tank interior Dz Dw 24 x MLI CL 2 x 25mm Gz (G) Gw</p>

<p>13</p>	<p>Insulation CL50+MLI36</p> <ul style="list-style-type: none"> • Insulation material: Cryo-lite + MLI • Insulation material placed on the outer wall of inner tank • Cryo-lite 2 x 25 mm =50 mm • 36 layers of MLI • Medium level vacuum 	<p>Outer tank wall Environment Vacuum Inner tank wall Insulation layer Tank interior Dz Dw 36 x MLI CL 2 x 25mm Gz (G) Gw</p>
<p>14</p>	<p>Insulation CL25+MLI24+CL25</p> <ul style="list-style-type: none"> • Insulation material: Cryo-lite + MLI + Cryo-lite • Insulation material placed on the outer wall of inner tank • Cryo-lite 25 mm • 24 layers of MLI • Cryo-lite 25 mm • Medium level vacuum 	<p>Outer tank wall Environment Vacuum Inner tank wall Insulation layer Tank interior Dz Dw CL 25mm 24 x MLI CL 25mm Gz (G) Gw</p>

15	<p>Insulation CL25+MLI36+CL25</p> <ul style="list-style-type: none"> • Insulation material: Cryo-lite + MLI + Cryo-lite • Insulation material placed on the outer wall of inner tank • Cryo-lite 25 mm • 36 layers of MLI • Cryo-lite 25 mm • Medium level vacuum 	
----	---	--

The simulations were carried out using 15 versions of insulation for every two pressures: 0.1Pa (medium level vacuum) and atmospheric pressure 0.1 MPa. Table 2.1 presents types and detailed dimensions of the insulation, for which the simulation tests were conducted.

2.3. THERMAL LOADS, BOUNDARY CONDITIONS AND MATERIAL PARAMETERS

Distribution of the thermal loads of the model is shown in fig. 2.4.

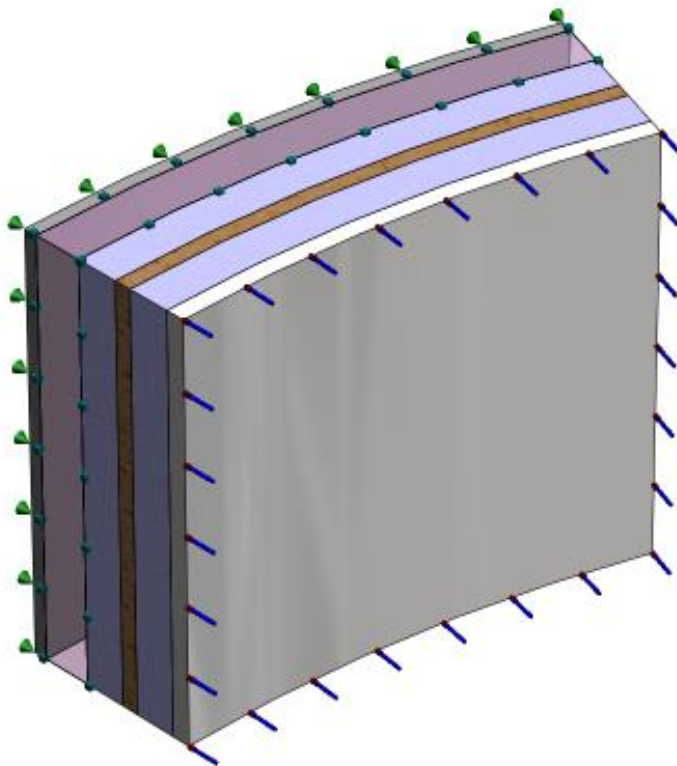


Fig. 2.4. Model of the tank section with symbols of thermal loads:
blue-red cylinders – temperature, green cones – convection,
green cubes – radiation

Simulation studies were conducted using SolidWorks Simulation Professional system. Thermal tests were carried out on a solid model, assuming steady state of the heat transfer process. The following loads and boundary conditions were used:

- constant temperature on the inside wall of the inner tank equal to 77.15 K (minus 196 °C),
- constant ambient temperature: 288.15 K (plus 15 °C),
- heat transfer by convection on the outer wall of the external tank with a convection coefficient equal to 10 W/(m²·K),
- emissivity of the external surfaces of insulation layers and the not insulated inner walls of the tank is equal to 0.1,
- thermal resistance between layers of insulation material and between the insulation and the tank wall equal to 1.0 (m²·K)/W.

Material properties important for the thermal examination in steady state were adopted under the literature, international standards or manufacturer's data. For the materials which can be used in a wide range of temperatures, the relevant material properties were assumed to be variable, depending on the temperature. Only for the P355NL1 steel, a constant thermal conductivity equal to 30 W/(m·K) was applied.

2.4. RESULTS OF SIMULATIONS

Thermal calculations were conducted for all versions of presented tank insulations. In each case maps of temperature distribution and the heat fluxes were obtained. Fig. 2.5 shows the temperature distribution of the version 1 insulation (medium level vacuum only, without any insulating material). In fig. 2.6 is presented distribution of the heat flux in a cross-section. As it arises from fig. 2.5, the temperature of the outer wall of the tank is close to zero degrees Celsius. This may cause ice accretion of the tank wall. Obtained value of the heat flow coefficient of the heat transfer into the cryogenic tank is about 20 W/m^2 .

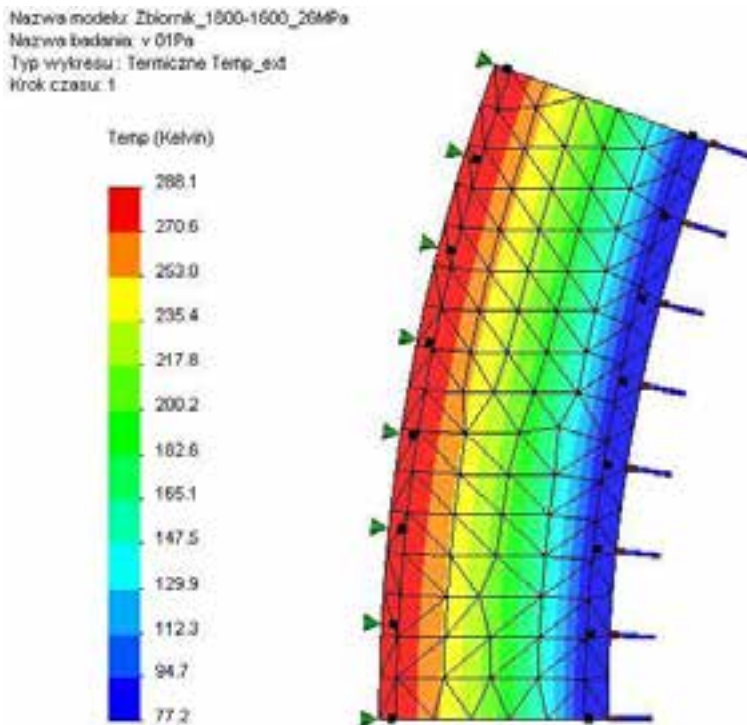


Fig. 2.5. Temperature distribution in the cross-section, version 1

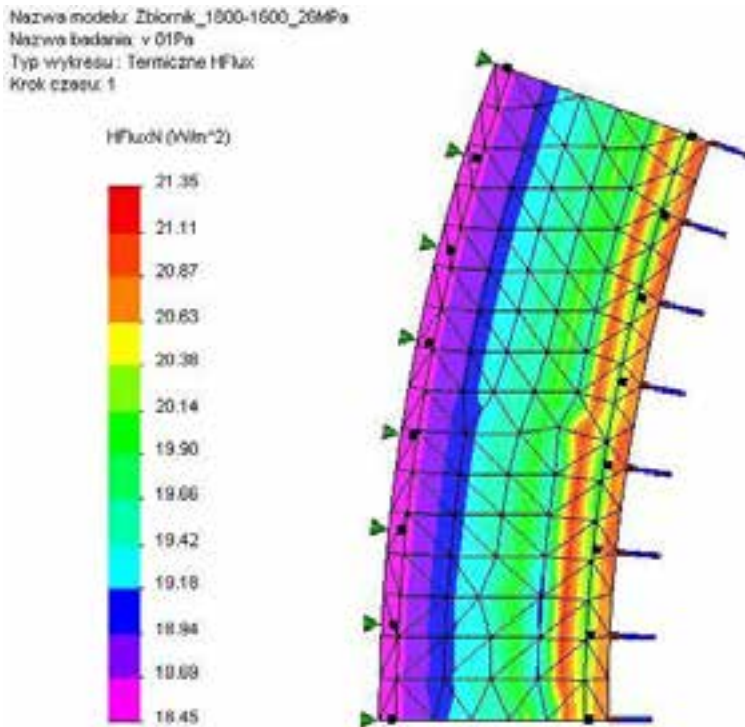


Fig. 2.6. Resultant heat flux distribution in the cross-section, version 1

In case of version 2 insulation (fig. 2.7 – 2.8), the temperature distribution in the space between walls is more advantageous. In this case, one 25mm layer of Cryo-lite placed on the outer wall of the inner tank, together with the medium level vacuum ($p = 0.1$ Pa) provides significant increase of the insulation efficiency. Temperature of the outer wall of the outer tank reached plus 14 degrees Celsius. Therefore, there is no danger to form the ice layer. Furthermore, the value of heat flux has been decreased by about 50 percent.

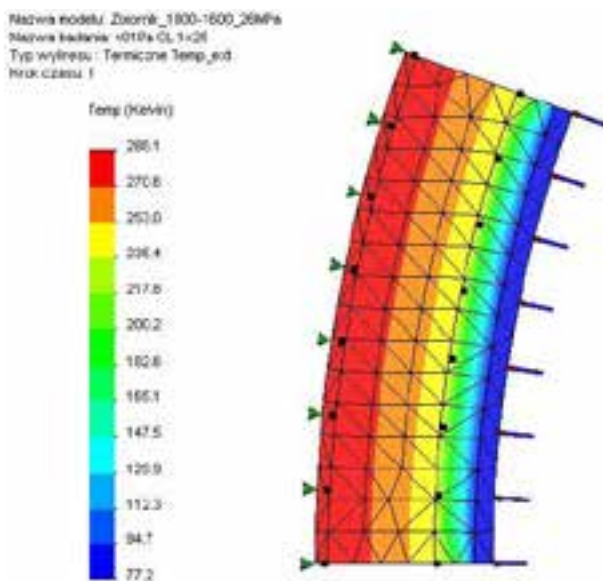


Fig. 2.7. Temperature distribution in the cross-section, version 2

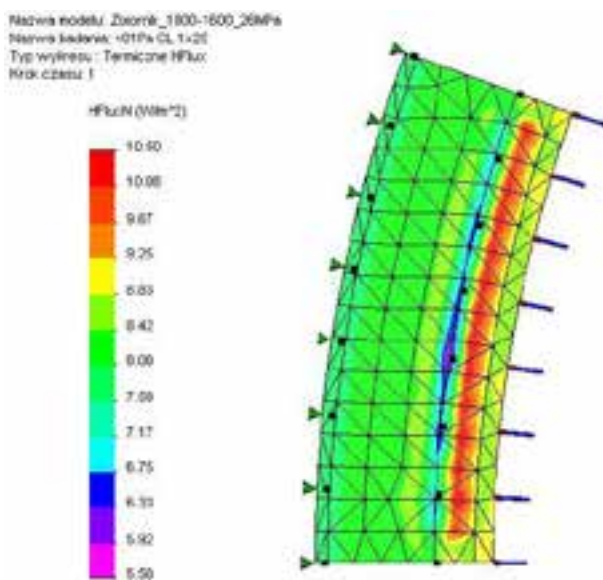


Fig. 2.8. Resultant heat flux distribution in the cross-section, version 2

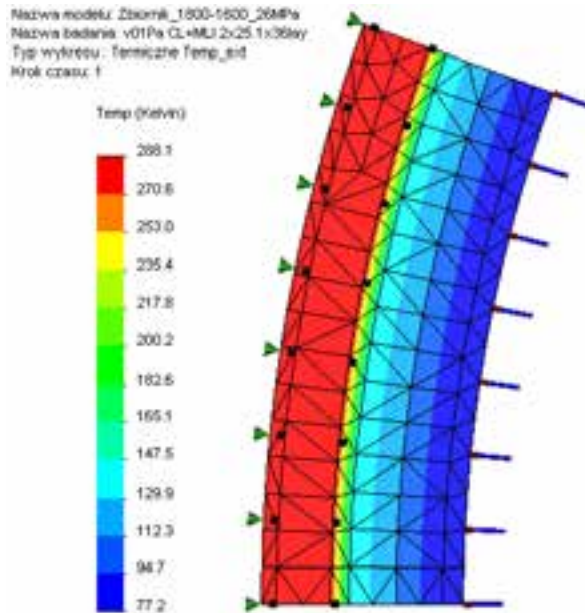


Fig. 2.9. Temperature distribution in the cross-section, version 13

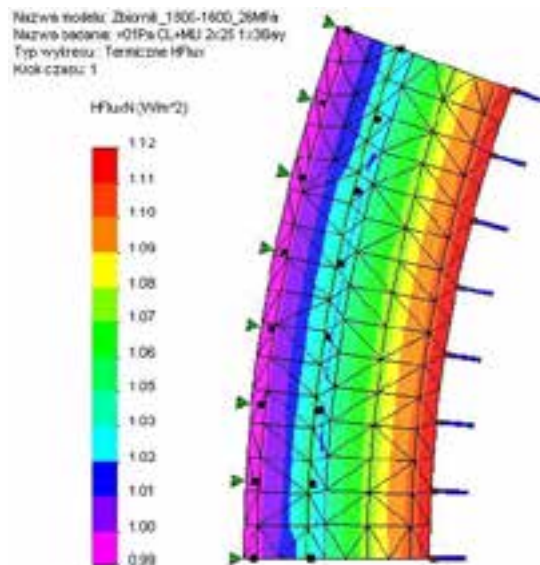


Fig. 2.10. Resultant heat flux distribution in the cross-section, version 13

The best result with a medium level vacuum was obtained for insulation version 13 (fig. 2.9– 2.10). This case involves a compound insulation, which consists of two 25 mm layers of Cryo-lite and 36 layers of Cryotherm.

Comparison of summarized heat flows and temperatures for various insulation versions are shown in fig. 2.11 – 2.13.

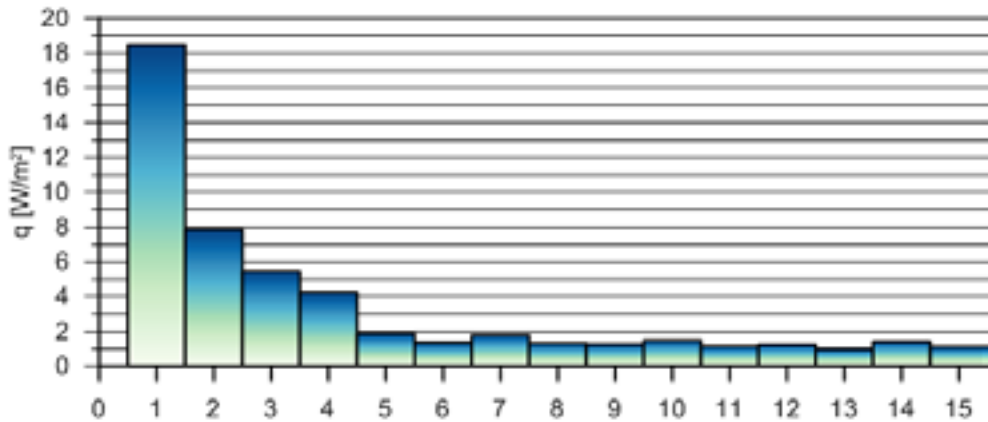


Fig. 2.11. Comparison of heat fluxes for various insulation versions at medium level vacuum ($p=0.1$ Pa)

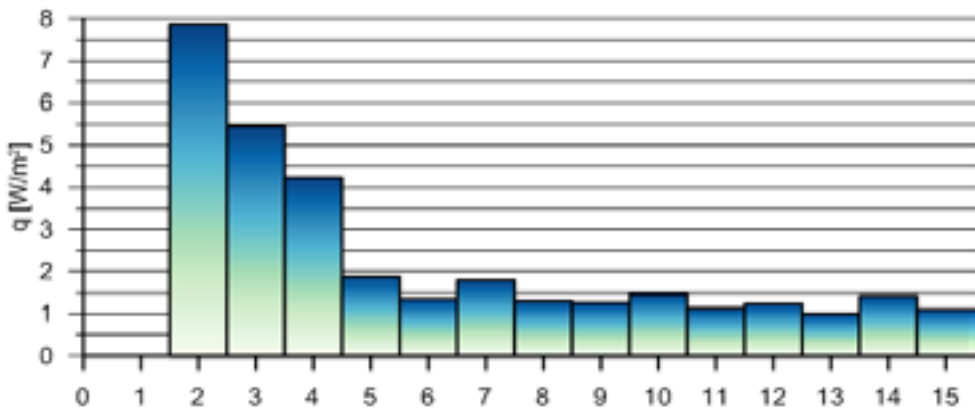


Fig. 2.12. Comparison of heat fluxes for various insulation versions at medium level vacuum ($p=0.1$ Pa) without version 1

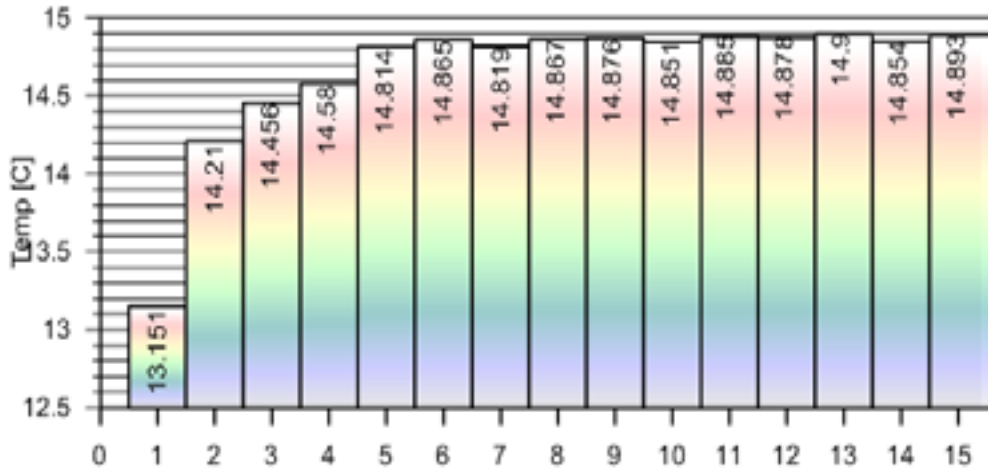


Fig. 2.13. Comparison of temperatures of the outer wall of the tank for various insulation versions at medium level vacuum ($p=0.1$ Pa)

The second set of simulations concerned the emergency situation, which consists in the loss of the vacuum. In these cases pressure between the inner and the outer tank was equal to 10^5 Pa.

The worst parameters of insulation efficiency, assuming a vacuum loss, were observed in versions 1 (no insulating material used) and 6 (36 layers of Cryotherm). The average heat flux was close to 37 W/m^2 and temperature of the outer wall of outer tank was decreased to 11.3 degrees Celsius. Temperature distributions and heat flux distributions in these cases are presented in fig. 2.14 – 2.17.

The best results, including the average heat flux of 27.6 W/m^2 and temperature of the outer wall of outer tank 12.2 degrees Celsius were obtained for insulation version 4 (three 25 mm layers of Cryo-lite) and 12 (two layers of Cryo-lite and 24 layers of Cryotherm).

Temperature distributions and heat flux distributions for insulations version 4 and 12 are presented in fig. 2.18 – 2.21.

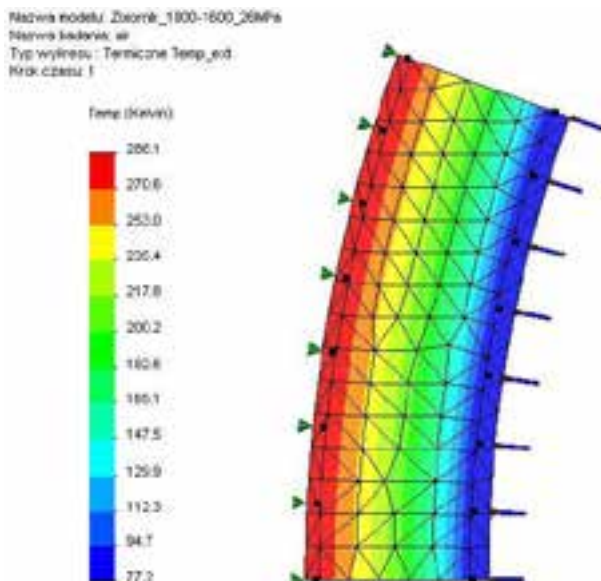


Fig. 2.14. Temperature distribution with a vacuum loss, version 1

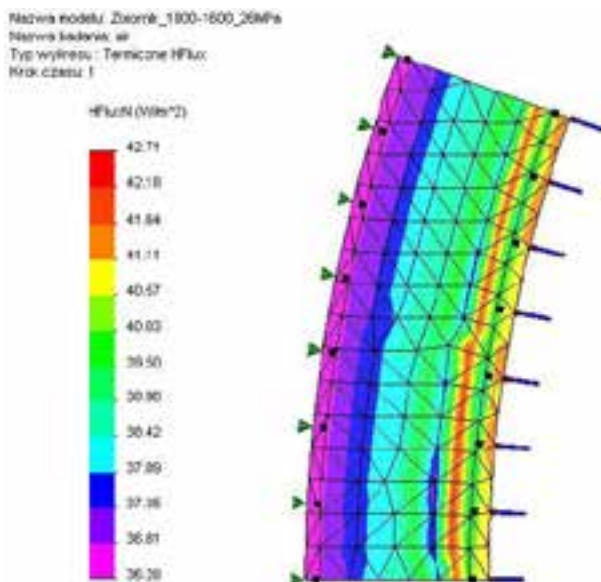


Fig. 2.15. Resultant heat flux distribution with a vacuum loss, version 1

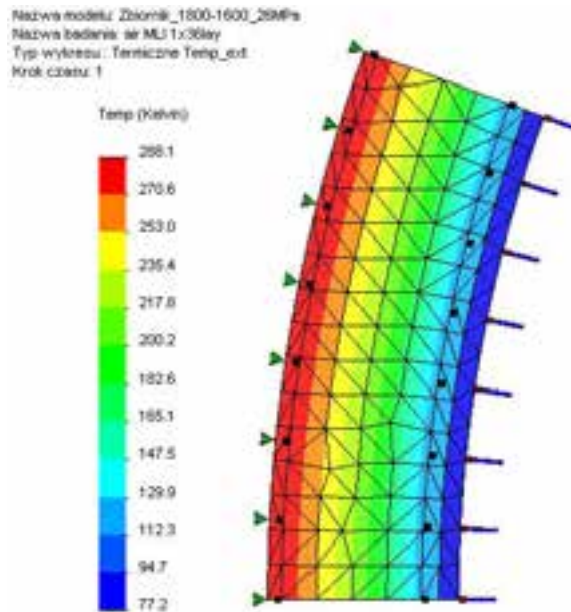


Fig. 2.16. Temperature distribution with a vacuum loss, version 6

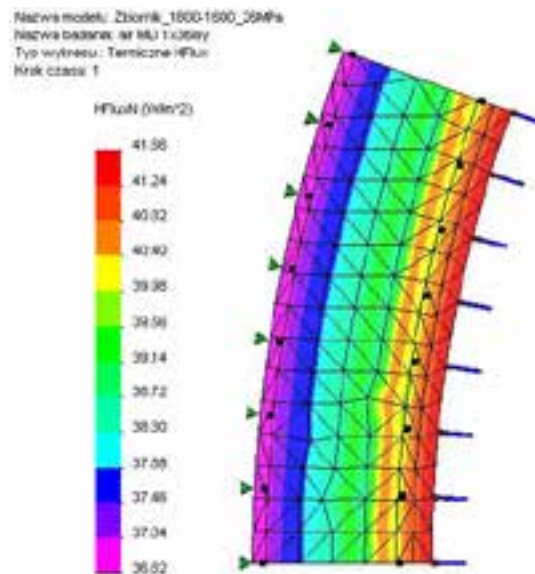


Fig. 2.17. Resultant heat flux distribution with a vacuum loss, version 6

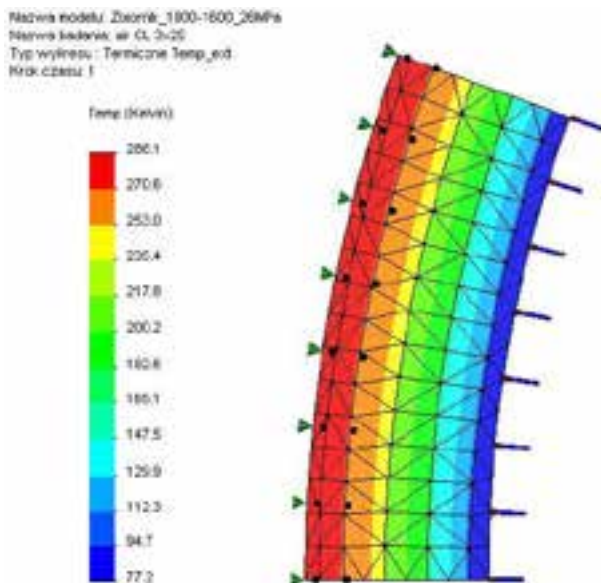


Fig. 2.18. Temperature distribution with a vacuum loss, version 4

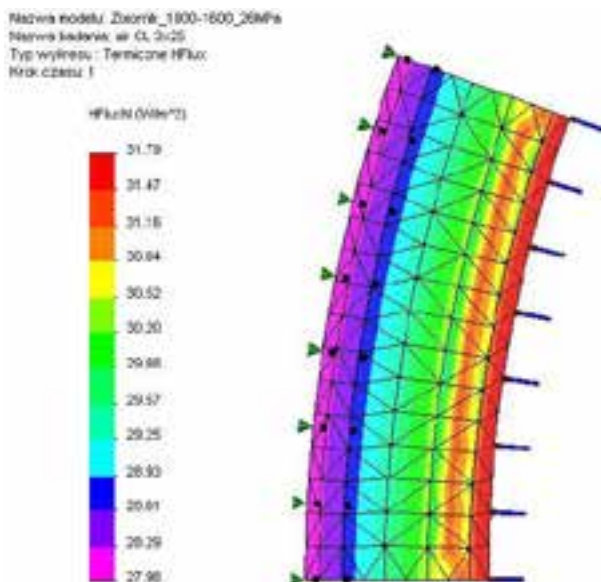


Fig. 2.19. Resultant heat flux distribution with a vacuum loss, version 4

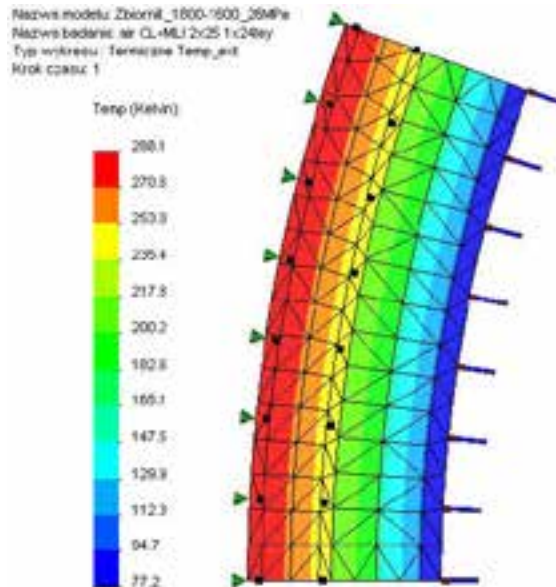


Fig. 2.20. Temperature distribution with a vacuum loss, version 12

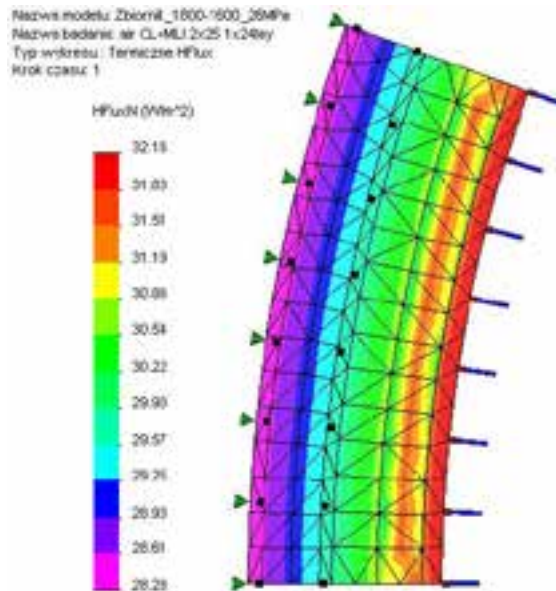


Fig. 2.21. Resultant heat flux distribution with a vacuum loss, version 12

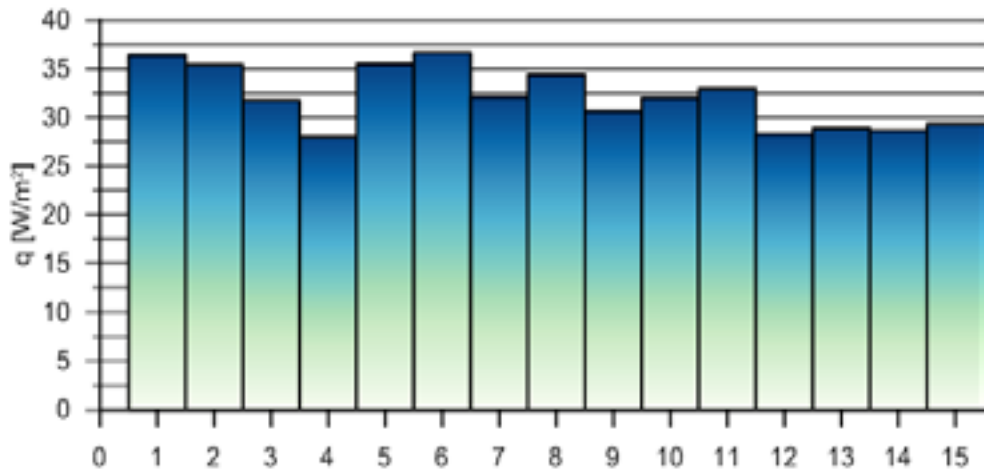


Fig. 2.22. Comparison of heat fluxes obtained for various types and configurations of insulation system without the vacuum ($p=10^5$ Pa)

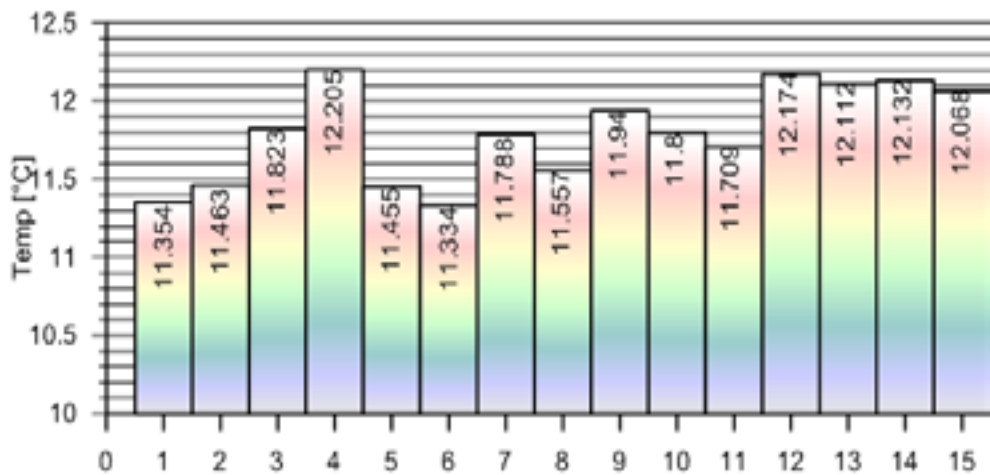


Fig. 2.23. Comparison of temperatures of the outer tank walls obtained for various types and configurations of insulation system without the vacuum ($p=10^5$ Pa)

2.5. SUMMARY

When choosing the insulation type and the insulation material, it should be taken into consideration, that in an emergency, vacuum insulated cryogenic tank can disappear. Therefore, the choice of insulating material must be made with two factors taken into account:

- The insulation should allow to obtain the lowest possible heat flux through the insulation material.
- The insulation should be characterized by the relatively low heat flux in case of the vacuum disappearance.

Results of simulations indicate, that the lowest heat flux in analyzed range of temperatures was obtained in the following cases:

- In medium level vacuum ($p = 0.1$ Pa) for the following versions of insulation: 6, 8, 9, 11 – 13 and 15. These are the MLI insulations (36 layers) or Cryo-lite + MLI (36 layers). All these insulations allow to obtain the heat flux lower than 1.4 W/m^2 .

In case of the vacuum disappearance, the divergence of results for various types of insulation is considerably less. Heat fluxes obtained in these cases are in range from 27.98 to 36.66 W/m^2 . The most advantageous values of the thermal conductivity coefficient have Cryo-lite + MLI insulations, versions 7, 9 – 15.

2.6. REFERENCES

- [1] Arkharov A., Marfenina I, Mikulin Ye.: *Cryogenic Systems*, Vol.1: *Basics of Theory and Design*, Moscow, 2000.
- [2] Bryson W. E.: *Cryogenics*, Hanser Gardner Publications, 1999.
- [3] Chorowski M.: *Kriogenika. Podstawy i zastosowania*, IPPU Masta, Gdańsk, 2007.

- [4] Czyżycki, W.; *Heat flow modelling on thermal insulation of cryogenics tanks using SolidWorks simulation package*, Technical Transactions vol. 4-M/2011A, Wydawnictwo PK 2011 (in polish).
- [5] Flynn T. M.: *Cryogenic Engineering*, 2nd edition, Dekker 2004.
- [6] Lisowski, E.; Czyżycki, W.; Łazarczyk, K.; *Simulation and experimental research of internal supports in mobile cryogenic tanks*, Technical Transactions, 8, 175-183, Wydawnictwo PK, 2010.
- [7] Lisowski, E.; Czyżycki, W.; *Transport and storage of LNG in container tanks*, Journal of KONES, 18, 3, 193-201, 2011.
- [8] Lisowski, E.; Czyżycki, W.; *Modelowanie elementów maszyn i urządzeń w systemie CAD 3D SolidWorks z aplikacjami CosmosWorks i FloWorks*, Wydawnictwo PK, 2008.
- [9] Lisowski, E.; Czyżycki, W.; Łazarczyk, K.; *Using of polyamide in construction of supporting blocks of cryogenic tanks on example of LNG container*, Archives of Foundry Engineering, 10, 3/2010, 81 - 86, 2010.
- [10] Lisowski, E.; Czyżycki, W.; *Transport ciekłego LNG w zbiornikach kontenerowych*, Zeszyty Naukowe Politechniki Świętokrzyskiej. Nauki Techniczne, 12, 2009.
- [11] Lisowski E., Filo G., Czyżycki W.: *Computer Aided Design in Mechanical Engineering*, ch. 4: Transport of Liquid Natural Gas by mobile tank container, Bergen University College 2009.

3. SIMULATION RESEARCH OF THE THERMAL INSULATION SUPPORTS OF CRYOGENIC TANK

Thermal insulation for cryogenic tank walls, proposed in the previous chapter, cannot carry mechanical loads resulting from the weight of the tank. Supporting the inner tank with supports made completely of steel implies too large heat losses. To keep heat losses low, supports should be highly lengthen and their cross-sections should be reduced. These changes would result in significant problems related to the strength and loss of structural stability. Therefore, a compromise is needed that would allow the transfer of substantial load and by the other hand, would not create thermal bridges. Previous work of authors related to the construction of horizontal cryogenic tanks. Plastic supports were applied in these constructions. They allowed to obtain satisfactory results [3, 5, 6, 8 – 11]. The support of the vertical tank has slightly different construction. Therefore, in this case it was decided to apply a mixed solution: steel structure of support with the plastic insert characterized by low thermal conductivity.

3.1. ARRANGEMENT OF INTERNAL SUPPORTS REGARD TO EXTERNAL SUPPORTS

In order to minimize heat transfer between the tanks, it is necessary to deploy internal supports in consideration of external supports respectively. The carried out calculations show, that it is preferable to maintain a maximum distance between internal supports and external supports. At a small distance of supports, the heat flow is raised due to increase of the surface of convection. The increase occurs due to inclusion of surface of the outer support in heat exchange. In this case the outer surface operates as a radiator [1, 2, 3, 4].

First, the simplified model of the tank was built. Then, calculations of the heat flux depending on the number of internal supports and their positions in relation to the external supports were carried out. Diagram of the geometrical model is shown in fig. 3.1, while the results are presented in fig. 3.2 and table 3.1.

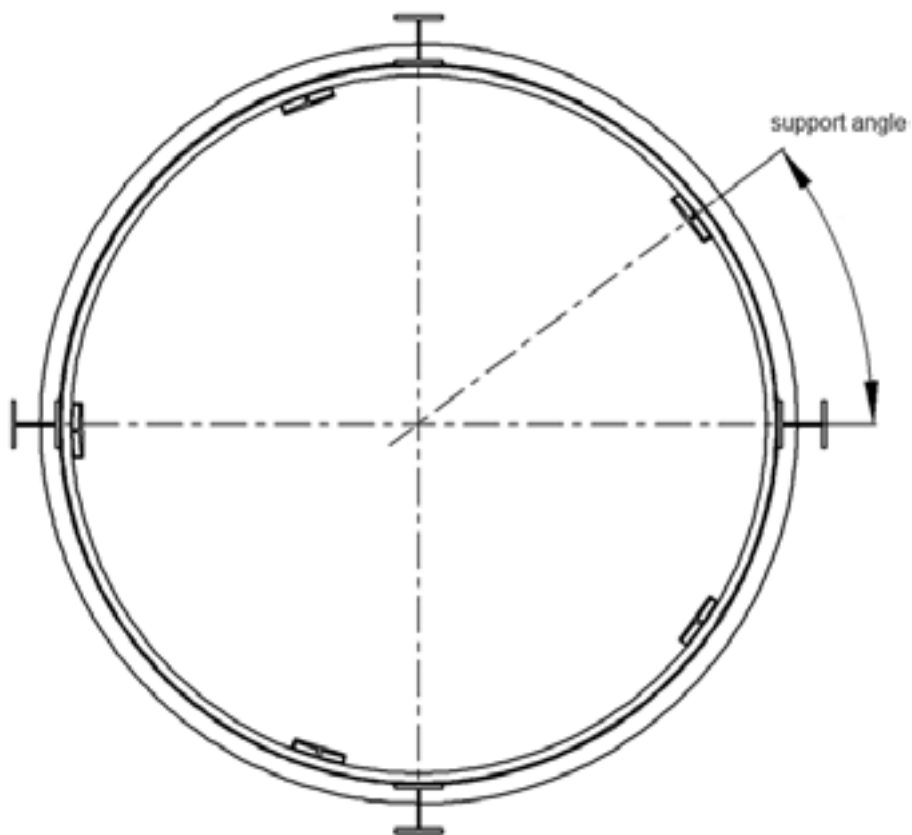


Fig. 3.1. Diagram of geometrical model for investigating the impact of internal supports positions relative to external supports on the average heat flux on the outer surface of the tank model

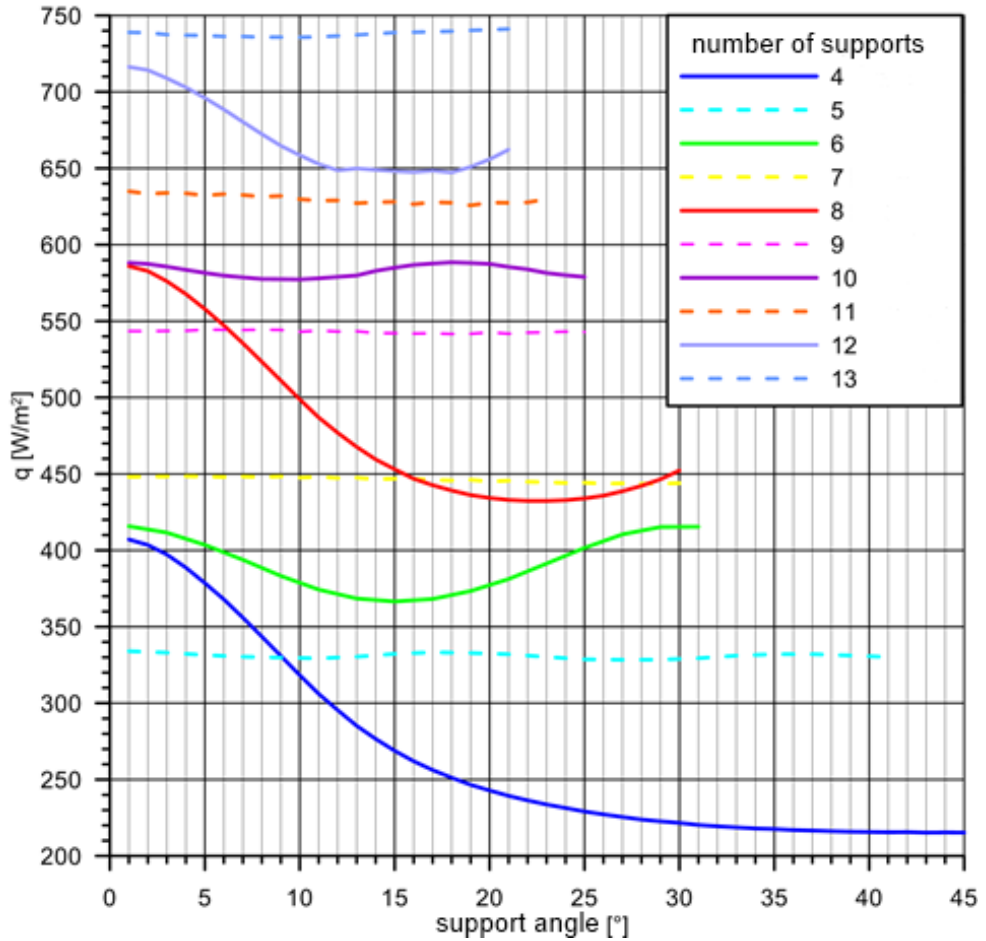


Fig. 3.2. The impact of the number of internal supports and their positions relative to internal supports on the average heat flux at the outer surface of the tank model

Tab. 3.1 Recommended angle between first internal support and plane of symmetry of external support

Number of internal supports	4	5	6	7	8
Recommended angle between first internal support and plane of symmetry of external support [°]	45	11	15	25,7	22,5
Number of internal supports	9	10	11	12	13
Recommended angle between first internal support and plane of symmetry of external support [°]	20	10	16,4	15	13,8

3.2. CONSTRUCTION AND MATERIALS OF INSULATION INSERTS FOR THE SUPPORTS

It was assumed, that the cryogenic tank supports located inside of the outer tank will be made of steel with thermo-insulating inserts. Thus, the steel elements were created using identical material as cryogenic tank, while the following materials for thermo-insulating inserts were tested: Polyamide – Tarnamid, PTFE – Tarflen, Polyacetal, Textolite, PVDE – Polyvinylidene Fluoride, PP – Polypropylene and PC – Polycarbonate. Schematic diagram of the cryogenic tank supports is shown in fig. 3.3.

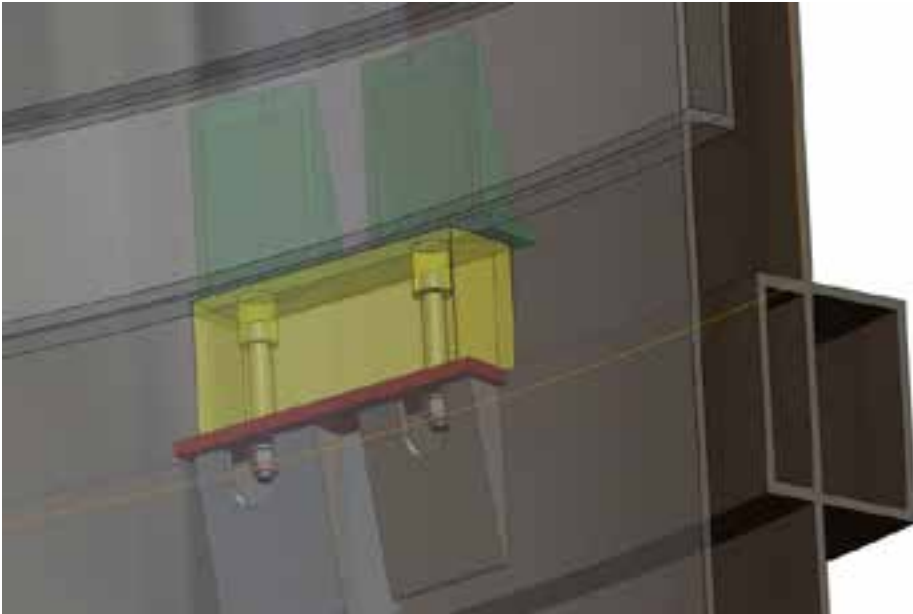


Fig. 3.3. Thermo-insulating insert of the support

Insulating insert is a block, which separates two steel elements of the support. Each insert was mounted using two standard stainless steel screws with cylindrical heads and hexagonal sockets.

Various design variants of inserts were selected for the simulation tests. The following figures show selected design options, that is:

- the basic version of solid insulating insert (fig. 3.4) – type 1,
- version with additional cutout (fig. 3.5) – type 2,
- version with additional cutout and lateral holes (fig. 3.6) – type 3.

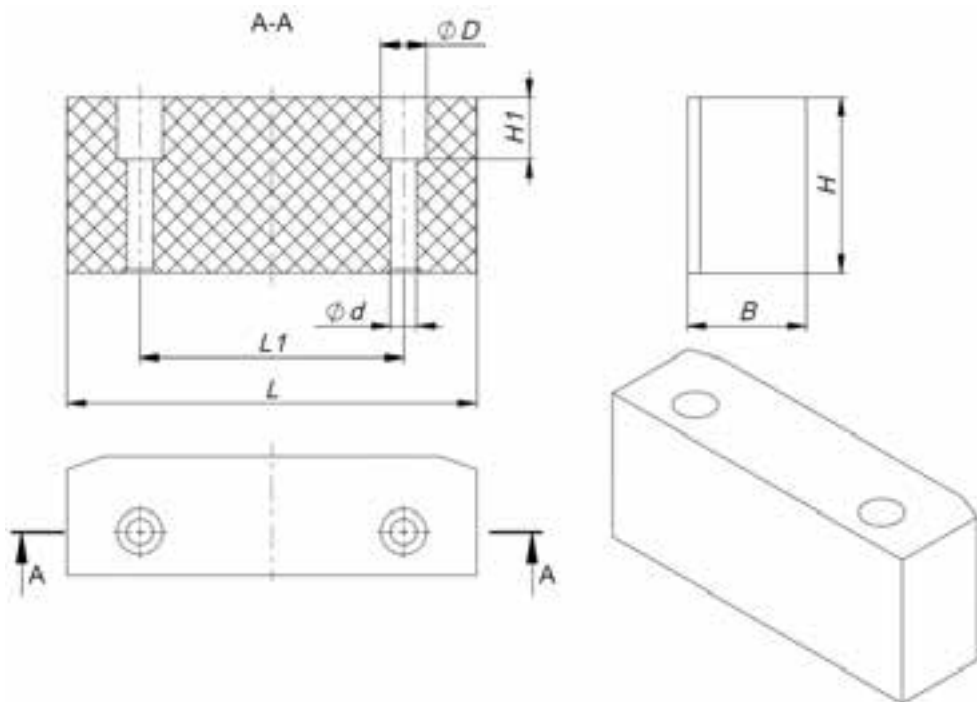


Fig. 3.4. Diagram of the default insert (type 1): H – height, L – length, B – width, $L1$ – spacing of mounting holes, D, d – diameters of screw sockets

Each type of insulation insert was applied in the model of the cryogenic tank for calculating the heat flux.

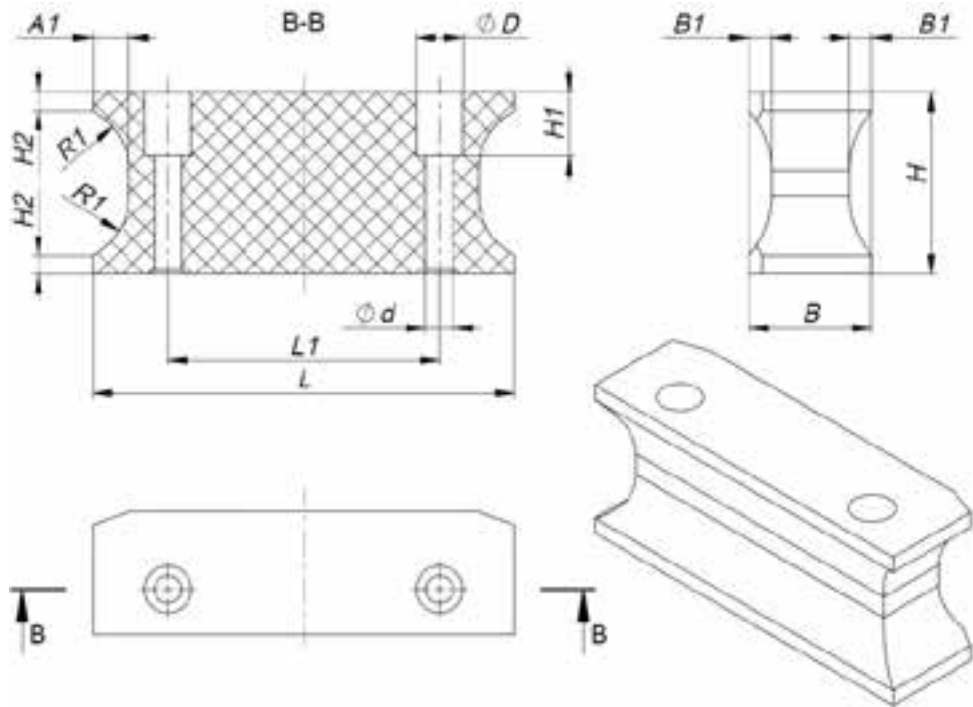


Fig. 3.5. Diagram of the undercut insert (type 2): H – height, L – length, B – width, $L1$ – spacing of mounting holes, D , d – diameters of screw sockets, $R1$ – undercut radius

3.3. ASSUMPTIONS FOR THE CALCULATIONS

Before the start of calculations, the following constructional and mechanical assumptions were made [1-4, 6, 11]:

- internal supports should carry loads resulting from the weight of the inner tank and mass of the stored LNG,
- masses of pipe and fittings were omitted,
- calculated value of acceleration in the vertical direction is equal to $2 \cdot g$,
- averaged surface pressures on the surface of support must not exceed 10 MPa,
- arrangement of supports is symmetrical (regular polygon),
- all variants of supports are screwed to the mountings of the external tank,
- inner tank deformations caused by changes of its temperature are taken into account in the design of support mounting,
- positioning of the tank is provided by additional alignment elements.

The main physical and material parameters assumed for calculations:

- | | |
|--|------------------------------|
| • internal temperature of the inner tank wall | 77 K |
| • initial temperature of the outer wall of outer tank | 288 K |
| • ambient temperature | 288 K |
| • convection type | natural; |
| • convection coefficient | $10.0 \frac{W}{m^2 \cdot K}$ |
| • material parameters of the inner tank wall
in function of the temperature | variable |
| • material parameters of external tank wall | constant |
| • material parameters of the support | constant |

- material of support polyamide PA6
- size of tank section: height 800mm, section angle: 30°.

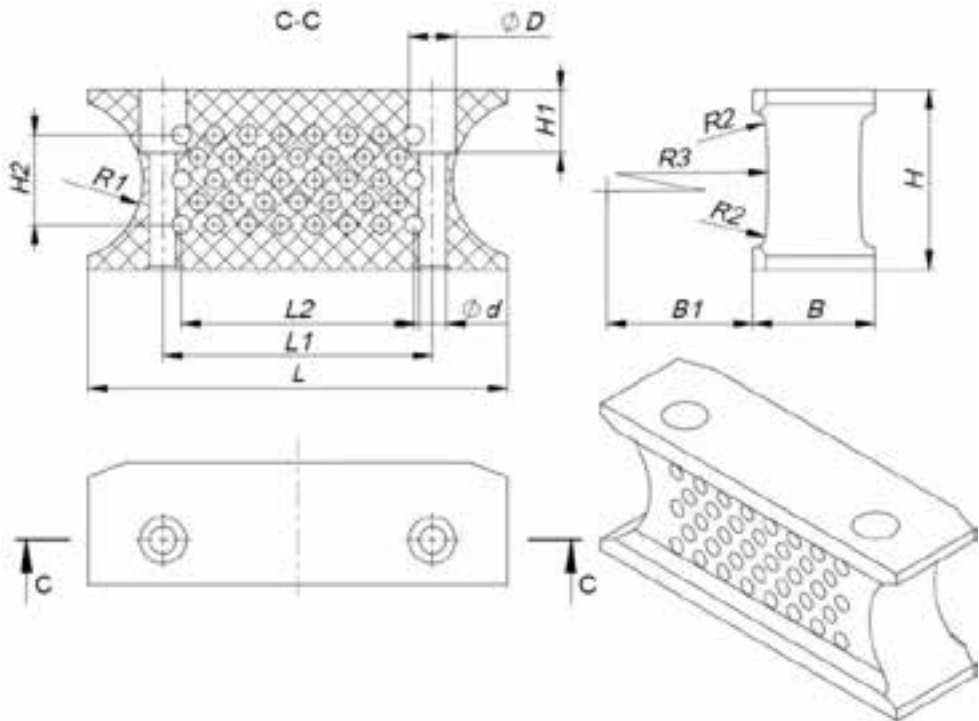


Fig. 3.6. Diagram of the i-undercuts insert (type 3): H – height, L – length, B – width, $L1$ – spacing of mounting holes, D , d – diameters of screw sockets, $R1$, $R2$, $R3$ – undercut radiuses, $L2$, $H2$ – dimensions of the openings area

3.4. SIMULATION RESEARCH OF INSULATING INSERTS OF SUPPORTS IN SOLIDWORKS

Models for calculations were created in the SolidWorks system [3, 7]. Then, in the Simulation module, models were discretized and boundary conditions were defined. Next, calculations were carried out and analysis of results was made.

In fig. 3.8 – 3.13 von Mises stress distributions for insert types 1, 2 and 3 are presented, while in fig. 3.14 – 3.25 are shown distributions of the heat flows and temperatures, respectively. Although the heat-insulating inserts were applied, values of the heat flows through supports were significantly higher than heat fluxes through the tank walls. Consequently, the temperature of the outer wall of outer tank within the area of the supports was considerably decreased.

Method of mounting insulating inserts between the inner tank and the outer tank is presented in fig. 3.7.

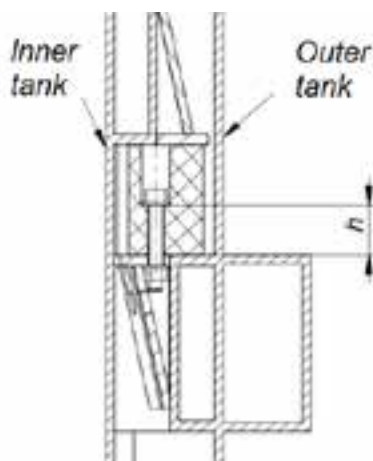


Fig. 3.7. Mounting of insulating insert between tanks,
 h – distance between the screw jack plane and the lower support plane

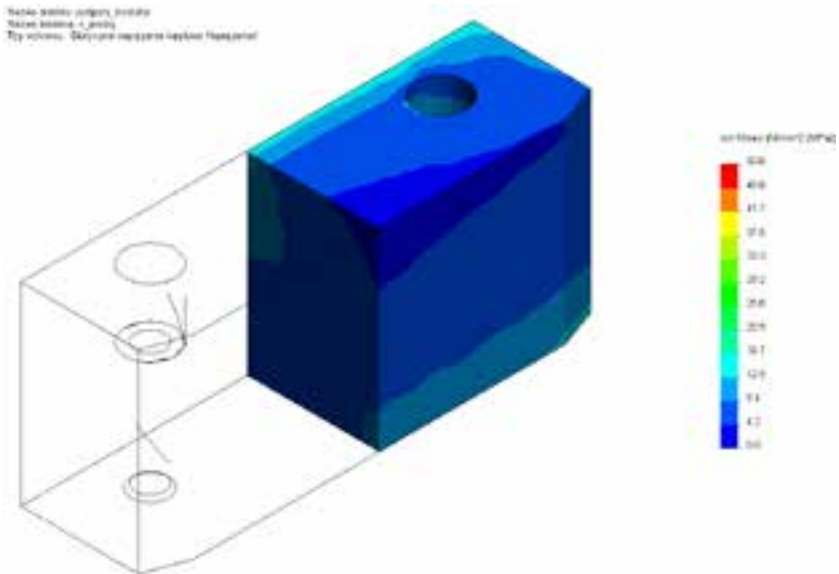


Fig. 3.8. Stress distribution, support type 1

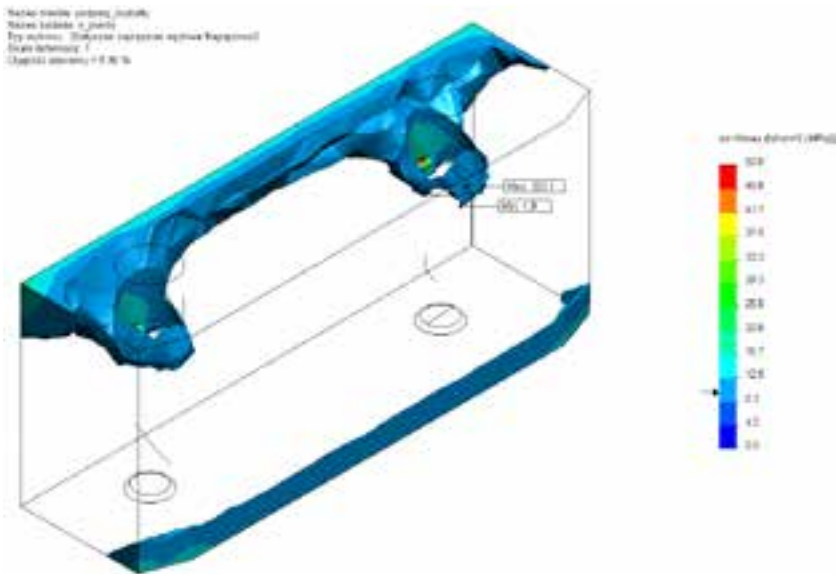


Fig. 3.9. Areas in which the stress is greater than 5 MPa, support type 1

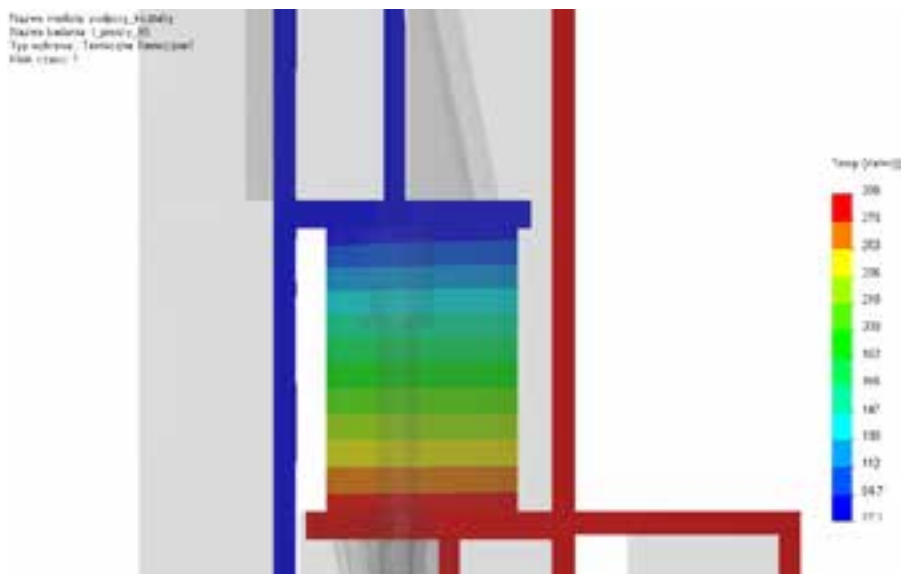


Fig. 3.14. Distribution of temperature in a section through the means of the support, support type 1

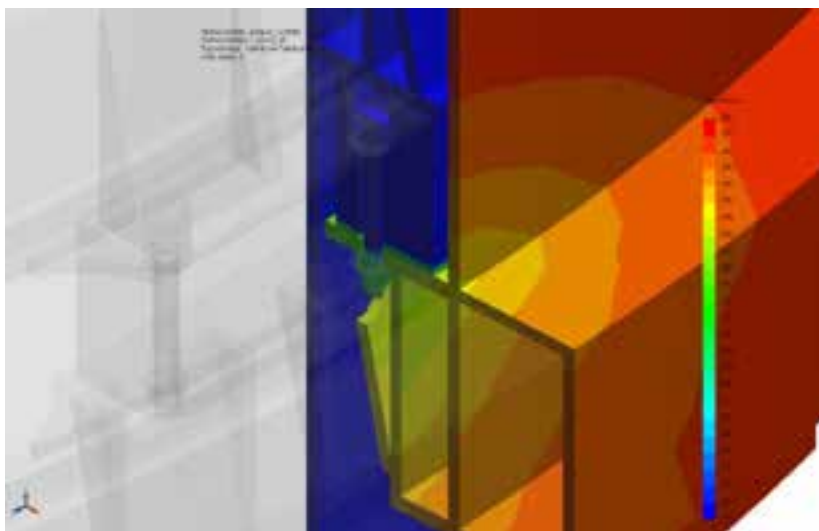


Fig. 3.15. Distribution of temperature in a section through the screw with the range narrowed to 273-288 K, support type 1

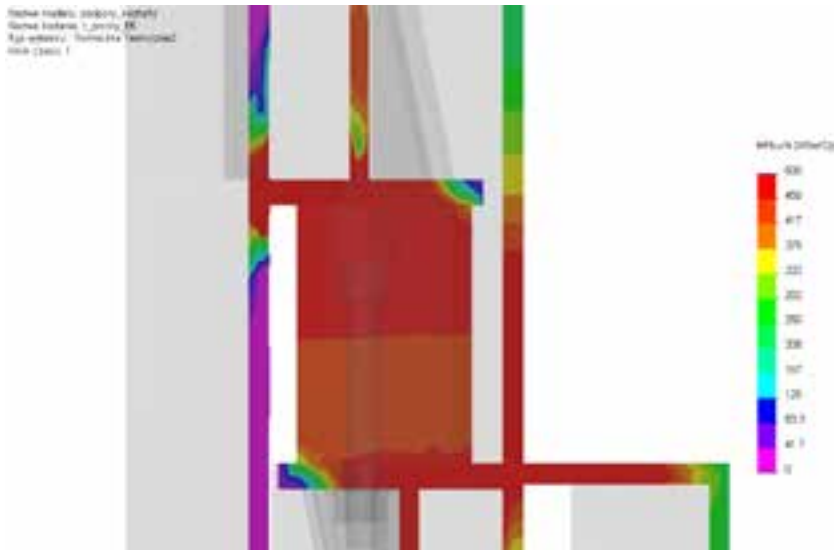


Fig. 3.16. Distribution of resultant heat flux in a section through the means of the support, support type 1

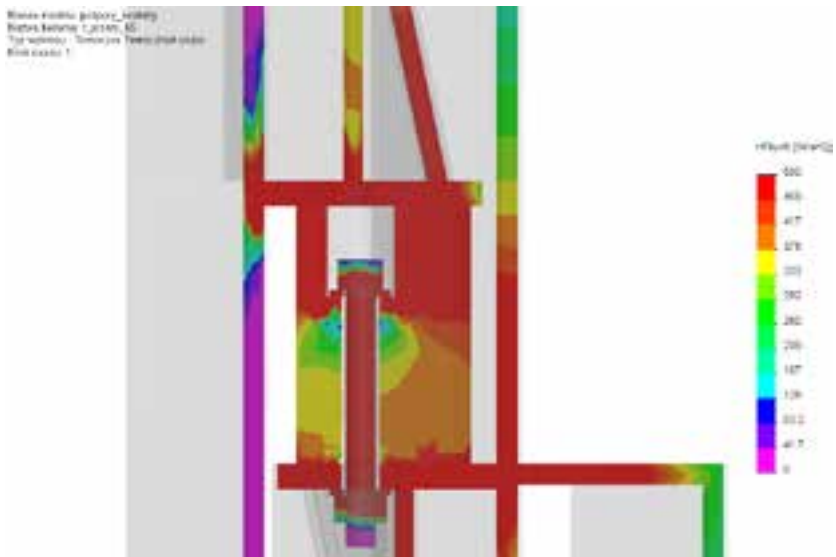


Fig. 3.17. Distribution of resultant heat flux in a section through the screw, support type 1

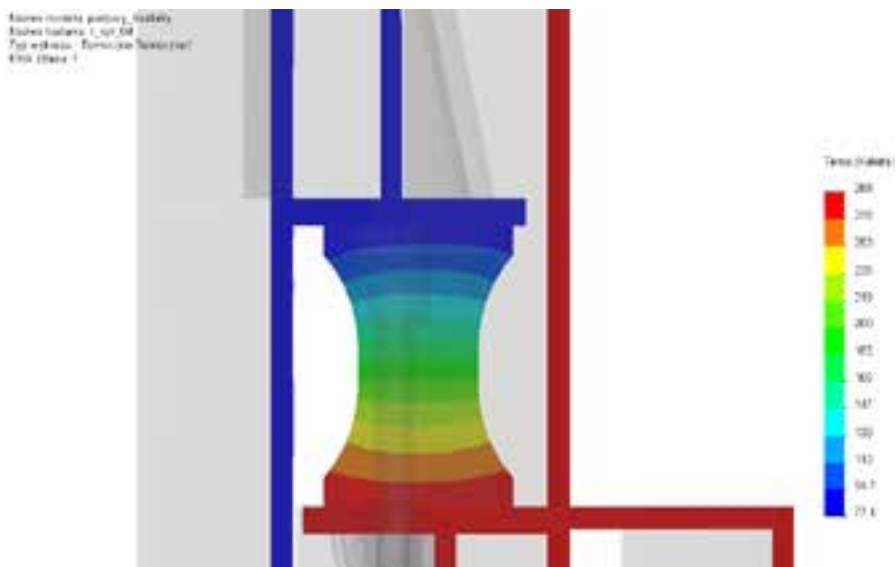


Fig. 3.18. Distribution of temperature in a section through the means of the support, support type 2

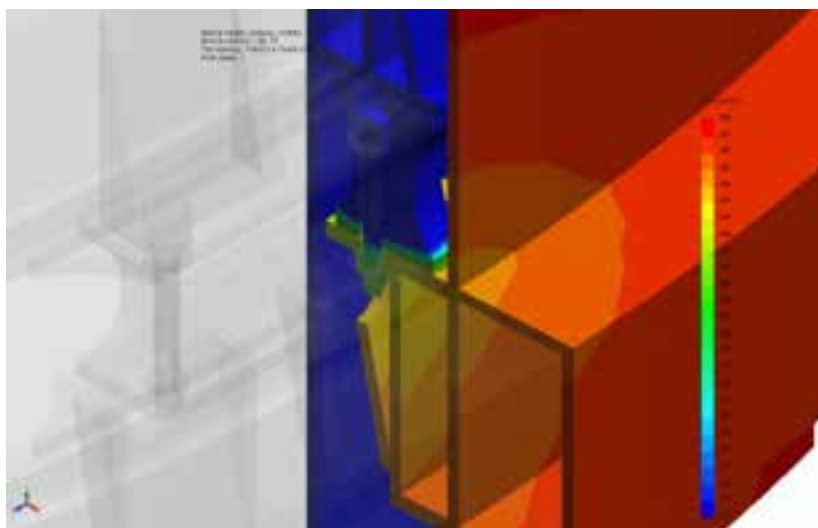


Fig. 3.19. Distribution of temperature in a section through the screw with the range narrowed to 273-288 K, support type 2

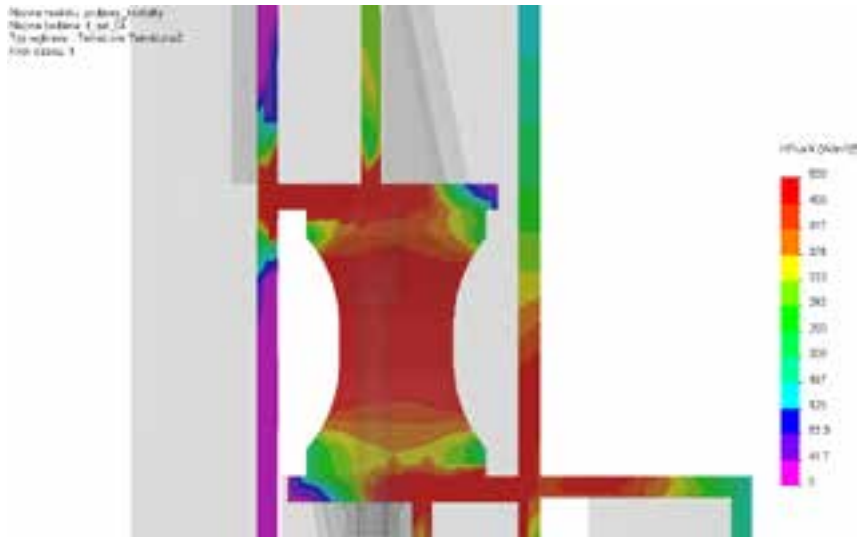


Fig. 3.20. Distribution of resultant heat flux in a section through the means of the support, support type 2

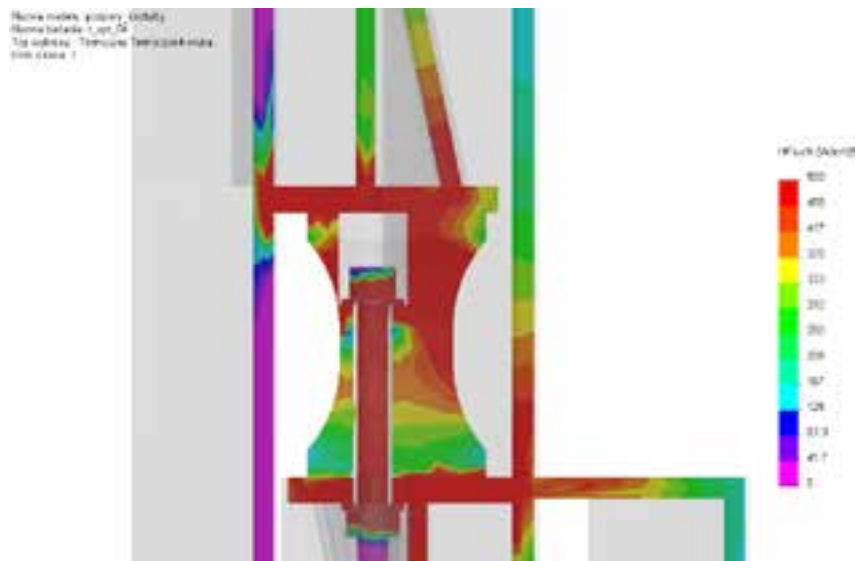


Fig. 3.21. Distribution of resultant heat flux in a section through the screw, support type 2

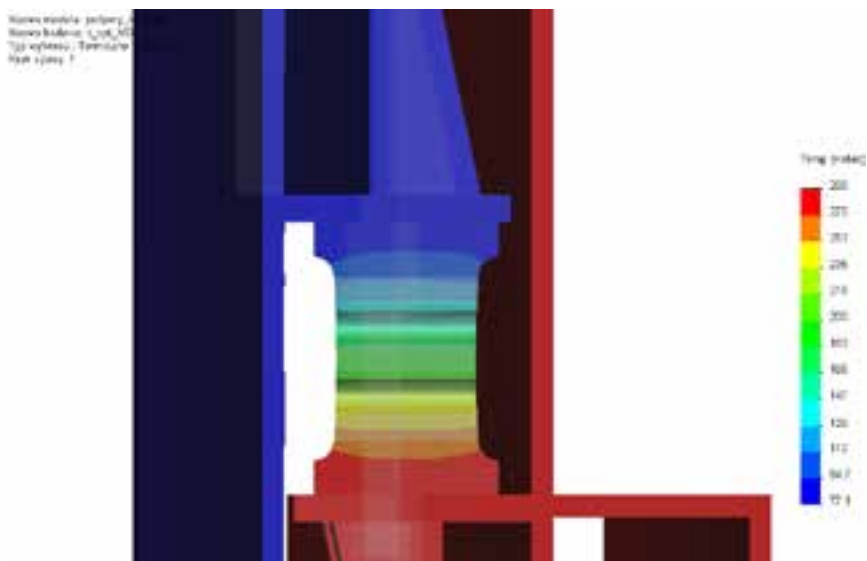


Fig. 3.22. Distribution of temperature in a section through the means of the support, support type 3

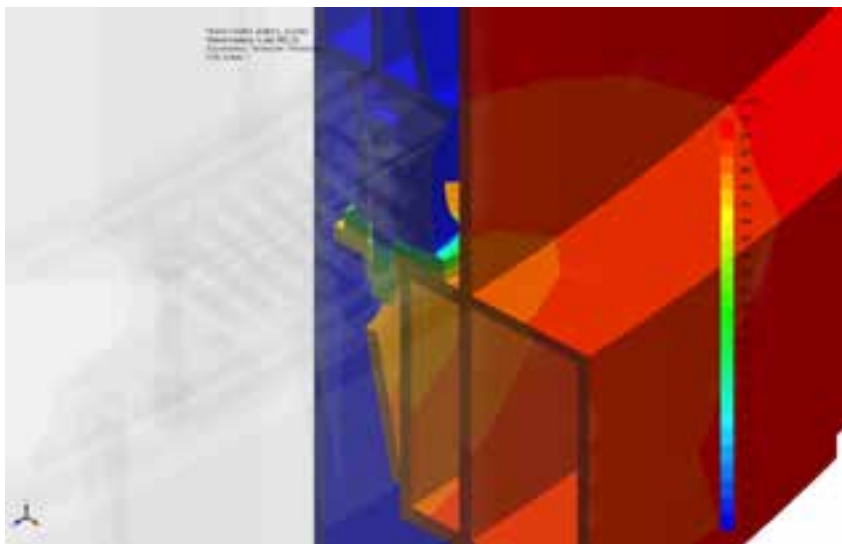


Fig. 3.23. Distribution of temperature in a section through the screw with the range narrowed to 273-288 K, support type 3

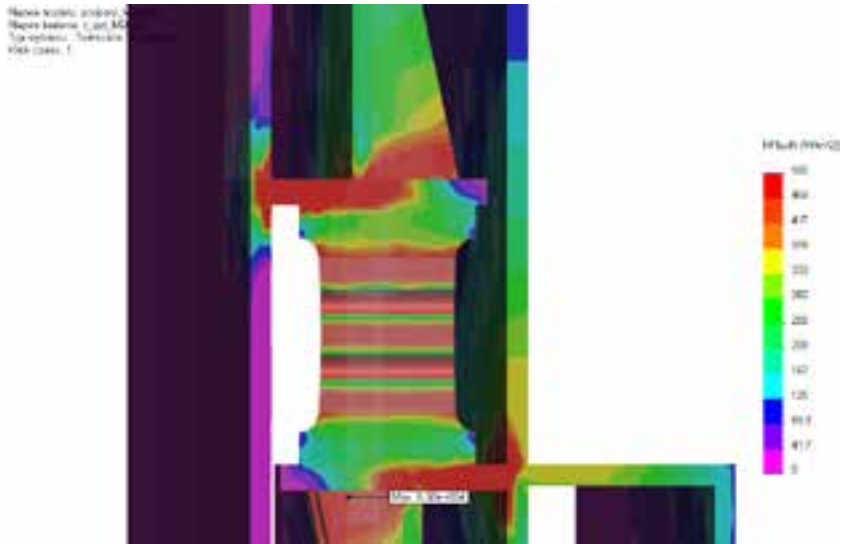


Fig. 3.24. Distribution of resultant heat flux in a section through the means of the support, support type 3

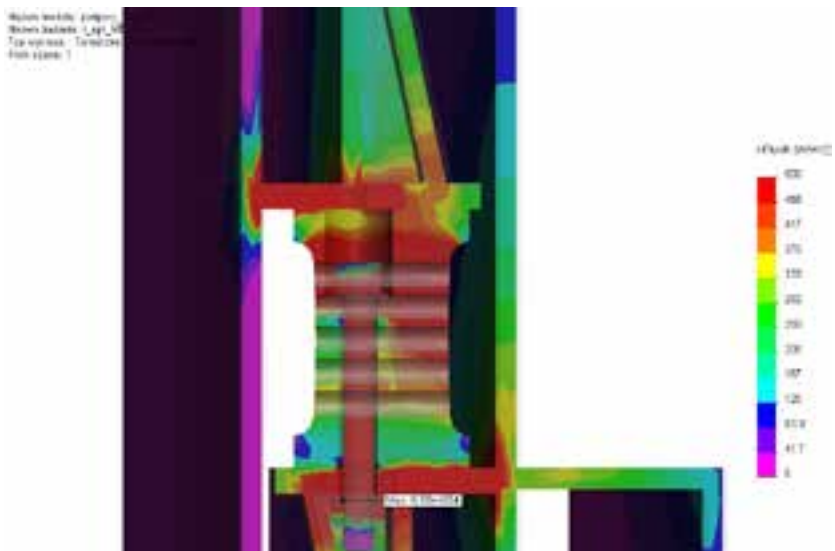


Fig. 3.25. Distribution of resultant heat flux in a section through the screw, support type 3

In fig. 3.26 is presented comparison obtained on simulation research of the heat flux through the wall of the outer tank using various constructions of supports. The most advantageous results were obtained for the type 3 insert, narrowed with transverse holes.

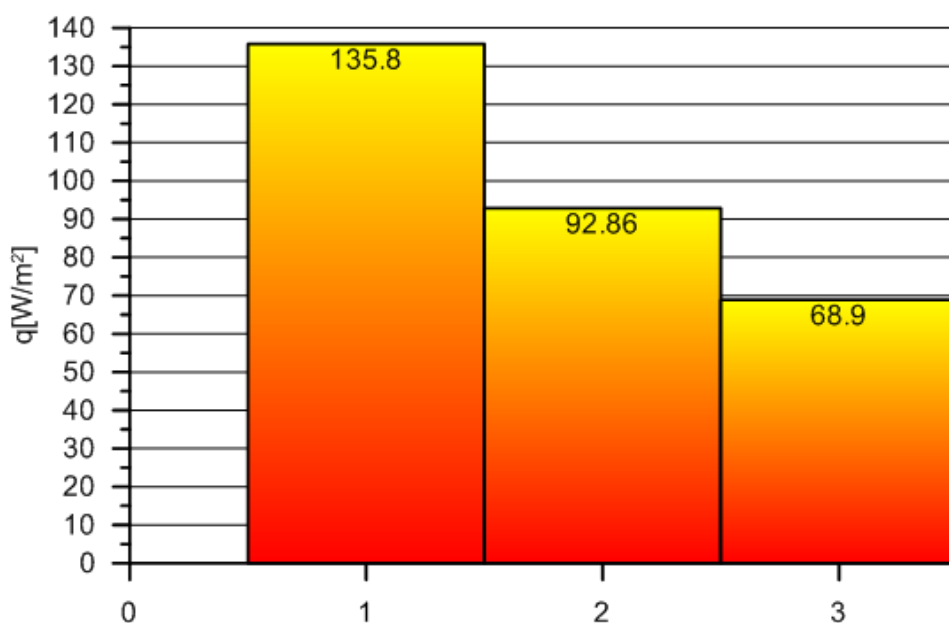


Fig. 3.26. Comparison of average heat fluxes on fragment of the outer wall of outer tank obtained with various types of inserts: 1 – standard insert (type 1), 2 – insert with cutout (type 2), 3 – insert with the i-undercuts (type 3)

3.5. CONCLUSIONS

In this chapter supports of the inner tank were proposed. Size of the supports were optimized according to the strength requirements as well as minimization of the heat flow. Several solutions were analyzed, in order to

reduce the heat flux passing through the support. On the basis of the results, the following conclusions can be formulated:

- best thermal results were obtained for the insert of type 3,
- inserts of polyamide PA 6 were used for the simulations. Possibilities of using other materials for construction of inserts were also analyzed. Due to the thermal and mechanical properties, it appears that application of Polyamide and Polyvinylidene Fluoride can be the superior solution,
- presented results obtained for the PA 6 will be similar in nature for other materials, including some differences in the value of thermal conductivity coefficient and contact effects,
- all analyzed material meets the strength requirements at normal ambient temperatures. The choice of material for the supports between the outer tank and the inner tank must be verified in further experiments,
- selection of construction material for supports should be based on results of strength calculations at low temperatures and thermal tests on the model of tank. Cost, availability and technology of assembling should be also considered while choosing type of the insulating material.

3.6. REFERENCES

- [1] Arkharov A., Marfenina I, Mikulin Ye.: *Cryogenic Systems*, Vol.1: *Basics of Theory and Design*, Moscow, 2000.
- [2] Bryson W. E.: *Cryogenics*, Hanser Gardner Publications, 1999;
- [3] Czyżycki, W.; *Heat flow modelling on thermal insulation of cryogenics tanks using SolidWorks simulation package*, Technical Transactions vol. 4-M/2011A, Wydawnictwo PK 2011 (in polish).

- [4] Flynn T. M.: *Cryogenic Engineering*, 2nd edition, Dekker 2004;
- [5] Lisowski, E.; Czyżycki, W.; Łazarczyk, K.; *Simulation and experimental research of internal supports in mobile cryogenic tanks*, Technical Transactions, 8, Wydawnictwo PK, 2010.
- [6] Lisowski, E.; Czyżycki, W.; *Transport and storage of LNG in container tanks*, Journal of KONES, 18, 3, 193-201, 2011.
- [7] Lisowski, E.; Czyżycki, W.; *Modelowanie elementów maszyn i urządzeń w systemie CAD 3D SolidWorks z aplikacjami CosmosWorks i FloWorks*, Wydawnictwo PK, 2008.
- [8] Lisowski, E.; Czyżycki, W.; Łazarczyk, K.; *Using of polyamide in construction of supporting blocks of cryogenic tanks on example of LNG container*, Archives of Foundry Engineering, vol.10, 2010.
- [9] Lisowski, E.; Czyżycki, W.; *Transport ciekłego LNG w zbiornikach kontenerowych*, Zeszyty Naukowe Politechniki Świętokrzyskiej. Nauki Techniczne, 12, 2009.
- [10] Lisowski, E.; Czyżycki, W.; Łazarczyk, K.; *Wdrożenie produkcji cystern kontenerowych do transportu i przechowywania gazów skroplonych*. Biuletyn Instytutu Spawalnictwa 2, 2012.
- [11] Lisowski E., Filo G., Czyżycki W.: *Computer Aided Design in Mechanical Engineering*, ch. 4: Transport of Liquid Natural Gas by mobile tank container, Bergen University College 2009.

4. EXPERIMENTAL RESEARCH

Experimental research contained investigations of thermal properties of plastics at cryogenic temperatures and strength tests of plastics at cryogenic temperatures.

4.1. RESEARCH OF THERMAL PROPERTIES OF PLASTICS AT CRYOGENIC TEMPERATURES

To perform comparative research of selected materials for heat flow through heat insulating insert, a special laboratory test stand was built. It was made as part of outer and inner tank shell, between of which was put a plastic insert. Created section with removal $\frac{1}{4}$ of material is presented in fig. 4.1. Along its height was mounted a temperature sensor, which electrical cables were led out toward side wall.

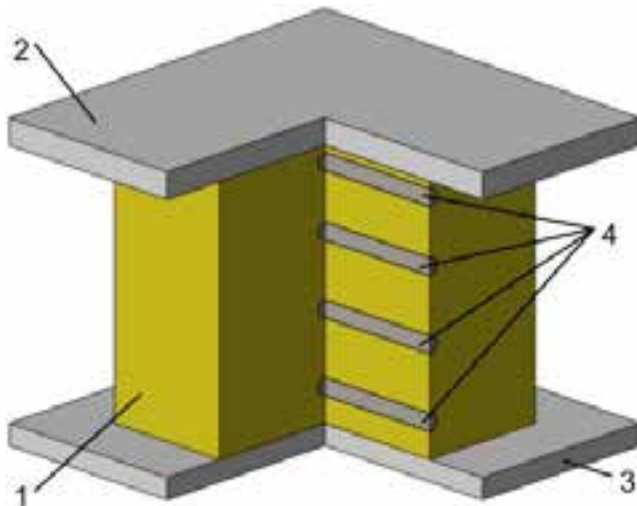


Fig. 4.1. Set for research: 1– heat insulating insert, 2– part of inner tank shell, 3– part of outer tank shell, 4– temperature sensors

For preliminary studies, there were prepared cuboidal samples of heat insulating inserts of edge length $l=100$ mm. The test stand allows to examine four heat insulating inserts at the same time.

a)



b)



Fig. 4.2. View of laboratory test stand: a) before insulating
b) with full insulation during the tests

Test results depend significantly of pressing force, because change of the temperature leads to change of length of testing element. In order to achieve required pressure, each of testing modules (fig. 4.2 and fig. 4.3) was equipped with pressure adjustment mechanism 6, pressure transmitter 5 and displacement sensor 8. Nitrogen was applied as the cryogenic fluid. Temperature of the medium at the time of measurement was about minus 196 °C.

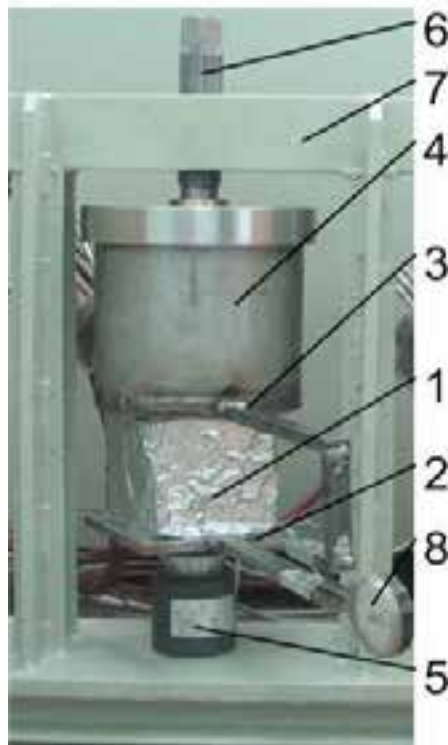


Fig. 4.3. Structure of single test cel: 1– heat insulating insert, 2– outer tank shell, 3– inner tank shell, 4– vessel with cryogenic fluid, 5– pressure transmitter, 6– pressure mechanism, 7– frame, 8– displacement sensor

Before beginning the major tests, the heat insulating insert and all side walls of testing stand were insulated with multilayer material, with a thermal conductivity of about $0.025 \frac{W}{m \cdot K}$ and was shielded using layers of aluminum film (fig. 4.2). At the beginning, required initial pressure was applied for each support and the vessels were filled with liquid nitrogen. Then, the pressure force was adjusted and recording of measured parameters values was started.

For tests were used materials selected on the basis of literature. Mechanical and thermal properties of the materials are shown in table 4.1:

- polyethylene PE10-UHMW,
- polyamide PA6G,
- polyoxymethylene copolymer POM-C,
- polyvinylidene fluoride PVDV.

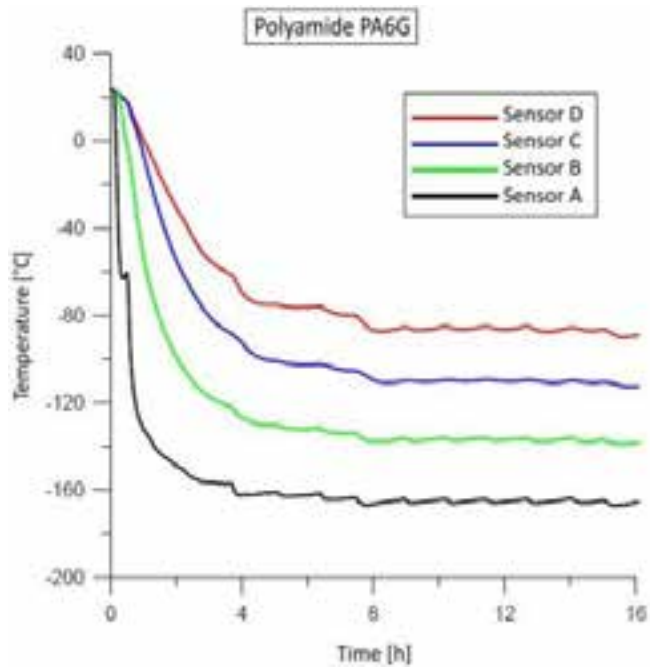
Table 4.1. Collation of selected properties of tested plastic materials^{*)}

Name of material	Thermal conductivity λ at 23 °C [W/(m·K)]	Yield stress Re [MPa] dry/wet	Elastic modulus [MPa] in tension/bendig test
PE10-UHMW	0,41	17 / --	650 / 800
PA6G	0,24	85 / 60	3300 / ----
POM-C	0,31	65 / --	2700 / ----
PVDF	0,11	50 / --	2000 / 2000

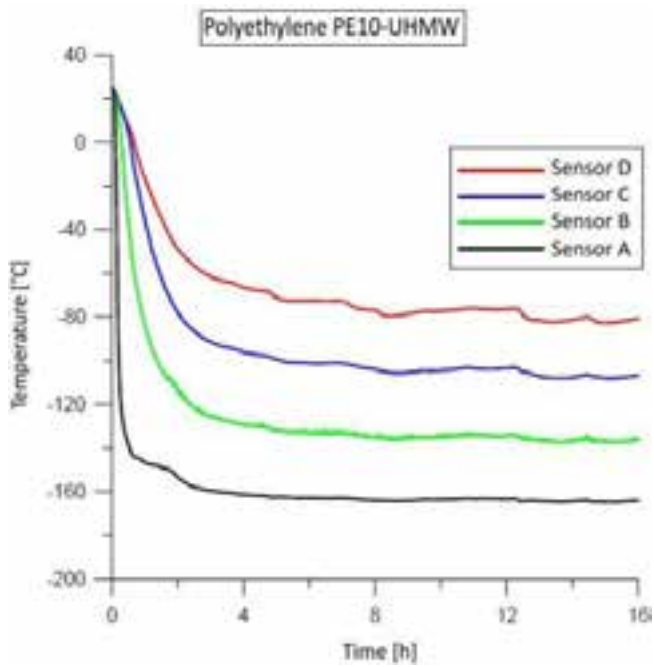
*) table was made basing on sheets of producer

Fig. 4.4 shows obtained temperature distribution in time, starting from the moment of filling vessel with liquid nitrogen.

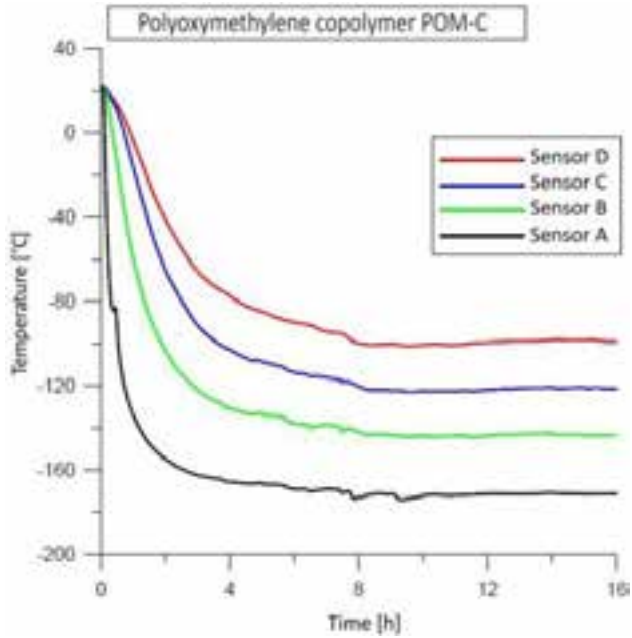
a)



b)



c)



d)

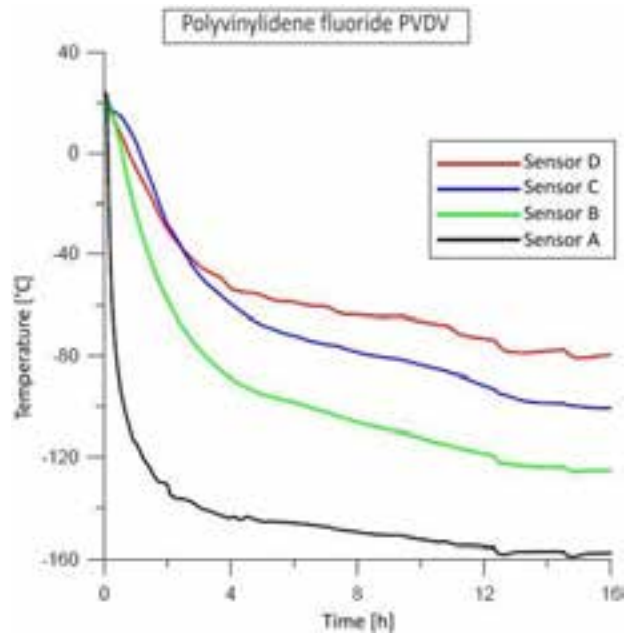


Fig. 4.4. Temperature plots in tested materials: a)PA6G, b)PE, c)POM, d)PVDF

According to this waveform, temperature of the first sensor from the side of the cryogenic vessel (sensor A) quickly reached the temperature close to the liquid nitrogen. After approximately 4 hours, the temperatures in other measuring points (sensors B, C and D) have also begun to stabilize. It was assumed, that steady state occurred within 6 hours after start of the experiment. The entire test cycle lasted for about 16 hours.

Basing on thermal conductivity coefficients shown in table 4.1, it can be assumed that the best insulator at ambient temperature is the PVDF material. However thermal properties of materials such as steel, but also plastics, usually vary with temperature. For example, thermal conductivity of austenitic stainless steel decreases by about 25% at the temperature range from plus 20°C to minus 220°C. Thermal conductivity of plastic materials is decreasing too with the drop of temperature. This phenomenon is beneficial for the insulating properties of the system, but the course of the change in thermal conductivity as a function of temperature is characteristic and different for each material. For steel these dependencies were precisely examined and described. In case of plastic materials, only some of them have been tested at low temperatures.

Conducted experiments helped to evaluate temperature change in heat insulating inserts for four different materials under the same conditions.

Collated results, as shown in table 4.2, allow to estimate variability of thermal conductivity tested materials for their insulating properties in specific temperature range from plus 20°C to minus 196°C. The PVDF material, which at temperature plus 23°C has the lowest thermal conductivity, reveals the smallest temperature decrease which means the worst insulating properties at low temperatures. The PE10-UHMW material which is characterized by the highest thermal conductivity among tested

materials at ambient temperature, reveals the highest temperature decrease which means the best insulating properties at low temperatures.

Table 4.2. Collation of temperatures at the cryogenic tank T1 and shielding tank T2 for tested materials

Name of material	λ at temp.23 °C [W/(m·K)]	Min temperature T1 [°C]	Max temperature T2 [°C]	Temperature decrease $\Delta T = T1-T2$ [°C]
PA6G	0,24	-167	-90	77
PE10-UHMW	0,41	-167	-82,5	82,5
POM-C	0,31	-160	-80,5	78,7
PVDF	0,11	-171,5	-99	72,5

Taking into consideration thermal properties, mechanical properties, availability of the material and easiness of shaping different geometrical forms, further studies were focused on material PA6G, which has slightly worse low temperature insulating properties than PE-10, but several times better strength properties (table 4.1).

By using temperature measurements in particular measuring points heat insulating insert made of polyamide PA6G, was estimated variability of thermal conductivity as show in fig. 4.5. In result of lowering the temperature from plus 20°C down to minus 200°C, thermal conductivity decreased fivefold what is beneficial due to the insulating properties of the supports.

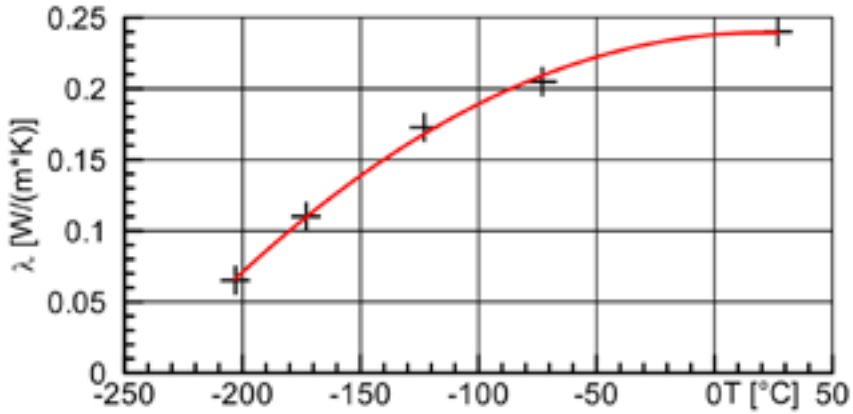


Fig. 4.5. Changes in the value of thermal conductivity as a function of temperature

Obtained results of thermal conductivity can be approximated by a polynomial of second degree with coefficients shown in the following equation:

$$\lambda(T) = -0,0503 + 0,0020 \cdot T - 3,4753 \cdot T^2. \quad (4.1)$$

The thermal tests of four selected materials have shown that the best insulator at low temperatures is polyethylene. However, given the thermal properties combined with strength, polyamide seems to be more advantageous option.

4.2. STRENGTH TESTS OF PLASTICS AT LOW TEMPERATURES

Compressive strength test was conducted on the samples made of material PA6G and PE, on a static universal testing machine class 1, type R-20 with the measuring range 0 – 100 kN (fig. 4.6).



Fig. 4.6. View of universal testing machine

For the tests there were prepared samples in the shape of roller with diameter $\phi 65\text{mm}$ and two heights: $L_1=40\text{mm}$ and $L_2=100\text{mm}$. Process of freezing the samples was performed in a calorimeter filled with liquid nitrogen at boiling point (temperature minus 196°C), under atmospheric pressure (fig. 4.7). The measurement was carried out using contact thermometer THERM 2250-1 with a measuring range from minus 199.9°C to plus 199.9°C (fig. 4.8).



Fig. 4.7. Cooling of the sample in the calorimeter



Fig. 4.8. Measuring temperature of the sample

Table 4.3. Test results on samples with dimensions of $\phi 65 \times 40 \text{ mm}$

No/Name of material	Dimensions ϕ / L	Dimension after cooling ϕ / L	Δh , load 20kN	Δh , load 100 kN	Sample dimensions after test
1 / PE	$\phi 65/40,0$	$\phi 63,8/39,3$	1mm	2mm	$\phi 64,9/39,7$
2 / PE	$\phi 65/40,0$	$\phi 63,8/39,3$	1mm	2,1mm	$\phi 64,8/39,7$
3 / PA	$\phi 65/40,0$	$\phi 64,2/39,9$	1mm	1,5mm	$\phi 64,6/39,9$

Table 4.4. Test results on samples with dimensions of $\phi 65 \times 100 \text{ mm}$

No/Name of material	Dimensions ϕ / L	Dimension after cooling ϕ / L	Δh , load 20kN	Δh , load 100 kN	Sample dimensions after test
1 / PE	$\phi 65,1/100,2$	64,2/98,1	1mm	2 mm	64,6/98,4* 64,5/98,5**
2 / PA	$\phi 65/100,0$	64,5/99,1	1,1mm	3mm	64,8/99,4* 64,6/99,0**

*/ sample dimensions under load of 20 kN

**/ sample dimensions under load of 100 kN

Before proceeding with the tests, the initial samples dimensions had been measured. After cooling down of each sample the measuring process was performed again to determine the real thermal contraction. Sample height measurement was also performed while conducting the test on a static universal testing machine after of each stage. Compressive test was conducted for two load values 20 kN and 100 kN. These loads, after

calculating, give on a cylinder area (diameter $\phi 65$ mm) pressure 6 N/mm^2 and 30 N/mm^2 respectively.

The results of frozen samples made of polyamide and polyethylene are contained in table 4.3 and 4.4.

4.3. CONCLUSIONS

As a result of low temperature, both materials show small thermal contraction. For polyethylene it is about 0.18 mm per 10 mm of initial thickness of the material, and for polyamide thermal contraction is almost twice less what is about 0.1 mm per 10 mm of initial thickness of the material.

Polyethylene under load of 20 kN was compressed by about 1 mm and under load of 100 kN by about 2 mm. Polyamide turned out to be more stiff. Under load of 100 kN, the shorter sample $\text{Ø}65 \times 40$ mm was shortened by about 1.5 mm, and the longer sample $\text{Ø}65 \times 100$ mm was elastically compressed by about 3 mm. For load of 20 kN deformation of polyamide was almost identical like this of polyethylene PE.

All of the samples after test did not show any defects like delamination, cracks or scratches. After cooling down, the material was shrinking slightly. Under the load, the material continues to shrink but only in the elastic range. After removal of the load the material returns to its initial dimensions.

4.4. REFERENCES

- [1] Alciatore D.: *Introduction to Mechatronics and Measurement Systems*, 4th edition, McGraw-Hill, 2011.
- [2] Arkharov A., Marfenina I, Mikulin Ye.: *Cryogenic Systems*, Vol.1: *Basics of Theory and Design*, Moscow, 2000.
- [3] Bryson W. E.: *Cryogenics*, Hanser Gardner Publications, 1999.
- [4] Chorowski M.: *Kriogenika. Podstawy i zastosowania*, IPPU Masta, Gdańsk, 2007.
- [5] Flynn T. M.: *Cryogenic Engineering*, 2nd edition, Dekker 2004.
- [6] Górski, Z., Cwilewicz, R., Konopacki, Ł., Kruk, K. *Proposal of propulsion for liquefied natural gas tanker (LNG carrier) supplying LNG terminal in Poland*, Journal of KONES, Vol. 15, No. 2, s. 103—108, Institute of Aviation, Warsaw 2008.
- [7] Lisowski, E.; Czyżycki, W.; Łazarczyk, K.; *Simulation and experimental research of internal supports in mobile cryogenic tanks*, Technical Transactions, 8, 175-183, Wydawnictwo PK, 2010.
- [8] Lisowski, E.; Czyżycki, W.; *Transport and storage of LNG in container tanks*, Journal of KONES, 18, 3, 193-201, 2011.
- [9] Lisowski, E.; Czyżycki, W.; *Modelowanie elementów maszyn i urządzeń w systemie CAD 3D SolidWorks z aplikacjami CosmosWorks i FloWorks*, Wydawnictwo PK, 2008.
- [10] Lisowski, E.; Czyżycki, W.; Łazarczyk, K.; *Using of polyamide in construction of supporting blocks of cryogenic tanks on example of LNG container*, Archives of Foundry Engineering, 10, 3/2010, 81 - 86, 2010.

- [11] Lisowski, E.; Czyżycki, W.; *Transport ciekłego LNG w zbiornikach kontenerowych*, Zeszyty Naukowe Politechniki Świętokrzyskiej. Nauki Techniczne, 12, 2009.
- [12] Lisowski E., Czyżycki W.: *Transport and storage of LNG in container tanks*, Journal of KONES Powertrain and Transport, Vol. 18, No. 3, p.p. 193-201, Warsaw 2011.

5. ONLINE MONITORING AND DIAGNOSIS SYSTEM OF THE LNG SUPPLY STATION

Cryogenic gas in the tank is stored as a liquid phase, and to some extent as a vapor which is formed by heating the fluid due to unavoidable heat leaks [3]. Power receiving system can use only the gaseous phase. For small consumption, the amount of gas generated by evaporation may be sufficient. At a higher consumption rate, it is necessary to vaporize liquid phase of the cryogenic liquid. In this case the liquid is pumped through the system of vaporizers, and therefore the gas flow is carried out by another method. Thus, the gas consumption can be realized in two ways: through direct input from the tank or by the system of vaporizers [4]. There is a need to control these systems. Activities associated with the control process can be implemented automatically. The use of an automatic system may include various parameters, such as pressures, temperatures and flow rates at different points in the installation.

Due to the nature of LNG station functioning and necessity of service continuity by the various seasons of the year, an own system of monitoring and diagnostics has been offered. The system will allow on-line tracking of selected parameters and remote access to selected data. Analysis of data on consumption of LNG is essential for the development of logistics supply, predicting repairs, etc.

5.1. MATHEMATICAL DESCRIPTION OF THE EVAPORATION PROCESS

The issue of the LNG consumption from the cryogenic tank is closely connected with the phenomenon of evaporation. Therefore, this chapter presents the problem of cryogenic liquids evaporation with a special

consideration given to LNG. Mathematical models of this process, which are applied in practice, are also presented in this chapter.

Description of the evaporation process determines the rate of the phase transition from liquid into gas. In general, we can distinguish the following cases in which the evaporation process occurs:

- volatile liquid at atmospheric temperature and pressure (acetone),
- superheated liquid
 - at ambient temperature, under high pressure (butane),
 - at high temperature and under high pressure (i.e. heated cyclohexane),
- cooled cryogenic liquefied gas - at low temperature but at atmospheric pressure (i.e. cooled methane, nitrogen, LNG).

The evaporation process of the liquid proceeds in a different way in these three cases. In the first case, after the flow out from the reservoir, the fluid is approximately in equilibrium. Therefore, the evaporation proceeds relatively slowly. In the second case the liquid is superheated and boils. Therefore, it is subjected to slow evaporation. The first category of the superheated liquid at ambient temperature and high pressure refers to liquefied gases. The second category, at high temperature and high pressure corresponds to liquids heated above their normal boiling point. The third case corresponds to the refrigerated liquefied gases which evaporate rapidly at the beginning, followed by a slow process.

5.1.1. EVAPORATION OF OVERHEATED LIQUID

Overheated liquid boils only partially, because some of its amount is cooled due to a decrease of the latent heat of vaporization and reaches atmospheric boiling point. Theoretically, some liquid, which boils

adiabatically (Theoretical Adiabatic Flash Fraction - TAFF) could be determined on the basis of the heat balance equation [2]:

$$\Phi = \frac{c_{pl}}{\Delta H_v} (T_i - T_b) \quad T_i > T_b, \quad (5.1)$$

where c_p – specific heat capacity, T – temperature on the absolute scale, ΔH_v – latent heat of vaporization, Φ – evaporated part of the liquid, and indexes b , i and l correspond to the boiling point, the initial point and the liquid point.

An alternative equation which takes into account the differential nature of the vaporization has the following form [2]:

$$(1 - \Phi)c_{pl}(-dT) = \Delta H_v d\Phi, \quad (5.2)$$

hence:

$$\Phi = 1 - \exp\left[-\frac{c_{pl}}{\Delta H_v} (T_i - T_b)\right] \quad T_i > T_b. \quad (5.3)$$

Expressions (5.2) and (5.3) give the theoretical amount of vapor formed. A sudden increase and release of vapor bubbles results in forming drops of liquid and liquid-spray. Mass of the liquid in the spray form is generally at the same level as during the initial boiling. Atomized liquid evaporates increasing the cloud of vapor or forms drops and falls down. The total amount of vapor formed from both the initial boiling and with the spray evaporation creates the final size of the cloud.

Rule of thumb often used for the liquid that forms a spray, says that this part of liquid is equal to the amount of spray formed during the initial boiling [3]. Another rule is that if the partial boiling is small, it is appropriate to assume that the quantity of atomized liquid is two or three times greater than the quantity formed during the initial point [7].

In [4] the author considers the effects of spraying liquids and precipitation accompanying outflow of boiling liquid, with particular reference to ammonia. You can consider two situations the flow: the flow of superheated metastable liquid and throttled two-phase flow. Both cases were modeled and examined.

In the case of non-strangled liquid flow, there is a large increase in diameter of the flow at the outlet. Increases of this type were observed during the research project "Desert Tortoise" [3]. In the case of strangled two-phase flow, the flow velocity is much greater. The part of liquid which boils is similar in both cases. The resulting droplets are sheared. Maximum size of drops, according to the Weber number, is:

$$We_d = \frac{u_d^2 d \rho_d}{\sigma_d}, \quad (5.4)$$

where d is a droplet diameter, u – velocity, ρ – density, σ – surface tension. The d index denotes droplet.

The range of precipitation depends on the balance of forces of inertia and gravity. Droplets have a greater inertia than steam particles, but in the case of droplets the effect of gravity is higher. The remaining part of the boiling liquid is in the normal boiling point. Evaporation takes place as a process with limited speed. This secondary evaporation with reduced speed is often considered as relatively less important compared to the initial boiling point, mainly due to the possibility of forming a cloud of flammable gases, in the case of discharge into the atmosphere.

5.1.2. MASS AND HEAT EXCHANGE DURING THE EVAPORATION FROM OPEN CONTAINER

Generally, the evaporation from an open container is a process with limited exchange of both mass and heat. However, in specific cases, one type of the exchange may be dominant. So, for the case of cryogenic liquid evaporation, the evaporation rate depends on the heat exchange between the substrate and the tank.

Considering an open container, there is only one way of mass transfer: between the liquid surface and the atmosphere. In contrast, there are many types of heat exchange: heat transfer by convection between the liquid surface and the atmosphere, by conduction between the liquid and the substrate, and by radiation.

Thus, the heat balance for an open container can be written as follows:

$$w \cdot c_{pl} \frac{dT}{dt} = -A_p (q_v - q_{cn} - q_{cd} - q_r), \quad (5.5)$$

where the following relationships are valid:

$$q_r = q_{rs} + q_{ra} - q_{rl}, \quad (5.6)$$

$$q_{rv} = m_v \Delta H_v, \quad (5.7)$$

w – mass of the liquid in the container, A_p – the open surface area of the container, c_{pl} – specific heat of a liquid in a container, m_v – is a stream of evaporating liquid mass per unit area, q_{cd} – heat flow per unit area resulting from the conductivity of the substrate to the tank, q_{cn} – heat flow per unit area resulting from the convection of air into the tank, q_r – net heat flow per unit area resulting from exposure to the tank, q_{ra} – heat flow per unit area resulting from radiation from the atmosphere into the tank, q_{rl} – heat flow per unit area resulting from radiation from the tank into the atmosphere,

q_{rs} – heat flow per unit area of solar radiation, q_v – heat required for the occurrence of the evaporation process per unit area, t – time.

Mass balance of the tank:

$$-\frac{d_w}{dt} = A_p m_v, \quad (5.8)$$

where the mass stream of evaporating liquid per unit area:

$$m_v = \frac{k_m M (p^0 - p^\infty)}{RT}, \quad (5.9)$$

k_m – mass transfer coefficient, M – molecular weight, p^0 – vapor pressure of liquid, p^∞ – partial pressure of fluid outside the tank. Usually it is assumed that the partial pressure of fluid outside the tank is equal to zero.

The equation (5.9) has been modified for multi-component liquids [2]:

$$m_v = \frac{k_m M_T^0 \sum x_i^0 M_i p_{is}}{RT n_T \sum x_i^0 M_i} \exp(-k p_{is} t) \quad (5.10)$$

where the k coefficient:

$$k = \frac{k_m A_p}{RT \cdot n_T}, \quad (5.11)$$

and M_i – molecular weight of the i -th component, M_T^0 – initial mass of the liquid, n_T – number of moles of the liquid, p_{is} – vapor pressure of the i -th component, x_i^0 – initial molar fraction of the i -th component, k – the constant value.

In general, the heat transfer can be correlated with a j_h coefficient and the mass exchange with the corresponding j_m coefficient [3]. In the case of geometry for which the characteristic dimension is the diameter d , the coefficients have the following form:

$$j_h = StPr^{0,67}, \quad (5.12)$$

$$j_m = \frac{k_m}{u} \frac{C_{Bm}}{C_T} Sc^{0,67}, \quad (5.13)$$

where: C_{Bm} –average logarithmic concentration difference, C_T – total concentration, k_m – mass transfer coefficient, u – characteristic velocity of liquid, St , Pr , Sc –Stanton, Prandtl and Schmidt number. Expression C_{Bm}/C_T is called the coefficient of lift.

Definitions and the relationship between the Reynolds number Re , Prandtl number Pr , Nusselt number Nu , Schmidt number Sc and Stanton number St are:

$$Re = \frac{u \cdot d \cdot \rho}{\mu}, \quad (5.14)$$

$$Pr = \frac{c_p \mu}{k}, \quad (5.15)$$

$$Nu = \frac{h \cdot d}{k}, \quad (5.16)$$

$$Sc = \frac{\mu}{\rho \cdot D}, \quad (5.17)$$

$$St = \frac{h}{c_p \rho} = \frac{Nu}{Re \cdot Pr}, \quad (5.18)$$

where: d – characteristic dimension (diameter of the tank), D – the diffusion coefficient, k – thermal conductivity, μ – dynamic viscosity.

Knowing the correlation for j_h , heat transfer coefficient h can be obtained from the definition of j_h in equation (5.12). Using an approximate identity:

$$j_m \approx j_h, \quad (5.19)$$

as well as definitions of j_h and j_m in equations (5.12) – (5.13), the following formula can be obtained:

$$k_m = \frac{h \cdot C_T}{c_p \cdot \rho \cdot C_{Bm}} \left(\frac{Pr}{Sc} \right)^{0.67}. \quad (5.20)$$

Alternatively, if the correlation for j_m is known, it can be used to determine j_h . For other types of geometry, the diameter is replaced with the value of the characteristic dimension.

Many researchers have measured the mass transfer from the surface of the liquid to gas, in particular for the evaporation of water. A special contribution was made by Coulson and Richardson. Their results were then correlated by T. K. Sherwood in terms of Reynolds number at the point of Re_x . In this case, the distance along the surface of the liquid to the considered point was set as a characteristic dimension. The result can be written using the formula:

$$j_m = 0.0415 \cdot Re_x^{-0.21}, \quad (5.21)$$

in the approximate range $10^4 < Re_x < 10^5$. Equation (5.21) can be used, in combination with (5.19) to obtain both: the mass transfer coefficient and the heat transfer coefficient.

The mass transfer coefficient can also be appointed directly using the number of Sherwood:

$$Sh = \frac{k_m \cdot d}{D}. \quad (5.22)$$

Fleischer gave the following relationship for the Sherwood number, assuming a flat surface of the liquid:

$$Sh = 0.037 \cdot Sc^{0.333} (Re^{0.8} - 15200) \quad (5.23)$$

Description of a heat flow from the substrate into the container is a complex issue because it should be considered as a transient process. A large contribution to the solution of unsteady heat transfer problems with the appointment of a number of specific cases brought Carslaw and Jaeger. The elementary heat flow equation has the form:

$$\frac{d^2\theta}{dz^2} = \frac{1}{\alpha_s} \frac{d\theta}{dt} \quad (5.24)$$

where:

$$\theta = T - T_s, \quad (5.25)$$

$$\alpha_s = \frac{k_s}{\rho_s c_{ps}}, \quad (5.26)$$

and α – heat dissipation factor, θ – temperature difference relative to the reference temperature or substrate, s index indicates is the substrate parameters.

If the temperature of the liquid in the tank is constant, the equation (5.24) can be solved with the following boundary conditions: $\theta = \theta_1$ for $z = 0$, $\theta = \theta_s$ for $z = \infty$. The solution is as follows:

$$\frac{\theta}{\theta_1} = \operatorname{erfc} \left[\frac{z}{2(\alpha_s t)^{\frac{1}{2}}} \right] \quad (5.27)$$

where z – vertical distance to the ground, the 1 index refers to liquid.

Considering the heat flux per unit area q :

$$q = -k \frac{d\theta}{dz}, \quad (5.28)$$

in conjunction with the equation (5.27) the formula can be written:

$$q = \left(\frac{k_s \rho_s c_{ps}}{\pi} \right)^{\frac{1}{2}} \frac{\theta_1}{t^{\frac{1}{2}}}. \quad (5.29)$$

The total heat flow through unit area:

$$Q = \int_0^t q dt = 2 \left(\frac{k_s \rho_s c_{ps}}{\pi} \right) \theta_1 t^{\frac{1}{2}} \quad (5.30)$$

A more complex case takes into account the variable temperature of the liquid. It can be solved with the following boundary conditions: $\theta = 0$ for $t = 0$, $\theta = \theta_1(t)$ for $z = 0$, $\theta = 0$ for $z = \infty$. The solution is as follows:

$$\theta = \frac{z}{2(\pi \alpha_s)^{\frac{1}{2}}} \int_0^t \frac{\theta_1}{(t-\tau)^{\frac{3}{2}}} \exp \left[-\frac{z^2}{4\alpha_s(t-\tau)} \right] d\tau. \quad (5.31)$$

Hence, reducing the temperature of the vaporizing tank will have approximately exponential character. The analytical solution of the equation (5.31) in the case when $\theta = \exp(-\lambda t)$ was presented by H. S. Carslaw and J.C. Jaeger.

The heat transfer by radiation is given by (5.6). The individual components of this equation are determined as follows:

$$q_{rs} = \psi(1 - a) \quad (5.32)$$

$$q_{ra} = \epsilon_a \sigma T_a^4 \quad (5.33)$$

$$q_{rl} = \epsilon_1 \sigma T_{a1}^4. \quad (5.34)$$

where: a – liquid surface albedo, ϵ – emissivity, σ – the Boltzmann constant, ψ – solar constant, the a index refers to the atmosphere. Value of the solar constant is $\psi = 1373 \text{ W}/\text{m}^2$ [2]. The values of albedo and emissivity were considered by Mackay'ai Matsugu. They suggested the

value of $a = 0.14$ and the emissivity of the atmosphere and the liquid equal to 0.75 and 0.95 respectively. The dependence of the angle of the sun on albedo for a tank of liquid were determined by Shaw and Briscoe. They obtained the results shown in table 5.1.

Table 5.1. The dependence of the angle of the sun on albedo

Angle [°]	90	50	40	20	10	0
Albedo	0.020	0.025	0.034	0.134	0.348	1.000

5.1.3. VAPORIZING OF CRYOGENIC LIQUIDS

In general, when considering the vaporization of cryogenic liquid or cooled liquefied gas, it is necessary to simultaneously take into account two processes: evaporation and expansion. At the beginning the process is dominated by evaporation, which is caused by the inflow of heat into the cryogenic liquid from the environment. There is a relatively short period of very rapid evaporation, followed by a slow process to the state approximately determined. Evaporation rate can be determined from the equation of heat flow, as it is shown in (5.29). The equation can be simplified to the form:

$$q = A_V t^{-\frac{1}{2}}, \quad (5.35)$$

where the coefficient

$$A_V = \left(\frac{k_s \rho_s c_{ps}}{\pi} \right)^{\frac{1}{2}} \theta_l \quad (5.36)$$

is known as an evaporation parameter. This equation was confirmed experimentally. It should be noticed that at the initial time ($t = 0$) equation

gives an infinite heat flux and cannot be used. However, the period of time with overestimated heat flux is very short.

Most studies in the field of cryogenic fluid vaporization concerns the liquefied natural gas (LNG) and ammonia. Studies of liquid ethylene were conducted on a large scale in Japan, by a team of prof. Hikita Tsuyoshi under the auspices of the Ministry of International Trade and Industry (MITI) since 1976. On the basis of obtained results, a utility model of the ethylene evaporation was developed:

$$v = 0.625\exp(-0.0507t), \quad (5.37)$$

where: t – time in seconds, v – speed of evaporation. The formula shows, that after approximately one minute the rate of evaporation is significantly reduced.

In summary, the evaporation of cryogenic liquid flowing from the reservoir exhibits features of the quasi–immediate process followed by slowing down to a steady state.

5.1.4. VAPORIZATION OF LIQUIFIED LNG

Study of LNG vaporization were carried out by many academic, research and industrial centers, among others by Burgess, Murphy and Zabetakis, Humbert–Basset and Montet, Kneebone and Boyle, Feldbauer, Raj and Kalelkar, the American Gas Association (AGA), Drake and Reid, Opschoor, Shaw and Briscoe.

On the basis of evaporation of liquid methane Zabetakis and Burgess developed a model describing the evaporation rate at the initial stage of the process. They found that the rate is limited by the supply of heat from the environment and is given by the formula:

$$v = \frac{k_2}{\rho_1 \Delta H_V} \frac{T_s - T_1}{(\pi \alpha_s t)^{\frac{1}{2}}}. \quad (5.38)$$

The formula presented in (5.38) is applicable only in the initial stage of evaporation, not exceeding the time of one minute after the start of the process. Double logarithmic plot of time course of evaporation has the form similar to a straight line.

LNG evaporation process has been particularly thoroughly studied by Drake and Reid. They conducted a series of experimental studies in relation to the results obtained by the American Gas Association and Gaz de France. They demonstrated that the rate of evaporation can be described by the formula (5.35), while the value of evaporation is very different depending on the type of environment in which the process occurs.

In particular, Drake and Reid studied the process of LNG evaporation after getting out of cryogenic tank (e.g. due to the failure). The values of the coefficients obtained for the vaporization of LNG from the surface at atmospheric pressure, ambient temperature $T_s = 16^\circ\text{C}$ and the LNG temperature $T_1 = -162^\circ\text{C}$ are shown in table 5.2.

V. J. Clancey in 1974 also developed a model describing the evaporation of cryogenic liquid such as LNG. Rapid evaporation in the initial period of time has been described using the following formula:

$$E_i = \frac{k_1(T_s - T_1)^2}{\Delta H_V}, \quad (5.39)$$

while in the steady phase:

$$E_s = \frac{k_2(T_s - T_1)}{\Delta H_V}, \quad (5.40)$$

where: E_i and E_s determine the mass evaporation rate per unit area and per

unit time $\left(\frac{kg}{m^2 \cdot s}\right)$, while ΔH_v determine the hidden heat of evaporation (J/kg). The k_1 and k_2 coefficients are dependent on the environment in which the evaporation takes place. For the flow of LNG to the substrate ground these coefficients take values presented in table 5.3.

Table 5.2. Parameters and the evaporation coefficients of LNG [7]

	ρ_s (g/cm ³)	c_{ps} (cal/g °C)	k_s (cal/s cm °C)	A_v (cal/s ^{1/2} cm ²)
Carslaw i Jaeger (1959)				
soil (medium quality)	2.5	0.2	0.0023	3.41
soil (sandy, dry)	1.65	0.19	0.00063	1.40
soil (sandy, 8% humidity)	1.75	0.24	0.0014	2.45
concrete (1:2:4)	2.3	0.23	0.0022	3.39
AGA tests				
compacted soil				8.5
Gaz de France				
soil (dry, 15°C)				18.2
soil (damped, 50°C)				12.7
soil (damped, 15°C)				5.68

Table 5.3. Values of coefficients determining evaporation rate of LNG [7]

Type of the base	k_1	k_2
medium-quality soil	7.1×10^{-4}	1.5×10^{-2}
concrete	7.5×10^{-4}	1.5×10^{-2}
sandstone	1.3×10^{-3}	2.6×10^{-2}

Rate of the LNG evaporation process was studied by S. J. Turner. Based on the results of his research G. Opschoor formulated the following mathematical formula:

$$q_w = 0.085 \cdot k_w \cdot \left(\frac{g \cdot \beta \cdot \Delta T^4}{\alpha_w \cdot \nu_w} \right)^{\frac{1}{2}}. \quad (5.41)$$

For the LNG, on the basis of the above equation, the following heat flux value can be obtained:

$$q_w = 2.3 \cdot 10^4 \left[\frac{W}{m^2 \cdot s} \right] \quad (5.42)$$

what leads to the mass of the evaporating LNG:

$$m_w = 0.045 \left[\frac{kg}{m^2 \cdot s} \right]. \quad (5.43)$$

This value was verified by experimental studies. G. Opschoor proposes a mass rate of the LNG evaporation $m_w = 0.05 \left[\frac{kg}{m^2 \cdot s} \right]$.

Opschoor has also developed mathematical formulas describing the mass evaporation rate of LNG in the case of a layer of ice formed. Assuming that the ice layer is formed after about 20-25 seconds, the process can be described using the following formulas:

$$m_v = 0.008 \cdot t \quad 0 \leq t \leq 25, \quad (5.44)$$

$$m_v = \frac{0.517}{(t-20)^{\frac{1}{2}}} \quad t > 25, \quad (5.45)$$

where t – time, m_v – mass evaporation rate per unit area and time $\left(\frac{kg}{m^2 \cdot s}\right)$.

For the case of simultaneous evaporation and expansion of LNG Burgess, Murphy and Zabetakis in 1970 proposed the following formulas:

$$r = k_3 t, \quad (5.46)$$

$$\frac{dm}{dt} = \pi \sigma v r^2. \quad (5.47)$$

Hence:

$$m = \pi \sigma v \int_0^t r^2(t) dt, \quad (5.48)$$

$$m = \frac{\pi}{3} \sigma v k_3^2 t^3, \quad (5.49)$$

where m – total mass of LNG evaporated, r – characteristic dimension (radius), k_3 – constant coefficient. The value has been determined experimentally $k_3 = 0.381$. Then, assuming the density of LNG $\sigma = 416 \frac{kg}{m^3}$, formula (5.49) can be simplified to the form:

$$m = 63.2 \cdot v t^3. \quad (5.50)$$

Lind in 1974 proposed a similar relationship, but with the value of the coefficient $k_3 = 0.635$. This value was based on the experiments carried out by Esso, described by Feldbauer. In this case the mass of evaporated LNG is calculated from the formula:

$$m = 175.7 v t^3 \quad (5.51)$$

A different approach was chosen by Fay, who started from the volume of the cylinder and the energy balance:

$$V = \pi r^2 h \quad (5.52)$$

$$\frac{dr}{dt} = (2g'h)^{\frac{1}{2}}. \quad (5.53)$$

After integration of energy balance for the boundary condition $r = 0$ for $t = 0$ the following relation was obtained:

$$r = \left(\frac{8g'V}{\pi}\right)^{\frac{1}{4}} t^{\frac{1}{2}} \quad (5.54)$$

Formulas (5.54) and (5.48) allow to determine the mass of vaporized LNG. Fay also established that heat conduction occurs through the layer of ice formed.

Ray and Kalelkar in 1973 designated the following relationship:

$$m = 1.712 \cdot \pi p v A^{\frac{1}{2}} t^2 \quad (5.55)$$

where A is the volume of evaporating cryogenic liquid.

5.2. IDEA OF MONITORING AND DIAGNOSTICS SYSTEM OF LNG SUPPLY STATION

Typical installation of the LNG supply station is constructed of the following components: a cryogenic tank for storing the LNG, a vaporizing installation, an odor-giving transmission system, system safety valves, and installation of pressure reduction. There is a need for carrying out tests of the following elements of the LNG station: filling and unloading installations, installation of the pressure building, system of evaporators. These tests have the following objectives:

- determine minimum time of filling the tank,
- identify a maximum flow rate of cryogenic fluid from the tank, which is possible to obtain as well as the minimum time of unloading the tank,
- determine a pressure recovery time inside the tank above the liquid surface for a given level of liquid in the tank and given initial value of the pressure,
- define parameters of automatic system for switching between the LNG vaporization installations,
- determine the actual temperature distribution, heat leakage and time to maintain the LNG inside of the tank.

5.2.1. IDENTIFICATION OF MEASURING POINTS

Before formulating requirements for the computer monitoring system of LNG supply station, an analysis of the number and arrangement of sensors needed was carried out. Simplified diagram of a local installation of the LNG supply station with specified measurement points is shown in fig. 5.1.

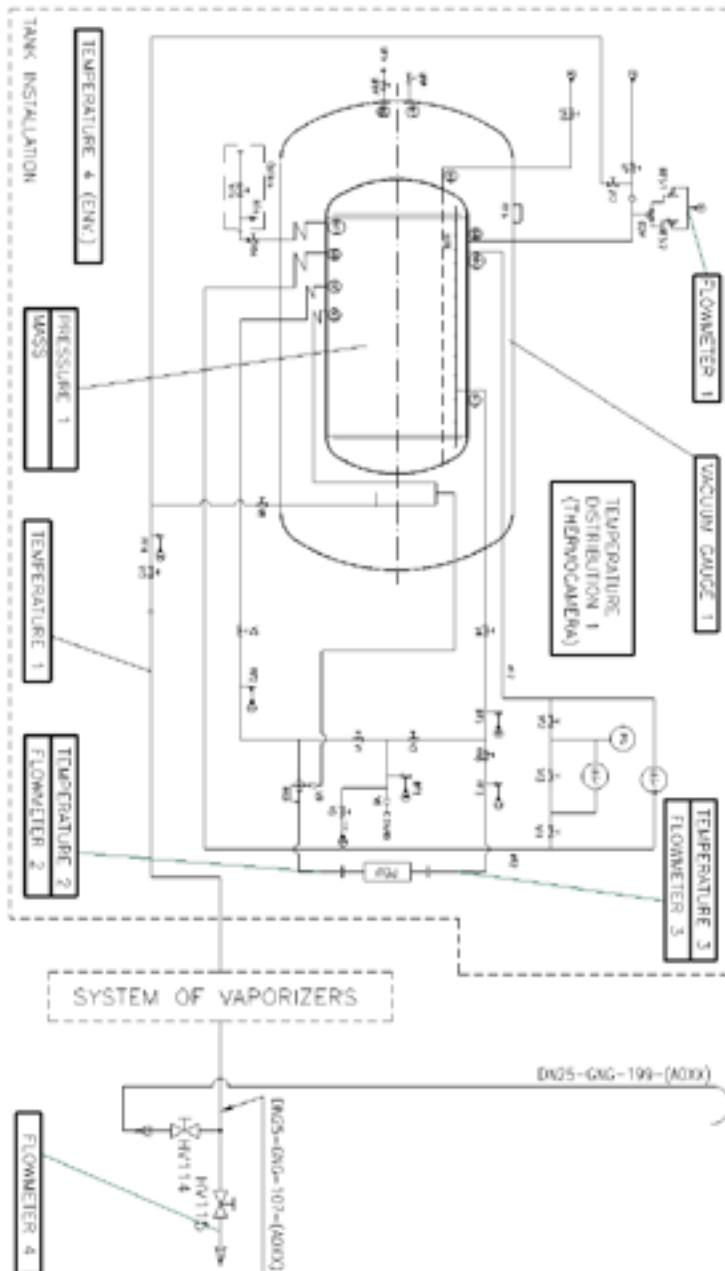


Fig. 5.1. Diagram of the installation of local LNG station with measuring points

As can be seen from the fig. 5.1, the following parameters of the LNG supply station will be subject to monitoring:

- PRESSURE 1 – LNG vapor pressure inside the cryogenic tank,
- VACUUM GAUGE 1 – level of vacuum between walls of cryogenic tank,
- TEMPERATURE 1 – gas temperature at the outlet from the tank,
- TEMPERATURE 2 and TEMPERATURE 3 – temperature before and after the pressure built unit (PBU),
- TEMPERATURE 4 – ambient temperature,
- TEMPERATURE DISTRIBUTION 1 – temperature distribution on the outer surface of the tank and installations obtained using a thermo vision camera
- FLOWMETER 1 – loss of LNG through the safety valve,
- FLOWMETER 2 and FLOWMETER 3 – mass flow before and after the pressure built unit (PBU),
- FLOWMETER 4 – actual consumption of LNG obtained by using the gas meter.

5.2.2. REQUIREMENTS FOR THE MONITORING AND DIAGNOSTICS SYSTEM

Design of the remote monitoring and diagnostics system of the local LNG station parameters was made taking into account a number of preliminary assumptions. Due to the diversity of functionalities performed, it was decided to decompose the system into modules. Individual modules have the form of desktop applications or applications running in the internet browser window. Desktop applications run under the systems of Microsoft Windows family, while the internet applications are available for browsers on any operating system, including mobile devices, smartphones, tablets,

PDA etc. Application for acquiring the measurement data supports typical data acquisition cards, such as Advantech or National Instruments. The measurement data are stored in a relational client server database, with support for transactions such as Firebird, MySQL or PostgreSQL.

From the user point of view, system of monitoring and diagnostics should provide the following functionalities:

- allow to acquire data from the transducers and store in a database for later processing and analysis,
- allow to observe time courses of selected parameters in both numerical and graphical form,
- enable secure remote access to data via the internet,
- enable messaging and alerting system using the short text messages (SMS) and e-mails,
- allow to optimize delivery of the LNG to the local supply station on the basis of the real-time consumption analysis,
- allow to control selected systems of the installation remotely by authorized personnel.

5.2.3. MAIN COMPONENTS OF THE SYSTEM

Diagram of the main components of the system is shown in fig 5.2.

On the basis of the analysis, the following components of the system have been extracted: monitoring subsystem, relational database server, visualization and diagnostic module, control module and subsystem of the LNG delivery optimization. Fig. 5.2 shows connections between the individual components.

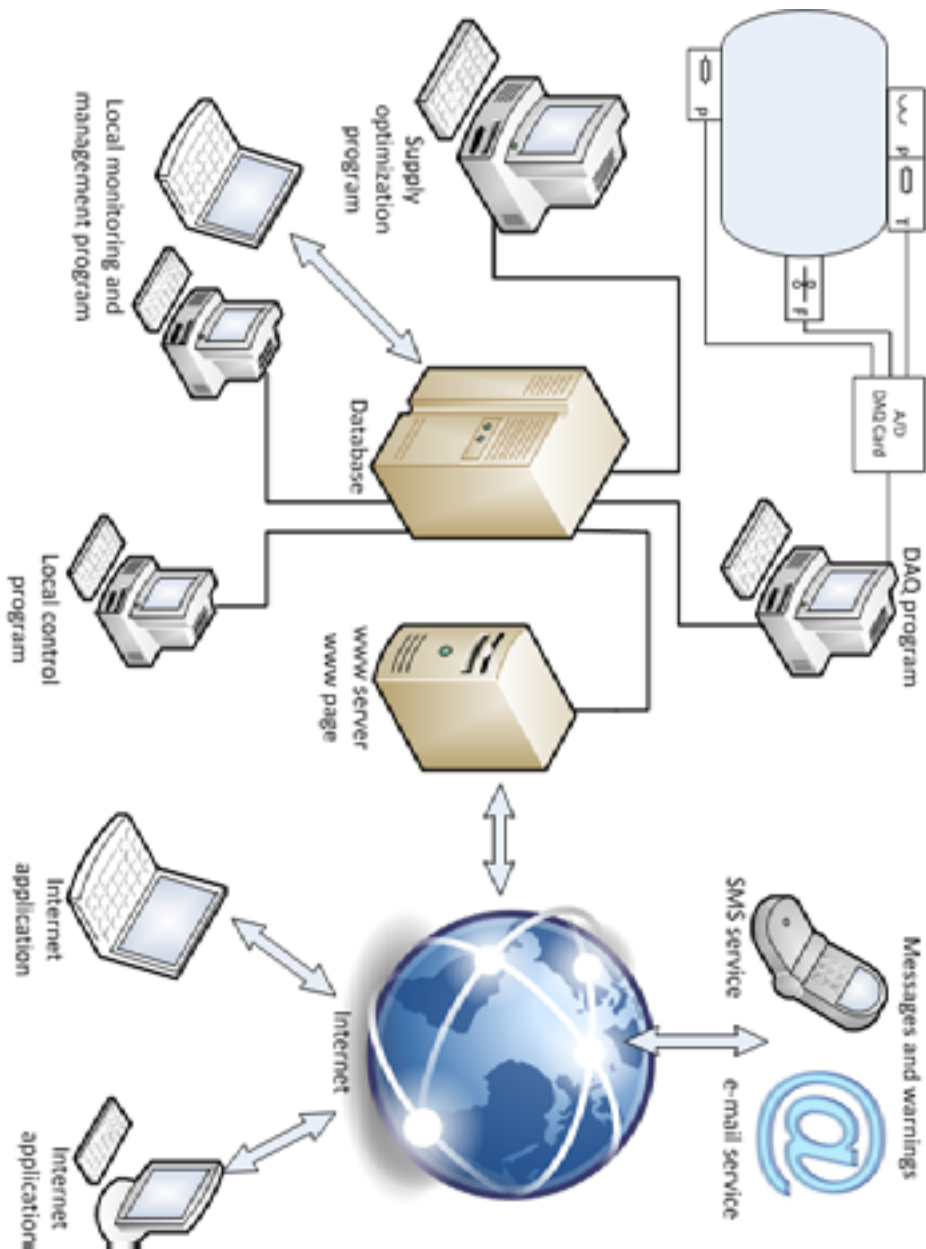


Fig. 5.2. Components of monitoring and diagnosis system

The monitoring subsystem includes sensors and transducers, DAQ card, a program for data acquisition, a program for management of monitoring parameters (e.g. frequency of readings from the transducers, measuring ranges, scaling parameters of the signals) and a program for transmission and acquisition of signals from the thermo vision camera. Relational database server is a central element of the system, almost all other components are connected with it. Visualization and diagnostics module can be used locally, via the desktop application or remotely, using a web server on the system side and internet browsers on the client side. Remote diagnosis includes sending messages, warning and alerts via SMS and e-mail. The control unit, for safety reasons, may be used only by authorized personnel via computers located in specially prepared sites within the LNG supply station. The optimal schedule for the delivery of LNG is determined by a separate application which is installed locally.

5.3. ELEMENTS OF THE MONITORING SUBSYSTEM

The monitoring subsystem includes sensors and transducers of measured parameters such as temperatures, pressures and flow rates, amplifiers, power supplies, connection cables and applications for both: data acquisition and management of parameters.

5.3.1. TEMPERATURE SENSORS AND TRANSDUCERS

The measurement of cryogenic temperatures can be performed using resistance sensors (RTDs) or thermocouples. In the proposed system, a Pt100 resistance sensors are used. This types sensors are present in different forms, which allow for measurement at various locations and environments. Fig. 5.3 shows the sensors to measure temperature of surface.

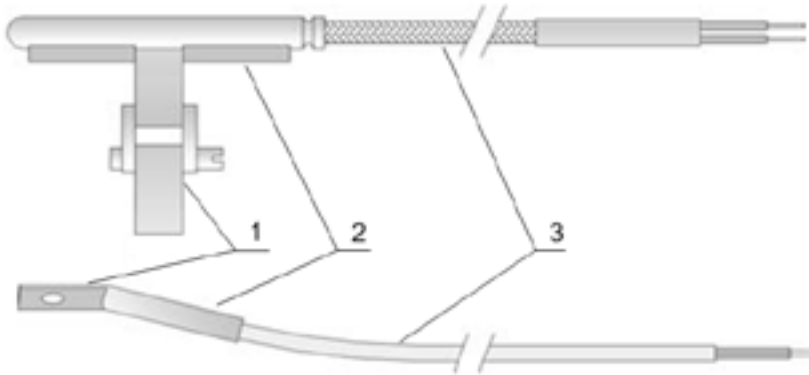


Fig. 5.3. Structure of a resistance sensor to measure temperature of surface
1 – mounting kit, 2 – sensor housing, 3 – wire

Types of RTDs presented in fig. 5.3 allow to measure temperatures of flat and oval surfaces. They are characterized by low weight and easy installation. They can be equipped with hose clamps or plates for easy installation.

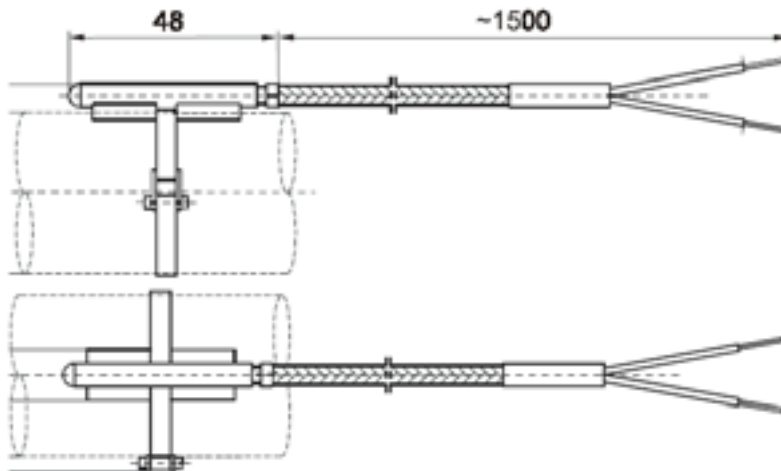


Fig. 5.4. RTD to measure temperature of a pipeline or a tank

Fig. 5.4 shows version of the sensor to measure a temperature inside a pipe, ventilation channel or container.

Sensors with connecting heads have usually a modular structure. The main components of the head are shown in fig. 5.5.

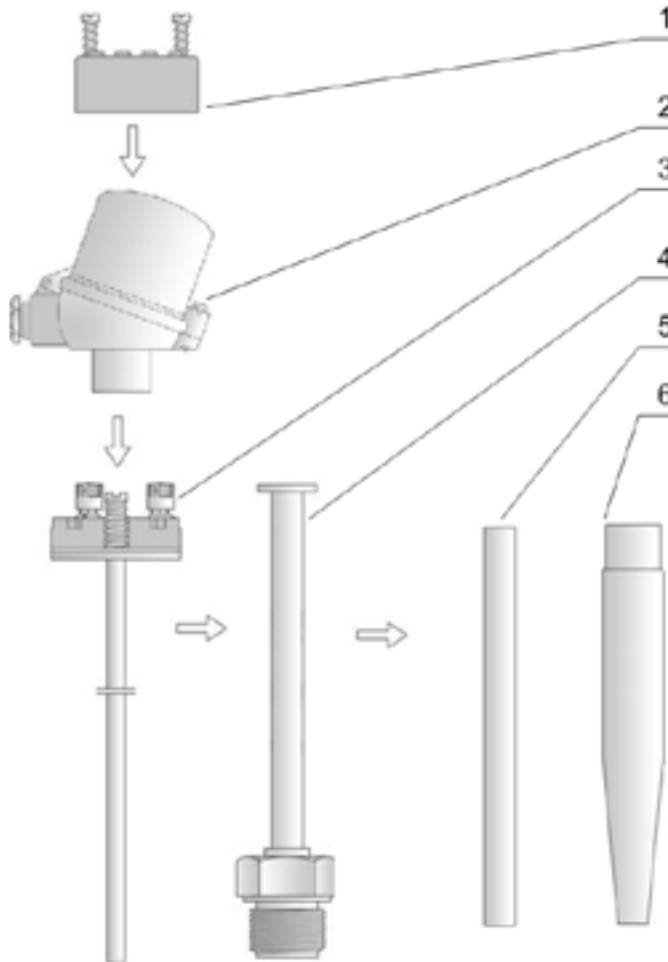


Fig. 5.5. Structure of the RTD sensor with the connecting head
 1 – temperature transducer, 2 – connecting head, 3 – the sensor,
 4 – spacer, 5 – protective tube, 6 – pressure cover

Standard measurement range of the resistance sensor comprises temperatures from minus 50 to plus 150 degrees Celsius or from minus 200 to plus 50 degrees Celsius. Sensing element is a thermometer Pt100, Pt500 or Pt1000. The measuring circuit can consist of two three or four wires. The cover and the heat sink are usually made of the MO59 brass.

The connecting head (2) can be made in different ways. Acceptable variants of realization are defined in the DIN 43 729 standard. The head can be made of aluminum, iron or plastic. The sensing element (3) consists of a ceramic block and a protective tube with a diameter of 3 to 8 mm. The tube is usually made of the material 1H18N9T (1.4541) material. The thermo resistor is located inside the tube.

Measuring element is a replaceable part of the sensor, what allows to reduce significantly the cost of modernization of measuring equipment at the facility. Resilient mounting of the ceramic block ensures perfect contact pressure of the measuring element to the bottom of the outer protective tube, fast response time, compensation in case of differences in size and reduction of natural vibration by double-sided fixing in the protective tube. Dimensions of measuring elements are made in accordance with DIN 43 762 standard. Items (4), (5) and (6) play an auxiliary and protecting role for the sensing element.

In a significant number of cases the temperature measurement can be performed using different types of the mantle sensors. In fig. 5.6 are presented basic design solutions of this kind of sensors. Typical measurement range of mantle sensors is from minus 200 degrees Celsius to plus 550 degrees Celsius. A Pt100 thermoresistor or derived (Pt500, Pt1000) can be used as a sensing element. The thermoresistor can be made in a class A or B in a measuring circuit with two, three or four wires. Standard range

of diameters is 3 mm to 8 mm. Depending on the needs, there are several design versions of the sensors:

- BT/T – without/with the tube, with free ends of the wires with a length of 20 mm to 50 mm,
- TKb – with a cable sleeve,
- BTW/TKbW – without/with the tube, with a flat mini plug,
- BTL/TKbL – without/with the tube, with a LEMO plug.

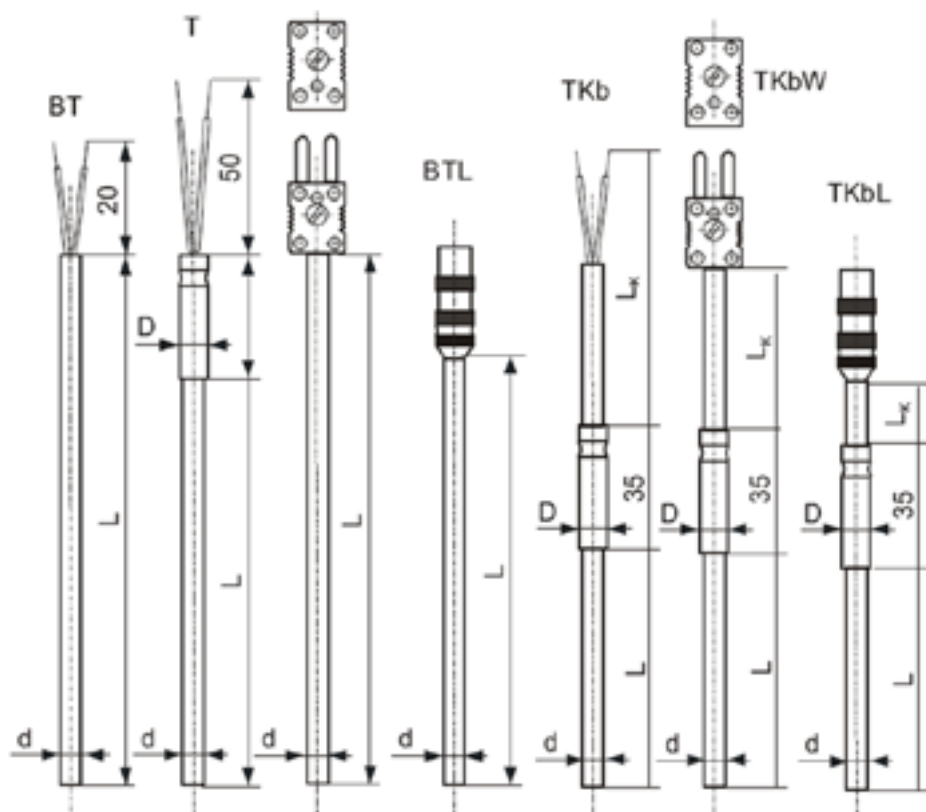


Fig. 5.6. Design solutions of mantle sensors

The signal generated by a Pt100 sensor must be amplified in order that its value could be processed by the DAQ card of the computer data acquisition system.



Fig. 5.7. PS-01 transducer for a resistance sensor

Typical transducers are PS-01 and PS-02. The PS-01 transducer (fig. 5.7) can process the temperature signal generated by a Pt100 sensor on the size of the current signal 4 to 20 mA in a two-wire circuit or voltage signal 0 to 10 V in a three-wire circuit. The transducer is adapted for mounting on a TS-35 rail.

5.3.2. MASS FLOW MEASUREMENT

Measurement of a mass flow of gas from the reservoir can be made by means of mass flowmeter, volumetric flowmeter or by measuring the weight change of the tank.

Mass flowmeters measure the flow in mass units. This type of measurement is unaffected by changes in temperature, density, pressure, viscosity, conductivity and fluid flow profile. Mass flowmeter provides accurate, fast and reliable measurements. It has no moving parts subject to wear. In the case of horizontal mounting the sensor is self-draining. Pipes

are placed in a sealed stainless steel housing, which allows to install the flowmeter in almost any environment.

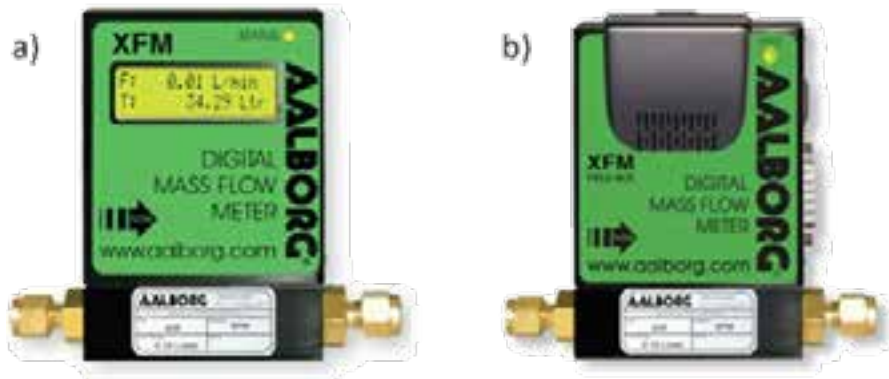


Fig. 5.8. Mass flowmeters: a) with an LCD display,
b) with the RS485 communication interface

Mass flowmeters may have a communication interface Profibus DP or RS-485 and RS-232 with or without the LCD display. The flowmeters are enclosed in housings made of stainless steel or aluminum. They provide self-diagnostic functions and allow to set the lower and upper threshold, beyond which an alarm is activated. The results of flow and volume measurements can be presented in many different units. The measurement accuracy is usually $\pm 1\%$ of the measuring range for standard conditions. Sample versions of the mass flowmeters are shown in fig. 5.8.

The mass flow rate can also be measured using the Coriolis flowmeter. The flowmeter operates on the basis of measurement of the Coriolis force arising during the flow of fluid through the appropriate section of the pipeline. The force is proportional to the mass of the liquid which flows through. In particular, it concerns the homomorphic fluids, that is, those that are not a mixture of substances having different physical states, such as

a liquid and gas. The resulting Coriolis force causes attenuation of the tube oscillations in the flow meter. The oscillations are measured using the appropriate sensors and then processed by the electronics. Coriolis flowmeters are characterized by numerous advantages. The main one is the accuracy that ranges from $\pm 0.1\%$ to $\pm 3\%$ depending on the particular installation. Flowmeters contain no mechanical parts that could be subject to rapid wear, so the time of their use is long. Examples of the Coriolis flowmeters are shown in fig. 5.9 – fig. 5.11.



Fig. 5.9. Mass Coriolis flowmeter PROMASS

Fig. 5.9 presents a PROMASS type mass flowmeter. This type of flowmeters can be used for liquids, vapors and gases. In addition to the mass flow, they can measure density and temperature of the medium. Unique detector design solution eliminates the vibration and mechanical stress in the system and ensures stable measurement of the mass in the actual process conditions. The accuracy of the measurements is also very high ($\pm 0.05\%$ of the nominal flow rate).

The Coriolis type flowmeters are suitable for measuring almost any medium at any conditions, as multiphase liquids, measurements in harsh process conditions, for liquids with high viscosity, which present big problems of measuring (the pressure drops during transport). Digital signal processing allows to obtain measurements with high accuracy and stability. Uncomplicated fluid flow path in the detector enables easy drainage, cleaning and use of dense liquids. Temperature range of measured liquid is from minus 200 to plus 400 degrees Celsius.



Fig. 5.10. Mass Coriolis flowmeter ROTAMASS

ROTAMASS flowmeters are equipped with an internal non-volatile EEPROM memory, which is used to save the configuration parameters. Thus, values of parameters are protected against loss in case of power failure. Communication interface is based on the HART protocol. The

flowmeter is intrinsically safe version, which is particularly important for measuring the parameters of LNG.

Coriolis mass flowmeters of MASSFLO type can be used to directly measure the following parameters: mass flow, total density, temperature, volumetric flow rate, total flow volume of the fraction and the percentage fraction. The flowmeters are characterized by high accuracy and wide temperature range of the fluid. An example of a MASSFLO flowmeter with a transducer is shown in fig. 5.11.



Fig. 5.11. Mass Coriolis flowmeter MASSFLO: a) MASS 2100 type, b) MASS 6000 transducer

Mass flow rate can be determined by measuring the volumetric flow rate of the gas. This way of calculating the mass flow has been described in DIN EN 12 213 standard. The calculation requires measurement of the following parameters: volumetric flow rate of the gas effluent stream, the pressure at the inlet of the flow meter and temperature of the gas effluent stream. The flow rate measurement can be realized e.g. using a turbine flowmeter. The turbine flowmeters are a group of measuring instruments of

the highest class of accuracy, which measure the current volumetric flow rate. The main element of this type of flowmeters is axially positioned turbine, which is propelled by the flowing medium. Rotational speed of the turbine is directly proportional to the velocity of the flowing medium and, consequently, to its volume. The turns of the turbine are converted into electrical signals by means of magneto-inductive sensor mounted in the outer housing of the sensor. An example of a turbine flowmeter, which can be used with cryogenic liquids or gases, Hoffer HO type, is presented in fig. 5.12.



Fig. 5.12. Turbine flowmeter HOFFER HO

Hoffer HO turbine flowmeter can be used to measure the parameters of liquids and gases at temperatures ranging from minus 270 to plus 180 degrees Celsius with ensured accuracy of 0.5%. There are versions of one or

two directions, with different types of connecting interfaces and a wide range of flow ranges.

Mass flow rate of gas from the reservoir can also be calculated based on mass measurements of the tank. In order to do this, a system of pressure sensors and an electronic adder must be built. The mass of the reservoir must be recorded during the experiment. An example diagram of the measurement system is shown in fig. 5.13.

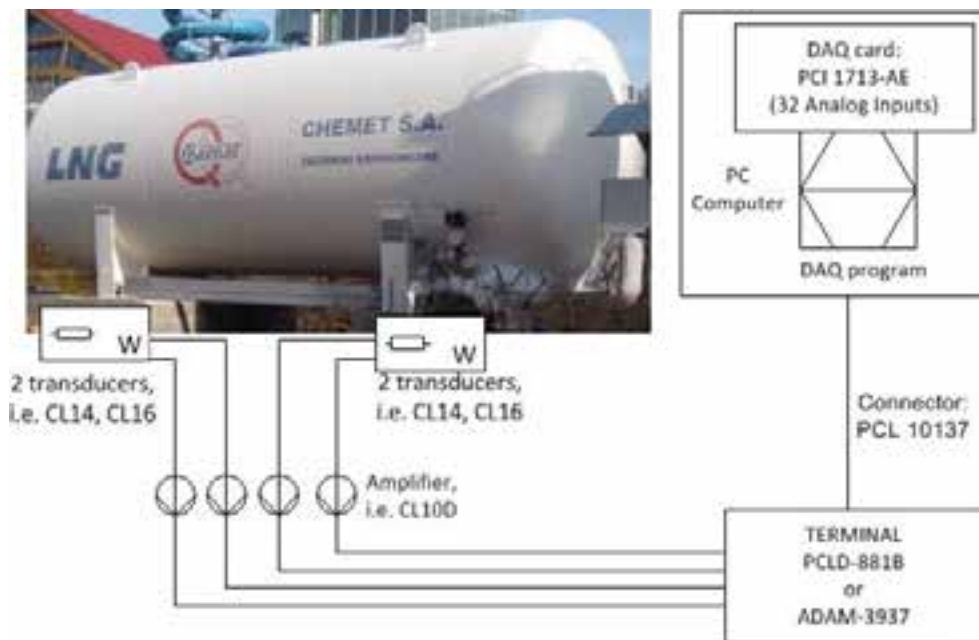


Fig. 5.13. Measuring system of cryogenic liquid mass flow based on change of the tank mass

In this case, the signals are transmitted from the force sensors (CL14 or CL16) through the amplifiers CL10D and the terminal board PCLD-881B or ADAM-3937 to the DAQ card (PCI 1713-AE). A computer program

summarizes indications of the individual sensors and calculates the value of the resultant force, which is finally converted into the mass.

5.3.3. MEASUREMENT OF THE PRESSURE

Measurement of the pressure inside the tank can be made by means of differential pressure gauges suitable for use in cryogenic conditions, such as Media 5 Media 6 These gauges can also be used to measure liquid level in the tank (including the cryogenic liquids) and flow rate. The pressure gauge includes a transducer which is controlled by a microprocessor. It is connected to the two-wire circuit. Measured values can be observed on the digital display and transmitted using a standard communication interface RS-232. There is also a possibility to use an output analog current signal of range from 4 mA to 20 mA. An example of a Media 6 pressure gauge is presented in fig. 5.14.



Fig. 5.14. Media 6 pressure gauge

The pressure within the elements of the cryogenic installation can be realized using strain sensors with built-in transducers, such as the Trafag NAT type or Trafag NAH type. Example models of the sensors are shown in fig. 5.15.



Fig. 5.15. Pressure transducers: a), b) – NAT type, c) NAH type

Strain gauge load cells of the NAH and NAT types can be adapted for different measuring ranges, e.g. from 0 bar to 10 bar. They may have, depending on the version, the current output signal from 4 mA to 20 mA or the voltage output signal from 0 V to 10 V. Typical accuracy of the measurement is of the order of 0.5 %.

5.3.4. STRUCTURE OF THE MEASUREMENT SYSTEM

Before the construction of the measuring system, different solutions have been analyzed. Using of the DAQ cards of the world-leading manufacturers, as Advantech, or National Instruments were considered. The measuring system can be built with an internal or external analog-to-digital (A/D) signal conversion [5, 9, 11]. A sample solution which uses the internal A/D converter, integrated with the DAQ Advantech PCI 1747 card (32 analog inputs) is presented in fig. 5.16.

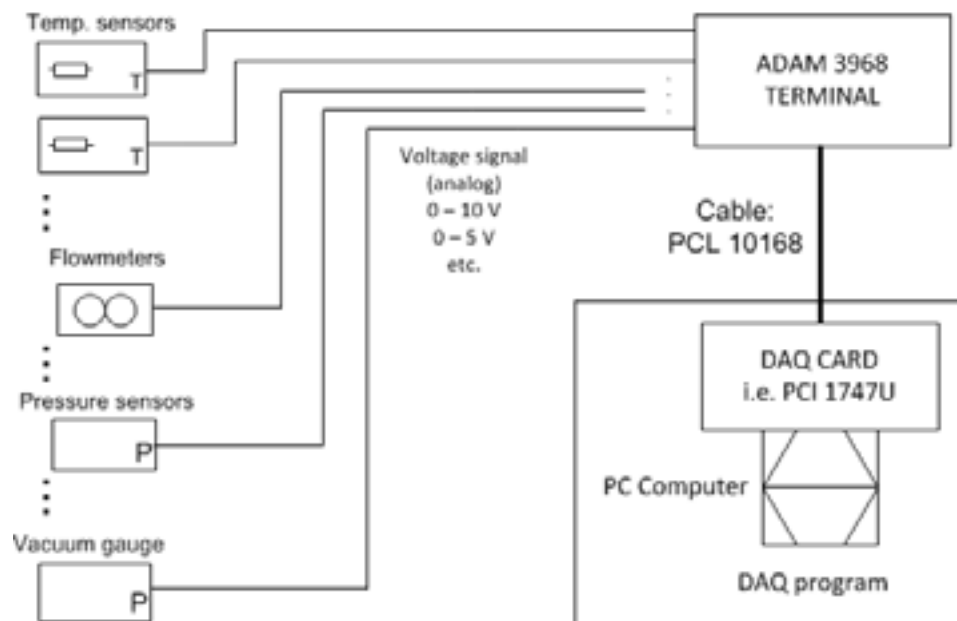


Fig. 5.16. Measuring system with an internal A/D converter

The proposed measurement DAQ card PCI 1713-AE is equipped with 32 configurable analog inputs for measuring ranges and 12-bit A/D converters. The card is installed inside a casing of a PC. A standard SCSI connector is used for communication with the sensors and transmitters. A SCSI connector cable is of the PCL 10 137 type. The cable connects the PCI DAQ card to the PCLD-881B (or ADAM-3937) terminal, designed for easy connection of the various transducers. The computer program for acquisition and presentation of the measured data can be developed using various object-oriented programming languages and software development environments, as Delphi, C++ or C#.

The diagram of the measuring system with an external A/D conversion and acquisition of measured values through the RS-232 serial ports is presented in fig. 5.17.

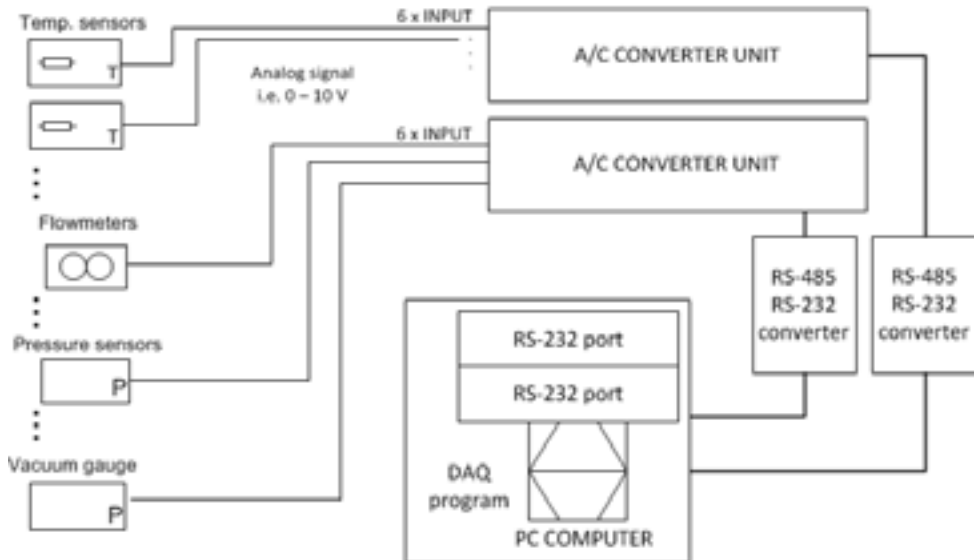


Fig. 5.17. Measuring system with an external A/D converter

In this case, the external A/D converter is installed. The output signal of the converter is transmitted through the serial interface (typically RS-485 industrial standard) according to a Modbus RTU [5] protocol. Modbus RTU provides a connection of the transmitters to a data acquisition system (which may be e.g. a PC) in the Master - Slave configuration. A master device is a PC, which sends requests for data to the transmitter. The transmitter, which is the slave device, sends data upon receiving of each data request. This type of connection of the measuring system to the PC requires usually an additional RS-485 to RS-232 converter, due to lack of RS-485 communication ports in the PC.

5.4. DESIGN OF THE SOFTWARE

5.4.1. THE DATA ACQUISITION PROGRAM

A program for data acquisition was designed and built with the following initial assumptions:

- the program is designed for Microsoft Windows. The program is being tested under Windows XP SP3, Windows Vista 32bit and Windows 7 32 bit;
- main program requirements: CPU min. Intel Core2Duo 2.0 GHz or equivalent, RAM min. 1024 MB (Windows XP) or 2048 MB (Windows 7), about 10 MB of hard disk space for the program, up to 40 GB for the measurement data;
- required the DAQ card, i.e. Advantech PCI-1713-AE or Advantech PCI 1747U with connecting terminals and wires;
- the program is designed to record data from the sensors and transducers for measuring the following parameters: force, temperature, pressure, mass flow rate etc. assuming the standard transducer output signal 0 – 10 V or 4 – 20 mA;
- the program collects the data from the transducers in the real time and stores it in a relational database.

In the development process of the data acquisition program the object-oriented programming techniques, such as a mechanism of inheritance, a polymorphism and a multithreading programming were used. Before the source code of the program was written, a preliminary project had been created using the application modeling language UML 2.0. The main functionalities of the program made available to the user are presented in the UML use case diagram in fig. 5.18.

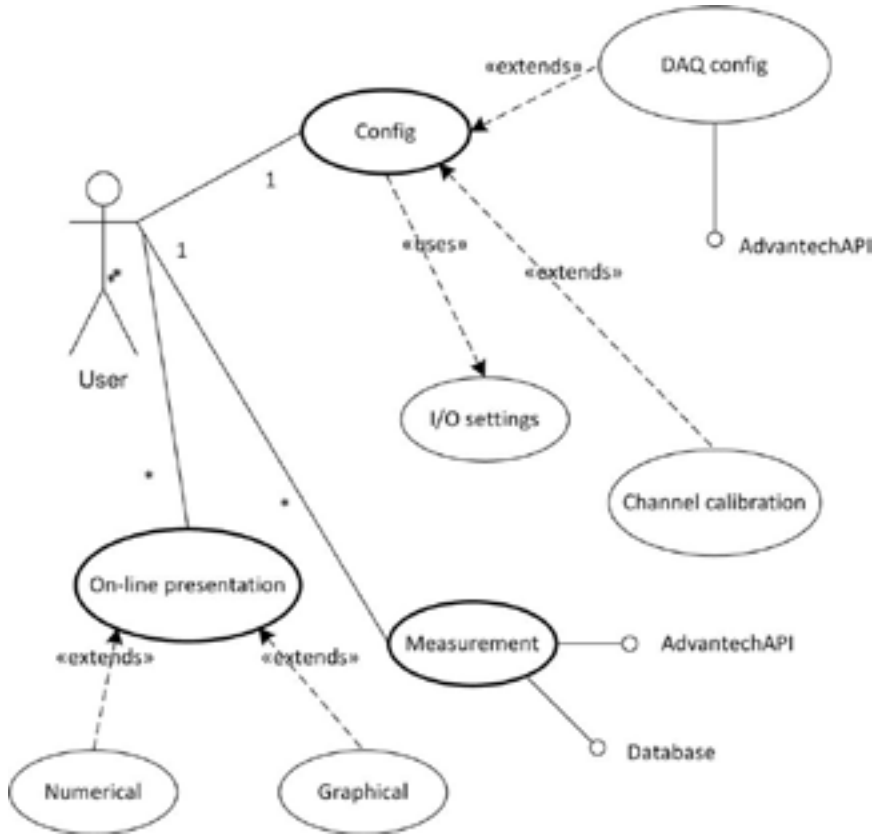


Fig. 5.18. The use-case diagram of the data acquisition program

The diagram shows the three main use cases available to the user of the program: configuring program parameters (*Config*), performing the measurement (*Measurement*) and the presenting values of the most recent measurements (*On-line presentation*). The configuration is done using the input and output settings (*I/O settings*) as paths, initialization files, output file formats, location and access parameters to the database. The configuration process also may include settings of the data acquisition card (*DAQ config*) as well as settings of the measurement channels (*Channel*

calibration). Each measurement channel has an individual range, a gain coefficient and a zero-point value (*Channel calibration*).

The following use cases: *DAQ config* and *Measurement* utilize the *AdvantechAPI* interface. In addition, the *Measurement* use case utilizes a database connection interface *Database*. Results of the most recent measurements can be presented in a numerical format (*Numerical*) or as a graphical time course (*Graphical*).

5.4.2. DATABASE DESIGN

The relational database consists of 12 data tables. Data Flow Diagram of the database shown in fig. 5.19.

In terms of the type of data stored in the database, the tables can be divided into three groups. The first group includes tables for storing the configuration data, the second group is for the user data and the third group is designed to record values of the measurements.

In the first group are included tablets which contain the configuration parameters of the measurement cards registered in the system. Basic parameters of DAQ cards are stored in the DAQCARD table. The parameters are: number of input and output analog channels, number of input and output digital channels, resolutions of the A/D and D/A converters, number of ranges available for the individual types of channels, version and name of the driver being used, etc. The values of individual measurement channels ranges available for the specified DAQ card are stored in DAQGAIN table, while the details of sensors connected to each channel are saved in DAQCHANNEL table.

Details of registered users of the application are stored in the USER table. The data include personal details, username, email and encrypted

password. Dates and times of logging users into the system are recorded in the USER_LOG table.

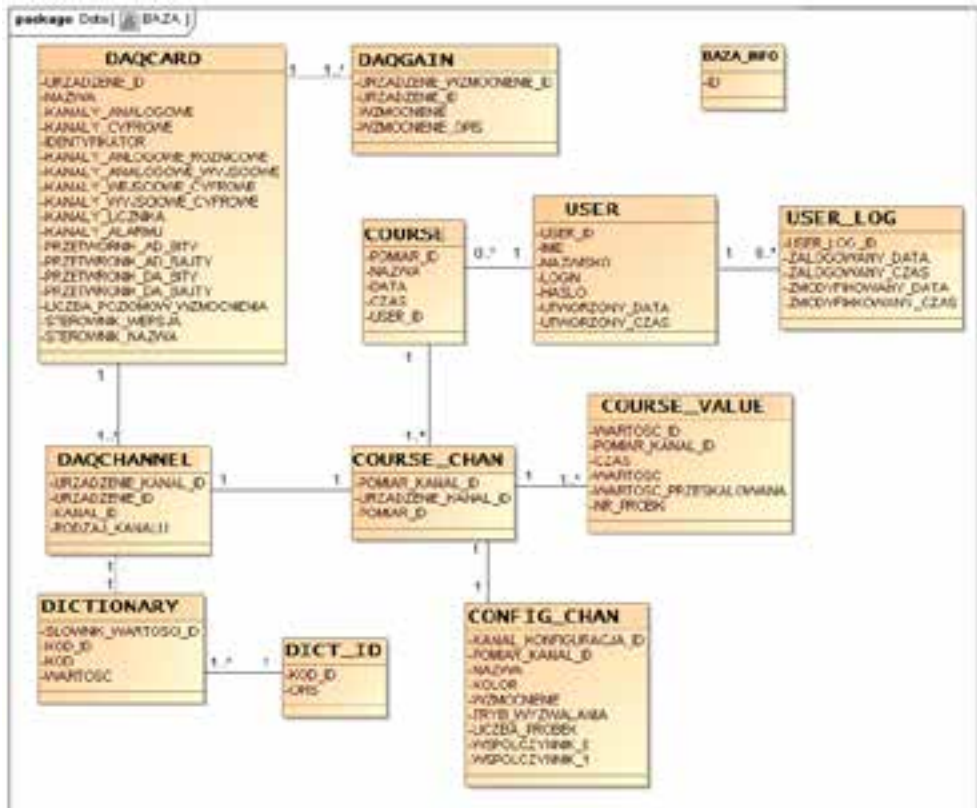


Fig. 5.19. Diagram of the relational database

The third group is the most important from the viewpoint of the database functionality. It includes tables for storing the measurement data of the carried out experiments. The primary table used to acquire the data is the COURSE table. It contains the name of the experiment, the start time and ID of the responsible user. Each experiment may include the acquisition of data from any number of available measurement channels whose parameters

are stored in the table COURSE_CHAN. The values read from the individual measuring channels are stored in the COURSE_VALUE table, while the configurations of individual channels for a given experiment are saved in the CONFIG_CHAN table.

The adopted form of the database allows to save data of any number of experiments. A multi-user access allows to carry out many experiments at one time. Configuration of the number and parameters of channels can be made independently for each experiment.

5.4.3. INITIAL ASSUMPTIONS ON THE MODULE FOR RESULTS VISUALIZATION

Visualization module is in a form of a web application. It is built based on the following initial assumptions:

- application should be compatible with popular web browsers, such as Internet Explorer, Firefox, Opera, Chrome, Safari,
- in order to ensure an adequate level of security, a user login system is built and an encrypted connection is used,
- logged user has access to the measurement data in the following areas:
 - on-line observation of the most recent values read from the various sensors and their time courses,
 - access to the monitoring data stored in a relational database,
 - observation of the values of monitored parameters in the selected time intervals,
 - the ability to create and analyze the time courses of individual parameters in the form of graphs.

The visualization module is being built using the PHP programming language and the Zend framework.

5.5. REFERENCES

- [1] Alciatore D.: *Introduction to Mechatronics and Measurement Systems*, 4th edition, McGraw-Hill, 2011.
- [2] Arkharov A., Marfenina I, Mikulin Ye.: *Cryogenic Systems*, Vol.1: *Basics of Theory and Design*, Moscow, 2000.
- [3] Bryson W. E.: *Cryogenics*, Hanser Gardner Publications, 1999.
- [4] Chorowski M.: *Kriogenika. Podstawy i zastosowania*, IPPU Masta, Gdańsk 2007.
- [5] Doebelin E.: *Measurement systems*, 5th edition, McGraw-Hill, 2003.
- [6] Filo Grzegorz, Lisowski Edward: *Metodyka programowania obiektowego z przykładami w C++*, podręcznik dla studentów szkół technicznych, Wydawnictwo PK, Kraków 2009.
- [7] Flynn T. M.: *Cryogenic Engineering*, 2nd edition, Dekker 2004.
- [8] Halpin T., Morgan T.: *Information Modeling and Relational Databases*, 2nd edition, Morgan Kaufmann, 2008.
- [9] Hughes I., Hase T.: *Measurements and their Uncertainties: A practical guide to modern error analysis*, Oxford University Press, USA, 2010.
- [10] Lisowski E., Czyżycki W.: *Transport and storage of LNG in container tanks*, Journal of KONES Powertrain and Transport, Vol. 18, No. 3, p.p. 193-201, Warsaw 2011.
- [11] Rabinovich S. G.: *Measurement Errors and Uncertainties: Theory and Practice*, 3rd edition, Springer, Germany, 2005.
- [12] Stanwick V., Fowler S.: *Web Application Design Handbook: Best Practices for Web-Based Software*, Morgan Kaufmann, 2004.